

SEISMIC LIQUEFACTION: 1-G MODEL TESTING SYSTEM AND SHAKE TABLE TESTS

**A Thesis Submitted to
the Graduate School of Engineering and Sciences of
İzmir Institute of Technology
in Partial Fulfillment of the Requirements for the Degree of**

MASTER OF SCIENCE

in Civil Engineering

**by
İrem KAHRAMAN**

**July 2013
İZMİR**

We approve the thesis of **İrem KAHRAMAN**

Examining Committee Members:

Assist. Prof. Dr. Nurhan ECEMİŞ

Department of Civil Engineering, İzmir Institute of Technology

Assoc. Prof. Dr. İsfendiyar EGELİ

Department of Civil Engineering, İzmir Institute of Technology

Assist. Prof. Dr. Devrim Şüfa ERDOĞAN

Department of Civil Engineering, Ege University

08 July 2013

Assist. Prof. Dr. Nurhan ECEMİŞ

Department of Civil Engineering, İzmir
Institute of Technology

Prof. Dr. Gökmen TAYFUR

Head of the Department of Civil
Engineering

Prof. Dr. R. Tuğrul SENGER

Dean of the Graduate School of
Engineering and Sciences

ACKNOWLEDGEMENTS

I would like to express my sincere gratitude to Asst. Prof. Nurhan Ecemiş, for her guidance and encouragement throughout the work for this thesis, as well as for her support throughout the entire studies at IZTECH. It was a great learning experience working with her and her assistance was very crucial.

I would like to thank Asst. Prof. Gürsoy Turan and Asst. Prof. Selçuk Saatçi for providing me a great opportunity to work at the IZTECH structural laboratory and providing me with valuable assistance whenever I needed.

This work herein was supported financially by TUBITAK (Project No:111M435). This support is gratefully acknowledged.

I would like to thank Research Assistant at IZTECH and my friend, Mustafa Karaman for his able and constant help during my research. I would like to thank Emre Özdeker for his valuable friendship as well as encouragements.

Last but not least, the deepest thanks and gratitude are extended to my father, Levent Kahraman, my mother, Şermin Kahraman and my sister, Nil Kahraman, for their never ending encouragement, support and love throughout every stage of my life. This work is dedicated to them.

ABSTRACT

SEISMIC LIQUEFACTION: 1-G MODEL TESTING SYSTEM AND SHAKE TABLE TESTS

Soil liquefaction is a crucial, interesting and complex seismic problem. Previous earthquake records and computational modelings have given general information about liquefaction, but many questions, such as; effects of silt content on liquefaction phenomena have not been clearly answered yet.

In this study, liquefaction phenomena in sands and silty sands were simulated by a large scale 1-g laminar box system. Three shake table tests were performed, where each test consisted of four shakes to analyze the initial-liquefaction and re-liquefaction phenomena. Instrumentations were used during shake table tests to measure laminate, soil response and settlement of ground. The soil deposit was prepared with different fines content using hydraulic filling method. Piezocone penetration tests (CPTu) were conducted, before and after each shake to determine the relative density of the soil model. Following results were found;

Silty sands were found to possess more liquefaction resistance than uniform fine sands. Soils with rounded shapes were more susceptible to liquefaction, than angular grained soils. Required time to trigger liquefaction increased with fines content and depth of the soil sedimentation. Liquefaction resistance of each tested sand decreased from 1st to the 2nd shaking, despite increase in relative density. Relative density values increased with each shake. Despite the increase in relative density, liquefaction resistance decreased. Relative density values have decreased, when fines content increased, but despite decreased in relative density, liquefaction resistance increased. Ground settlement values after the shaking was more than during the shaking. Ground settlement values have increased with fines content of the soil model.

ÖZET

SİSMİK SIVILAŞMA: 1-G MODEL DENEY DÜZENEĞİ VE SARISMA TABLASI DENEYLERİ

Kum sıvılaşması çok önemli, ilginç ve karışık bir sismik problemdir. Geçmiş depremler ve bilgisayar modellemeleri, sıvılaşma sırasında kumun davranışı hakkında genel bir bilgi vermektedir, fakat sıvılaşma üzerindeki silt yüzdesinin etkileri gibi sorular hala açıkça cevaplanmamıştır.

Bu çalışmada, büyük ölçekli laminer kutu ile sıvılaşma olayı taklit edilmektedir. 3 adet sarsma tablası deneyi yapılmıştır. Ön-sıvılaşma ve tekrar-sıvılaşmayı incelemek için her bir sarsma deneyi dört sarsmadan oluşmaktadır. Sarsma tablası deneyleri sırasında katmanların, kumun tepkisini ve yüzeysel oturmayı ölçebilmek için enstrümantasyonlar kullanılmıştır. Kum çözeltisi hidrolik doldurma metodu kullanılarak farklı silt yüzdeleri ile hazırlanmıştır. Kum modelinin rölatif yoğunluğuna karar verebilmek için her bir sarsma öncesi ve sonrasında koni penetrasyon deneyi uygulanmıştır.

Siltli kumların sıvılaşma direncinin, düzgün ince kumlara göre daha fazla olduğu bulunmuştur. Yuvarlak daneli ince kumlar, köşeli olanlara göre sıvılaşmaya karşı daha duyarlıdır. Sıvılaşmayı tetiklemek için gerekli süre, silt yüzdesi ve derinlik arttıkça artmaktadır. 1. Sarsmadan 2. Sarsmaya geçildiğinde, rölatif yoğunluğun artmasına rağmen, her bir test zemini için sıvılaşma direnci azalmaktadır. Her bir sarsma ile beraber rölatif sıklık değerleri artmaktadır. Rölatif sıklık her bir sarsmayla artmasına rağmen, sıvılaşma direnci düşmektedir. Silt yüzdesi arttığı zaman rölatif sıklık düşmektedir, rölatif yoğunluktaki azalmaya rağmen, sıvılaşma direnci artmaktadır. Sarsmadan sonraki yüzeysel oturma, sarsma sırasındaki oturmadan daha fazladır. Oturmalar silt yüzdesi ile artmaktadır.

TABLE OF CONTENTS

LIST OF FIGURES	xi
LIST OF TABLES	xvi
LIST OF SYMBOLS	xvii
CHAPTER 1. INTRODUCTION	1
1.1. General	1
1.2. Problem Statement and Scope of the Study	1
1.3. Organization of the Thesis	3
CHAPTER 2. REVIEW OF SOIL LIQUEFACTION	4
2.1. Introduction	4
2.2. Liquefaction Phenomena	4
2.2.1. Flow Liquefaction	5
2.2.2. Cyclic Mobility	6
2.2.2.1. Level Ground Liquefaction	7
2.3. Effects of Liquefaction	8
2.3.1. Alteration of Ground Motion	8
2.3.2. Sand Boils	9
2.3.4. Settlement	11
2.3.5. Instability	12
2.3.6. Bearing Capacity	14
2.4. Factors Known to Influence Liquefaction Potential	15
2.4.1. Soil Type	15
2.4.2. Relative Density	16
2.4.3. Void Ratio	17
2.4.4. Groundwater Level	17
2.4.5. Earthquake Magnitude and Distances	17
2.4.6. Earthquake Duration	18
2.4.7. Historical Evidence	19

2.4.8. Grain Size Distribution	19
2.4.9. Grain Shape	21
2.4.10. Depositional Environment	21
2.4.11. Age of Deposits	22
2.4.12. Initial Confining Pressure	22
2.4.13. Drainage Conditions.....	22
CHAPTER 3. LITERATURE REVIEW FOR MODEL TESTS	23
3.1. Introduction.....	23
3.2. Model Tests.....	23
3.2.1. Shake Table Tests	24
3.2.2. Centrifuge Tests	25
3.2.3. Literature Review of Shake Table Tests	26
3.2.3.1. Shake Table Tests Conducted by S. R. Pathak et al.....	
(2001)	27
3.2.3.2. Shake Table Tests Conducted by Tzou-Shin Ueng et al.....	
(2006)	28
3.2.3.3. Shake Table Tests Conducted by S.K Prasad et al.....	
(2004)	28
3.2.3.4. Shake Table Tests Conducted by Thenavanayam et al.....	
(2009)	28
CHAPTER 4. ONE-DIMENSIONAL LAMINAR BOX SYSTEM	30
4.1. Introduction.....	30
4.2. Strong Floor	31
4.3. 1-D Shake Table	31
4.4. Crane	31
4.5. One-Dimensional Laminar Box.....	31
4.5.1. I-Beam.....	32
4.5.2. Plate on Reinforced Welding and Angle Brackets.....	33
4.5.3. Roller Mechanism between Laminates	34
4.5.4. Box Stoppers and Rubber Stoppers.....	35
4.6. Membrane	36
4.7. Instrumentation	38

4.7.1. Submersible Accelerometer	39
4.7.2. Traditional Accelerometers	40
4.7.3. Pore Pressure Transducers	41
4.7.4. Potentiometers	44
4.8. Data Acquisition System.....	45
4.9. Sample Preparation Box	49
4.10. CPTu System	50
CHAPTER 5. SHAKE TABLE AND INITIAL LAMINAR BOX PERFORMANCE.....	
TESTS.....	55
5.1. Introduction.....	55
5.2. Shake Table Performance Test	55
5.3. Laminar Box Pull and Push Tests.....	56
CHAPTER 6. SOIL PREPARATION FOR THE SHAKE TABLE TESTS	58
6.1. Introduction.....	58
6.2. Preparation of Soil Samples.....	58
6.2.1. Laboratory Tests.....	59
6.2.1.1. Sieve Analysis	59
6.2.1.2. Hydrometer Test	60
6.2.1.3 Specific Gravity Test.....	61
6.2.1.4. Maximum and Minimum Void Ratio Tests.....	62
6.2.1.5 Falling Head Permeability Test	63
6.3. Hydraulic Filling Method	64
CHAPTER 7. CONE PENETRATION TESTS AND SHAKE TABLE TESTS	70
7.1. Introduction.....	70
7.2. CPTu Tests.....	70
7.2.1. CPTu Tests Results	74
7.2.1.1. Test 1- CPTu.....	74
7.2.1.2. Test 2 - CPTu.....	75
7.2.1.3. Test 3 - CPTu.....	76
7.3. Shake Table Tests	77
7.3.1. Shake Table Test 1	78

7.3.1.1. Soil Properties.....	78
7.3.1.2. Instrumentation Plan of Test 1.....	80
7.3.1.3. Input Motions of Test 1	81
7.3.1.4. Results of Test 1	82
7.3.1.4.1. Data Filtration	82
7.3.1.4.2. Acceleration Response of the Soil Model.....	85
7.3.1.4.3. Acceleration Response of Laminates	86
7.3.1.4.4. Excess Pore Water Pressure Response.....	88
7.3.1.4.5. Displacement Response of the Laminates.....	90
7.3.1.4.6. Settlement Response	91
7.3.1.4.7. Cross Comparison between Instruments	93
7.3.2. Shake Table Test 2	95
7.3.2.1. Soil Properties.....	95
7.3.2.2. Instrumentation Plan of Test 2.....	96
7.3.2.3. Input Motions of Test 2	97
7.3.2.4. Results of Test 2	98
7.3.2.4.1. Acceleration Response of the Soil Model.....	98
7.3.2.4.2. Acceleration Response of the Laminates	99
7.3.2.4.3. Excess Pore Water Pressure Response.....	101
7.3.2.4.4. Potentiometer	103
7.3.2.4.5. Horizontal Displacement Performance of the.....	
Laminates	103
7.3.2.4.6. Ground Surface Settlement Response.....	104
7.3.3. Shake Table Test 3	106
7.3.3.1. Soil Properties.....	106
7.3.3.2. Instrumentation Plan of Test 3.....	109
7.3.3.3. Input Motions of Test 3	110
7.3.3.4. Results of Test 3	110
7.3.3.4.1. Excess Pore Water Pressure Response.....	111
7.3.3.4.2. Displacement Response	112
7.3.3.4.3. Ground Settlement Response	113
 CHAPTER 8. ANALYSES OF THE TEST RESULTS.....	 116
8.1. Analyses of the Shake Table Tests	116

CHAPTER 9. CONCLUSIONS	125
9.1. Summary of Findings.....	125
9.2. Suggestions for Future Research	126
REFERENCES	127
APPENDIX A. DESIGN OF LAMINAR BOX	130

LIST OF FIGURES

<u>Figure</u>	<u>Page</u>
Figure 2.1. (a) Situation of Soil Particles Before Liquefaction Phenomenon, (b).....	
Connection between Soil Particles Before Liquefaction Phenomenon,.....	
(c) Connection between Soil Particles After Liquefaction Phenomenon.	5
Figure 2.2. Stress Path Zone of Susceptibility to Flow Liquefaction	6
Figure 2.3. Stress Path Zone of Susceptibility to Cyclic Mobility	7
Figure 2.4. (a) After 1999 Marmara Earthquake, Building Sank into the Ground, (b).....	
After 1999 Marmara Earthquake, The Sidewalk Bulged and Split.....	
Longitudinally	9
Figure 2.5. Schematic Explanation of Sand Boil Mechanism	10
Figure 2.6. (a) Small Sand Boils from the 1979 Imperial Valley Earthquake, (b) Large...	
Sand Boil during The Loma Prieta Earthquake, 1989	10
Figure 2.7. Examples of Settlement of Buildings after Marmara Earthquake, 1999.....	11
Figure 2.8. Lower San Fernando Dam after San Fernando Earthquake of 1971.....	13
Figure 2.9. (a) Before 1971 San Fernando Earthquake, Image of the Lower San.....	
Fernando Dam, (b) After 1971 San Fernando Earthquake, Image of the.....	
Lower San Fernando Dam	13
Figure 2.10. Lateral Spreading Problem After the 1964 Niigata Earthquake.....	14
Figure 2.11. Bearing Capacity Problem After 1964 Niigata Earthquake	14
Figure 2.12. Relationship between the Epicentral Distance (R_c) and the Moment.....	
Magnitude	18
Figure 2.13. Number of Equivalent Stress Cycles versus Earthquake Magnitude	18
Figure 2.14. The 1st Chinese Criteria	19
Figure 2.15. The 1 st and the 2 nd Chinese Criteria.....	20
Figure 2.16 Modified Chinese Criteria	21
Figure 3.1. Shaking Table with Soil Bin Used for Dynamic Earth Pressure Research...24	
Figure 3.2. Cross Section through a Geotechnical Centrifuge	26
Figure 4.1. I-beam.....	33
Figure 4.2. Angle Brackets	33
Figure 4.3. Roller Mechanism	35

Figure 4.4. Components of Bottom Laminate, Connection of Shake Table and Bottom... Laminate (1- Shake Table, 2-Laminate, 3- Strong Floor, 4- Box Stopper,... 5-Roller, 6- Rubber Stopper, 7- Angle Bracket, 8- L-Profile).....	36
Figure 4.5. Placement of the Rubber Membrane	37
Figure 4.6. Submersible Accelerometer Used in the Shaking Table Test	39
Figure 4.7. Traditional Accelerometer Used in the Shaking Table Tests.....	41
Figure 4.8. (a) Filter of the Pore Pressure Transducer, (b) Filter was Placed inside the.... Pore Pressure Transducer, (c) Pore Pressure Transducer Used in the..... Shaking Table Tests	42
Figure 4.9. Submersible Accelerometers and Pore Water Pressure Transducers Tied..... on Nets	42
Figure 4.10. (a) Pore Water Pressure Transducers and Submersible Accelerometers..... Tied on Nets and Nets are Placed in the Laminar Box, (b) Nets Tied on..... the Wood to be Tight	43
Figure 4.11 : (a) X-Potentiometers Measure the Displacement of Laminates, (b)..... Z-Potentiometers Measure Settlement	44
Figure 4.12. NI SCB-68 Connector Block for Data Acquisition Devices.....	45
Figure 4.13. NI SCXI-1520 Strain Gage Input Module	46
Figure 4.14. NI SCXI-1531 Accelerometer Input Module.....	46
Figure 4.15. Preparation Boxes.....	49
Figure 4.16. (a) Side View of CPTu System (N-S), (b) Figure B.2. Side View of..... CPTu System (W-E)	51
Figure 4.17. Components of the CPTu System	52
Figure 4.18. CPTu Probe; 1)Point, 10 cm ² , 2) O-ring, 3) Filter Ring, 4) X-ring, 5)..... Support Ring, 6) O-ring, 7) O-ring, 8) O-ring, 9) Friction Sleeve, 10)..... Cone Body, 11) O-ring (Source: Geotech Nova CPT Acoustic Manual)...	52
Figure 4.19 (a). Keeping the Rings and Cone Tip Point in Glycerin, (b) Mount of..... X-ring, Filter Ring and Point in Funnel	53
Figure 4.20. CPTu System Used in This Study.	54
Figure 5.1. (a) Shake Table Test with Soil Bags, (b)Acceleration vs Time of the Input... Motion and Accelerometer	56
Figure 5.2. (a) Load Cell Attached on the Laminate, (b) Static Force per Laminate	57
Figure 6.1. (a) Ranged the Sieves #4 to #230, (b) Sieves Column were Placed on the.... Mechanical Shaker.....	59

Figure 6.2. Control Cylinder and Hydraulic Stem.....	60
Figure 6.3. (a) Desiccator and Vacuum Pump, (b) Pycnometer, Distilled Water and..... Weight (Left to Right)	62
Figure 6.4. (a) Mold and Weight, (b) The Mold Attached to the Vibrating Table.....	62
Figure 6.5. Permeability Test Setup.....	64
Figure 6.6. Hydraulic Filling Schematic View	65
Figure 6.7. Hydraulic Filling Process	65
Figure 6.8. Bucket Density Process for Test 1	66
Figure 6.9. Locations of Buckets	67
Figure 6.10. Density Buckets Used for Bucket Density Test	68
Figure 6.11. (a) Test 1, (b) Test 2 and (c) Test 3 Filling Process	69
Figure 7.1. (a) Microphone was Placed on the Probe, (b) Hydraulic Pump was Raised,... (c) Rod was Added , (d) Microphone was Placed on the Rod, (e) The..... Rod and Probe was Penetrated to the Soil	72
Figure 7.2. Terminology for Cone Penetrometers	72
Figure 7.3. Location of CPTu Tests – Top View.....	73
Figure 7.4 Summary of CPT Test Results for Test 1.....	75
Figure 7.5. Summary of CPTu Test Results for Test 2.....	76
Figure 7.6. Summary of CPTu Test Results for Test 3.....	77
Figure 7.7. Grain Size Distribution and Soil Properties for Clean Nearly Uniform..... Sand.....	79
Figure 7.8. SEM images of Soil Sample with 0% Fines Content.....	79
Figure 7.9. (a) Test 1 Side View of Instrumentation Plan, (b) Top View of..... Instrumentation Plan	81
Figure 7.10. Input Motions of Test 1; (a) 1 st Shake, (b) 2 nd Shake, 3) 3 rd Shake and,..... (d) 4 th Shake	82
Figure 7.11. Print screen of the LabView Programme	83
Figure 7.12. Print screen of the Front Panel and Block Panel on the LabView..... Programme	84
Figure 7.13. Test 1; (a) 1 st Shake, (b) 2 nd Shake, (c) 3 rd Shake, (d) 4 th Shake..... Acceleration Response from Submersible Accelerometers (SA5, SA3,..... SA1)	86

Figure 7.14. Test 1; (a) The 1 st Shake, (b) The 2 nd Shake, (c) The 3 rd Shake, (d) The..... 4 th Shake Acceleration Response from Laminate Accelerometers (LA8,..... LA7, LA4, LA3,LA)	87
Figure 7.15. Test 1; (a) 1 st Shake, (b) 2 nd Shake, (c) 3 rd Shake, (d) 4 th Shake Excess Pore Water Pressure Response	88
Figure 7.16. Test 1; (a) 1 st Shake, (b) 2 nd Shake, (c) 3 rd Shake, (d) 4 th Shake..... Displacement Responses (XP6 , P5, XP7, XP4, XP2, XP1, XP3)	90
Figure 7.17. Test 1; 1 st Shake Settlement Results.....	91
Figure 7.18. (a) 1 st Shake, (b) 2 nd Shake, (c) 3 rd Shake, (d) 4 th Shake, Comparison..... of LA4 and XP7	93
Figure 7.19. Test 1; (a) The 1 st Shake, (b) The 2 nd Shake, (c) The 3 rd Shake, (d) The..... 4 th Shake Comparison of SA1, LA1 and XP3.....	94
Figure 7.20. Test 1; (a) The 1 st Shake, (b) The 2 nd Shake, (c) The 3 rd Shake, (d) The..... 4 th Shake Comparison of BA1 and Input Motion	94
Figure 7.21. Grain Size Distribution for Silty Sand and Soil Properties with 15%..... Fines Content	95
Figure 7.22. SEM Image of Soil Sample with 15% Fines Content	96
Figure 7.23. (a) Test 2 Side View of Instrumentation Plan, (b) Top View of..... Instrumentation Plan	97
Figure 7.24. Test 2; Input Motion of the (a) 1 st Shake, (b) 2 nd Shake, (c) 3 rd Shake..... and (d) 4 th Shake	98
Figure 7.25. Test 2; (a) 1 st Shake, (b) 2 nd Shake, (c) 3 rd Shake, (d) 4 th Shake..... Acceleration Response from Submersible Accelerometers (SA8, SA4,..... SA3, SA7, SA2).....	99
Figure 7.26. Test 2; (a) 1 st Shake, (b) 2 nd Shake, (c) 3 rd Shake, (d) 4 th Shake..... Acceleration Response from Laminate Accelerometers (LA8, LA7,..... LA6, LA5, LA4, LA3, LA2, LA1)	100
Figure 7.27. Test 2; (a) 1 st Shake, (b) 2 nd Shake, (c) 3 rd Shake and (d) 4 th Shake..... Excess Pore Pressure Response	101
Figure 7.28. Potentiometer Results (a) 1 st Shake, (b) 2 nd Shake, (c) 3 rd Shake,..... (d) 4 th Shake (XP6, XP5, XP7, XP4, XP2, XP1, XP3).....	104
Figure 7.29. Z-Potentiometers	104
Figure 7.30. Test 2; (a) 1 st Shake, (b) 2 nd Shake, (c) 3 rd Shake, (d) 4 th Shake..... Settlement Response (ZP1, ZP2)	105

Figure 7.31. Fines Content of the Soil Model in the Laminar Box	107
Figure 7.32. Grain Size Distribution of Silty Sand and Soil Properties with 25%.....	
Fines Content	108
Figure 7.33. SEM Image of Silty Sand with Less Than 25% Fines Content.....	108
Figure 7.34. (a) Test 2 Side View of Instrumentation Plan, (b) Top View of.....	
Instrumentation Plan	109
Figure 7.35. Test 3; Input Motion of the (a) 1 st Shake, (b) 2 nd Shake, (c) 3 rd Shake and	
(d) 4 th Shake.....	110
Figure 7.36. Test 3; (a) 1 st Shake, (b) 2 nd Shake, (c) 3 rd Shake and (d) 4 th Shake.....	
Excess Pore Water Pressure Response	111
Figure 7.37. Test 3; (a) 1 st Shake, (b) 2 nd Shake, (c) 3 rd Shake, (d) 4 th Shake.....	
Displacement Response (XP6, XP5, XP7, XP4, XP2, XP1, XP3).....	113
Figure 7.38. Test 3; (a) The 1 st Shake, (b) The 2 nd Shake, (c) The 3 rd Shake, (d) The.....	
4 th Shake Settlement Response	114
Figure 8.1. r_u values during; (a) Shake-1, (b) Shake-2, (c) Shake-3 and (d) Shake-4..	117
Figure 8.2. Required Number of Cycles for initiation of Liquefaction in; (a) Test 1,.....	
(b) Test 2, (c) Test 3.....	119
Figure 8.3. Initiation Time for Liquefaction in; (a) Test 1, (b) Test 2, (c) Test 3	121
Figure 8.4. Relative Density (D_r) in; (a) Test 1, (b) Test 2, (c) Test 3.	122
Figure 8.5. Relative Density Values to Initiate Liquefaction in; (a) Test 1, (b) Test 2,.....	
(c) Test 3.	123
Figure 8.6. Ground Settlement During and After the Shaking in Each Test.	124
Figure 8.7. Ground Settlement Variation with Fines Content of the Soil Model.	124

LIST OF TABLES

<u>Table</u>	<u>Page</u>
Table 1.1. A Summary of the 1-g Shake Table Tests Conducted Using 1-g Laminar Box	2
Table 2.1. Liquefaction Potential with Respect to Relative Density of Fine Sands	16
Table 3.1. Scaling Factors for Centrifuge Modeling	25
Table 3.2. Internal Dimensions and Laminates Number of Laminar Boxes	27
Table 4.1. Properties of Submersible Accelerometer	40
Table 4.2. Properties of the Pore Water Pressure Transducers	43
Table 4.3: Connection of Accelerometers and Potentiometers to Module	48
Table 6. 1. Summary of Properties of Soils which were Inside the Soil Bags	63
Table 6.2. Properties of Slurry Pump	64
Table 6.3. (a) Test 1, (b) Test 2, (c) Test 3 Bucket Density Tests Results	67
Table 6.4. (a) Test 1, (b) Test 2, (c) Test 3 Water Content.....	68
Table 7.1 Technical Specification of Hydraulic Power Unit.....	71
Table 7.2. Filter Type of Instrumentations	84
Table 7.3. Summary of Test 1.....	89
Table 7.4. Test 1; Ground Surface Settlement Measured by the Potentiometer.....	92
Table 7.5. Test 1; Ground Settlement Measured Manually	92
Table 7.6. Summary of Test 2.....	102
Table 7.7. Measured by Potentiometer	106
Table 7.8. Ground Settlement measured by Potentiometer	106
Table 7.9. Summary of Test 3.....	112
Table 7.10. Ground Settlement Measured by Potentiometer	114
Table 7.11. Ground Settlement Measured Manually	115

LIST OF SYMBOLS

a_{\max}	= Maximum acceleration amplitude of ground acceleration
BA	= Bottom accelerometer
A_c	= Area of the cone
A_s	= Surface area of the friction sleeve
C_c	= Coefficient of gradation
C_u	= Uniformity coefficient
CPTu	= Cone penetration test
d	= Diameter
D_{10}	= Diameter through 10% of the total soil mass passed
D_{30}	= Diameter through 30% of the total soil mass passed
D_{60}	= Diameter through 60% of the total soil mass passed
D_r	= Relative density
e	= Void ratio
e_{\min}	= Minimum void ratio
e_{\max}	= Maximum void ratio
FC	= Fines Content
f_s	= Sleeve friction
F _s	= The total force acting on the friction sleeve
g	= Acceleration due to gravity
G_s	= Specific gravity
h	= Height
H_o	= Original height
k	= Permeability
LA	= Laminate accelerometer
LL	= Liquid limit
M_s	= Weight of dry loose soil
No-Liq	= No Liquefaction
PP	= Pore water pressure
q_c	= Cone tip resistance
Q_c	= Total force acting on the cone
R_e	= Epicentral distance

R_f = Fault distance
 r = Radius
 r_u = Pore pressure ratio
 s = Settlement
SA = Submersible accelerometer
SEM = Scanning electron microscope
 u = Pore water pressure
 u_1 = Pore pressure on the cone
 u_2 = Pore pressure behind the cone
 u_3 = Pore pressure behind the cone
 V = Volume
 V_m = Volume of the mold
 V_s = Soil volume after compaction
 w = Water content
 W = Weight
 W_O = Weight of dry soil sample
 W_A = Weight of pycnometer and distilled water
 W_B = Weight of the empty pycnometer
XP = X-Potentiometer
ZP = Z- Potentiometer
 ε = Vertical strain
 ΔH = Vertical deformation
 Δu = Excess pore pressure
 Ω = Rotational speed
 \emptyset = Diameter
 μ = Friction
 $\gamma_{\text{dry-min}}$ = Density of the dry loose soil
 $\gamma_{\text{dry-max}}$ = Density of the dry compact soil
 γ_{sat} = Saturated unit weight
 σ_{v_o}' = Effective vertical stress

CHAPTER 1

INTRODUCTION

1.1. General

Earthquakes, hurricanes, tornados and floods occur naturally. These natural hazards cause significant damages around the world and lead to deaths, injuries and property damages. Generally earthquakes are referred to seismic hazards. The most significant seismic hazards are ground shaking, structural hazards, liquefaction, landslides, retaining structure failures, lifeline hazards, tsunami and seismic hazards.

One of the most devastating examples of earthquake damage is liquefaction. It occurs when saturated sands and silty soil deposits lose their strength and effective stress is equal to zero. Soil deposits appear to flow as fluids. Due to liquefaction phenomena related to saturated soils, liquefaction is usually observed near bodies of water such as rivers and bays.

1.2. Problem Statement and Scope of the Study

Since 1964, Niigata Earthquake has been attracting engineers' concern on the phenomena of soil liquefaction. Researchers have managed lots of aerial surveys to explain the failures caused by liquefaction. As a result of these surveys, various semi-empirical methods are proposed to characterize the ground failure during earthquake. However, aerial surveys give information about the site before and after an earthquake. Thus, model tests are used to characterize the behavior of soil during an earthquake.

Model tests can be divided into two main groups: Centrifuge modeling and 1-g shaking test. Centrifuge modeling was first used in 1970s at Cambridge University England for studying problems related to liquefaction, laterals spreading and related problems. However; scale factor is a significant problem. Besides scaling problem, dense instruments cannot be placed inside the soil, to measure the soil response.

Because of these disadvantages, most researchers have focused on large scale shake table tests in spite of they are extremely expensive.

Full scale shake table tests simulate the real world boundary conditions nearly, Dense array of instruments could be placed inside the soil. To understand the exact physics behind the soil behavior and to apply suitable engineering design guidelines, 1-g shake table tests are needed.

In this research, three 1-g shake table tests were conducted at the Civil Engineering Department's structural laboratory. Each test, 4 subsequent shakings were also performed. These are labeled as Shake-1, Shake-2, Shake-3 and Shake-4. At each subsequent shaking, only the peak acceleration value was changed. These three tests were conducted to study the behavior of sand and silty sand with different fines content (FC) to observe the effect of silt content on the liquefaction phenomena during and after the shaking. Table 1.1 summarizes these three shaking table tests. They were aimed at studying the pore pressure response, lateral deformations and ground settlements.

Table 1.1. A Summary of the 1-g Shake Table Tests Conducted Using 1-g Laminar Box

Test Name	Shaking Number	Model Height	Shaking Duration	Peak Acceleration	Frequency of Motion	Fines Content (FC)
-	-	<i>m</i>	<i>sec</i>	<i>g</i>	<i>Hz</i>	<i>%</i>
Test_1	Shake-1	1.40	12	0.05		0
	Shake-2	1.40	12	0.11	2	0
	Shake-3	1.40	12	0.48	2	0
	Shake-4	1.40	12	0.56	2	0
Test_2	Shake-1	1.44	12	0.04	2	15
	Shake-2	1.44	4.3	0.08	2	15
	Shake-3	1.44	12	0.34	2	15
	Shake-4	1.44	12	0.49	2	15
Test_3	Shake-1	1.44	12	0.05	2	25
	Shake-2	1.44	12	0.19	2	25
	Shake-3	1.44	12	0.43	2	25
	Shake-4	1.44	12	0.62	2	25

The two main focus of the experimental work included in this thesis are;

1. to influence the performance of the shake table and 1-g model testing system
2. to study the effects of fines content on the pore pressure response, lateral deformations and,
3. ground settlements

1.3. Organization of the Thesis

The thesis consists of seven chapters. The first chapter, the current chapter, presents an introduction that is related to the entire work. Chapter 2, presents a literature review of liquefaction, Chapter 3 presents literature review of model tests. Design of the laminar box system is submitted in Chapter 4. Chapter 5 presents performance tests, These tests are ‘pull and push’ tests and shake table tests with soil bags. Preparation processes for the shake table tests are presented in Chapter 6. Chapter 7 presents shake table tests and the results of the shake table tests. Before each shake table test, CPTu tests were conducted inside the laminar box to determine the relative density. Results of these tests also present in this chapter. In chapter 8, summary and findings of this study are presented. This chapter is followed by a list of references. Design drawings of the laminar box are given in Appendix A at the end of this thesis

CHAPTER 2

REVIEW OF SOIL LIQUEFACTION

2.1. Introduction

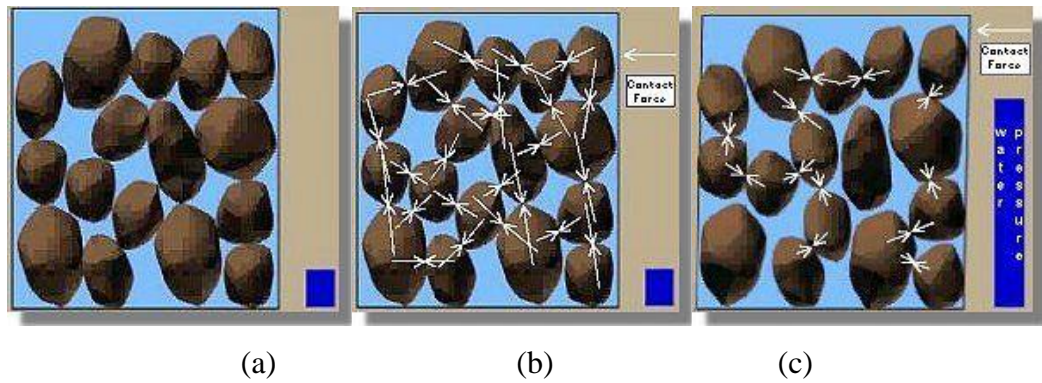
Soil liquefaction is one of the most important, interesting, complex and controversial seismic problem. Liquefaction has been seen occurred during large earthquakes or immediately after the earthquakes. Effects of the liquefaction phenomena were observed after the Alaska Earthquake (1964), Niigata Earthquake (1964), San Fernando Valley Earthquake (1971), Haicheng Earthquake (1975), Tangshan Earthquake (1976), Imperial Valley Earthquake (1979), Armenia Earthquake (1988), Loma Prieta Earthquake (1989), Kobe Earthquake (1995), and Marmara Earthquake (1999). Hence, more than four decades, researchers have studied liquefaction phenomena around the world.

In the following sections; information about liquefaction phenomena, effects of liquefaction, factors known to influence the liquefaction potential will be presented in detail.

2.2. Liquefaction Phenomena

The term liquefaction has historically been used in conjunction with a variety of phenomena that involve soil deformations caused by monotonic, transient or repeated disturbance of saturated cohesionless soils under undrained conditions. (Mogami and Kubo, 1953)

The generation of excess pore pressure is the main feature of liquefaction phenomenon under undrained conditions. When saturated cohesionless soils under undrained conditions are induced by rapid loading, due to tendency for densification, when excess pore pressure increases and effective stress decreases.



Note : Blue column represents the level of pore water pressure in the soil. The arrows represent the contact force between soil particles.

Figure 2.1. (a) Situation of Soil Particles Before Liquefaction Phenomenon, (b) Connection between Soil Particles Before Liquefaction Phenomenon, (c) Connection between Soil Particles After Liquefaction Phenomenon. (Source: [www.ce.washington.edu.html](http://www.ce.washington.edu/html))

As illustrated in Figure 2.1, each soil particle is in contact with neighbor particles before and during an earthquake. The weights of the overlying soil particles generate contact forces between the particles. The particles are hold in place by these contact forces that provide strength. The contact forces are large, while because the pore water pressure is low. When earthquake shaking starts, pore water pressure increases. The contact forces are decreased with time and soil deposits behave like a liquid than a solid. This phenomenon is called ‘liquefaction’.

Liquefaction phenomenon is divided into two main groups. These are (1) flow liquefaction and (2) cyclic mobility. Both flow liquefaction and cyclic mobility are extremely important. However, cyclic mobility is observed much more than flow liquefaction. Result of the flow liquefaction is usually more serious than cyclic mobility. Cyclic mobility can occur under a much broader range of soil and site conditions than flow liquefaction.

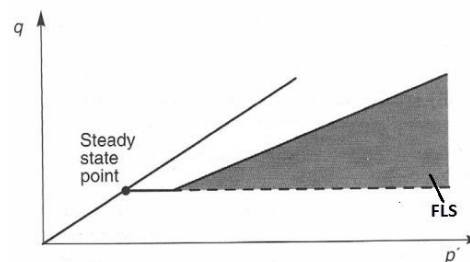
2.2.1. Flow Liquefaction

Flow liquefaction generates more dramatic effects than cyclic mobility. Tremendous instabilities known as flow failures are produced by flow liquefaction.

When shear stress required for static equilibrium of a soil mass is bigger than the shear strength of the soil, flow liquefaction occurs. In the field, shear stress required for static equilibrium, which are caused by gravity, remain essentially constant until large deformations develop. After triggering, large deformations produced by flow liquefaction are driven by static shear stress. Cyclic stresses may simply bring the soil to an unstable state, when its strength decreases adequately to allow the static stresses to produce the flow failure.

Flow liquefaction can occur in loose soils and failures of flow liquefaction develop suddenly with speed, and liquefied soils move over large distances. The flow slide failures of Sheffield Dam and Lower San Fernando Dam are examples of flow liquefaction.

When initial conditions fall within shaded zone in Figure 2.2, flow liquefaction occurs, if undrained disturbance brings the effective stress path from the point describing the initial conditions to the Flow Liquefaction State (FLS). If the initial stress conditions plot near the FLS, like under drained conditions an element of soil subjected to large shear stresses, flow liquefaction can be triggered by small excess pore pressures (Kramer & Seed, 1988). If the initial stress conditions are farther from the FLS, the liquefaction resistance will be greater (Kramer, 1996).



Note; q =Shear Stress, p' =Effective Stress

Figure 2.2. Stress Path Zone of Susceptibility to Flow Liquefaction
(Source: Kramer, 1996)

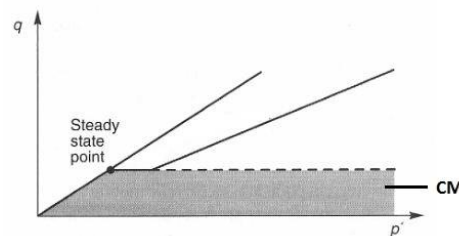
2.2.2. Cyclic Mobility

Cyclic mobility can also produce unacceptably large permanent deformations during earthquake shaking. In contrast to flow liquefaction, cyclic mobility occurs when

the static shear stress required for static equilibrium is less than the shear strength of the liquefied soil.

The deformations produced by cyclic mobility failures are driven by both cyclic and static shear stresses and develop increasingly during an earthquake shaking. These deformations are called lateral spreading that can occur at very gently sloping ground or nearby water.

Cyclic mobility can occur, when initial conditions plot to stay within the shaded zone. The shaded zone, in Figure 2.3 is susceptible to cyclic mobility. The shaded zone extends from very low to very high effective confining pressures because cyclic mobility can occur in loose and dense soils (Kramer, 1996)



Note; q =Shear Stress, p' =Effective Stress

Figure 2.3. Stress Path Zone of Susceptibility to Cyclic Mobility
(Source: Kramer, 1996)

2.2.2.1. Level Ground Liquefaction

Level ground liquefaction can be a part of cyclic mobility group. Static horizontal shear stresses which cause lateral deformations do not exist. During shaking, level ground liquefaction can produce large chaotic movement, but this movement causes little permanent lateral deformations.

Consequently, these deformations can cause significant damages. Flow liquefaction can produce major flow slides. Flow liquefaction contributes to the sinking and tilting of structures, the floating of light buried structures and also to the failure of retaining structures. Slumping of slopes, settlement of buildings, lateral spreading and retaining wall failure are observed as a result of cyclic mobility. Substantial ground oscillation, ground surface settlement, sand boils and post-earthquake stability failures can occur at level ground sites.

2.3. Effects of Liquefaction

Buildings, bridges and other constructed facilities can be affected by the liquefaction phenomena. Effects of liquefaction phenomena are categorized in main five groups; 1) alteration of ground motion, 2) sand boils, 3) settlement, 4) instability and 5) bearing capacity.

Niigata Earthquake (1964) raised the engineering awareness of earthquake induced liquefaction. The recorded magnitude was 7.4 on the Richter scale. Niigata lies on the banks of the Shinano River, where river and sea meet. As a result, liquefaction damages occurred mainly in low-lying areas. Buildings, which are founded on sand, tilted about 80 degrees because failure of bearing capacity in the liquefied ground (Figure 2.11). Besides building damages, underground structures such as, septic tanks, storage tanks, sewage conduits and manholes were damaged. Water was ejected from sand flows and mud volcanoes, shortly after the shaking and lasted for 20 minutes. City was covered with 25 cm thick sand deposits. Showa Bridge was also damaged because of lateral support loss from liquefaction. Five supported girders fell, when pier foundation piles deflected (Figure 2.10.).

2.3.1. Alteration of Ground Motion

As a result of positive excess pore water pressure during an earthquake shaking, soil stiffness decreases. Although a deposit of liquefiable soil is relatively stiff at the beginning of the earthquake shaking, at the end of the shaking, it may be much softer. The amplitude and frequency of the surface motion may change the degrees of the stiffness.

If the layer is so low, high frequency components of a bedrock motion cannot be transmitted to the ground surface in the most extreme case.

Surface acceleration amplitudes decrease, when pore pressure increases. This situation does not reduce the potential damage, because low acceleration amplitudes at low frequencies can produce large displacements. These displacements may be related to buried structures and failure in utilities and structures supported on pile foundations that extend through liquefied soils. Liquefied soils can be decoupled from the surficial

soils, when liquefaction occurs at depth beneath a flat ground surface and this phenomenon produces large transient time dependent ground oscillations.

The surficial soils are divided into blocks by fissures. These fissures can open and close during shaking. Ground waves with depth of up to several meters have been observed during ground oscillation, but generally permanent displacements are small.



(a)

(b)

Figure 2.4. (a) After 1999 Marmara Earthquake, Building Sank into the Ground (Source: www.geology.knoji.com), (b) After 1999 Marmara Earthquake, The Sidewalk Bulged and Split Longitudinally (Source: www.geerassociation.org)

Marmara Earthquake (August 17, 1999) is an example to the alteration of ground motion. Buildings sank into the soil and failed by the shaking and high numbers of oscillation cycles. Sidewalks are lifted up, due to the ejection of soil materials during shaking. Figure 2.4 illustrates the building which sank into the ground and the sidewalk which bulged and split longitudinally after 1999 Marmara Earthquake. Earthquake was measured 7.4 on Richter scale with 17km local depth. The event has lasted for 37 seconds. Marmara Earthquake caused serious human and economic losses.

2.3.2. Sand Boils

Generally liquefaction occurs along with the development of sand boils. Excess pore pressures induce and pore water dissipates predominantly by the upward flow during and following the earthquake shaking. This flow cause upward-acting forces on

soil particles. In such cases, the water velocity may carry soil particles to the surface. Figure 2.5 explains the sand boil mechanism, schematically.

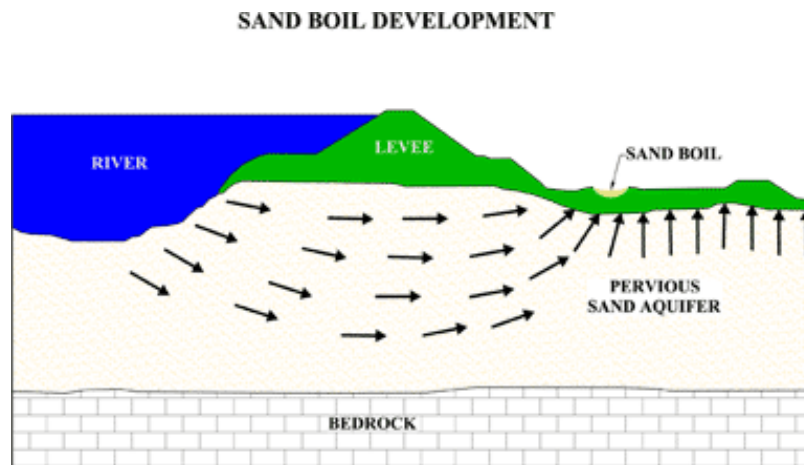


Figure 2.5. Schematic Explanation of Sand Boil Mechanism
(Source: www.sciengineering.com)

If soil conditions are not uniform, escaping pore water flows at high velocity through the localized cracks and channels. Sand particles can be carried with pore water through these channels and cracks up to the ground surface to form sand boils.

Development of sand boils depends on the magnitude of the excess pore water pressure, the thickness, density and depth of the zone of excess pore water pressure and the thickness, permeability and intactness of any soil layers that overlay the zone of high excess pore water pressure (Kramer, 1996).



(a)



(b)

Figure 2.6. (a) Small Sand Boils from the 1979 Imperial Valley Earthquake (Source: www.sciencedirect.com), (b) Large Sand Boil during The Loma Prieta Earthquake, 1989 (Source: www.walrus.wr.usgs.gov)

Many examples of existence can be given for the sand boils. For example, during Imperial Valley Earthquake and Loma Prieta Earthquake, sand boils were observed (Figure 2.6). These phenomena provide evidence of extensive liquefaction at depth. Imperial Valley Earthquake took place on October 15, 1979 with magnitude of 6.4 on the Richter scale and having 7 km local depth. Loma Prieta Earthquake occurred on October 17, 1989. Magnitude of earthquake was 6.9 on the Richter scale and local depth was 18km. The shaking has lasted for 10-15 seconds.

2.3.4. Settlement

During shaking, sand tends to densify. Subsurface densification is observed at the ground surface in the form of ground surface settlement. Such settlement causes distress to structures supported on shallow foundations, damage to utilities that serve pile-supported structures and lifelines that are buried at shallow depths.

Generally settlement of dry sand is completed by the end of the earthquake. The densification of dry sand related to earthquake loading, density of the sand, the amplitudes of shear strain cycles (Silver & Seed, 1971). The settlement could occur, when earthquake induced pore water pressures dissipate.

Dry sand settlement occurs in less time, compared to the settlement of a saturated sand deposit. Occurrence of settlement of saturated sand depends on the permeability and compressibility of the soil and the length of the drainage path. The maximum shear strain and the amount of excess pore water pressure are generated by the earthquake influence by the post shake earthquake densification of saturated sand.



Figure 2.7. Examples of Settlement of Buildings after Marmara Earthquake, 1999
(Source: www.nisee.berkeley.edu.html)

Figure 2.7 (a) illustrates the building, which settled and shifted laterally and opening a gap between the sidewalk. Figure 2.7. (b) displays the staircase that was sheared, due to the settlement. Figure 2.7. (c) presents the building tilted, because of the differential settlement

2.3.5. Instability

Liquefaction induces instabilities. Instability is the one of the most damaging of all earthquake hazards. Flow slides, lateral spreads, retaining wall failures and foundation failures the observed in earthquakes all over the world. Instability failures can occur, when the shear stresses are more than shear strength of liquefied soil. Then the soil deform, until shear stress is not exceeded by the shear strength.

If undisturbed sample is taken from the liquefied soil, the shear strength may be evaluated by the laboratory testing in comparison with some in-situ test parameters and back-calculated strengths, which are taken from some liquefaction case histories.

Flow failures occur when the shear stresses required for static equilibrium are greater than the shear strength of the liquefied soil. This case can appear during an earthquake and/or after an earthquake very quickly. Flow liquefaction produces large soil movements.

Flow failure occurred in some previous earthquakes, causing the collapse of earth dams, slopes and the failure of foundations. San Fernando Valley Earthquake occurred on February 9, 1971. The magnitude of the earthquake was 6.6 on the Richter scale with local depth of 8.4km. The shaking lasted nearly for 60 seconds. Lateral spreading caused by liquefaction, damaged a regional water filtration plant and a local government building. Liquefaction caused a partial collapse of an earthen dam.

San Fernando Dam was constructed with hydraulic filling method in 1912-1915. The older part of the dam consisted of clay core with silty sand outer zones. In hydraulic filling method, mixed soil and water were transported to dam with pipelines and the fill and water deposited on the embankment. This method allowed the water to drain away. In this filling method soil was loose and suitable for liquefaction. Figure 2.8 illustrates the water level close to the maximum level.

Water level
close to the
maximum level



Figure 2.8. Lower San Fernando Dam after San Fernando Earthquake of 1971.
(Source: www.academic.emporia.edu.htm)

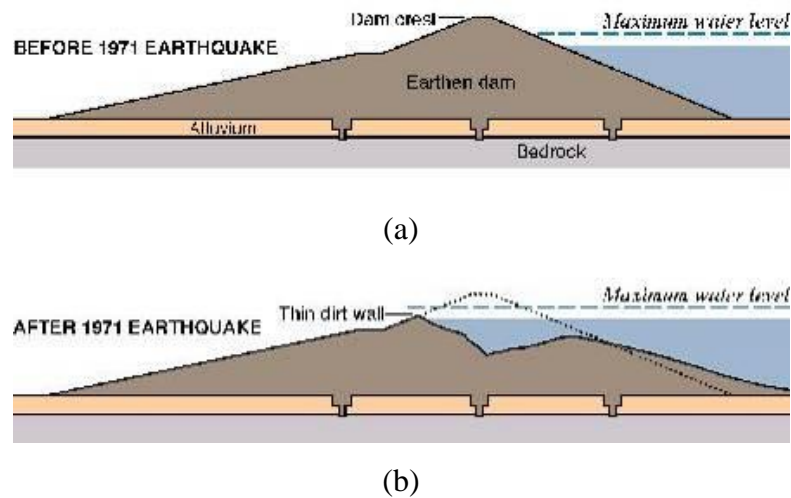


Figure 2.9. (a) Before 1971 San Fernando Earthquake, Image of the Lower San Fernando Dam, (b) After 1971 San Fernando Earthquake, Image of the Lower San Fernando Dam (Source: www.academic.emporia.edu.htm)

Figures 2.9 (a) and (b) illustrate the cross section of the Lower San Fernando Dam, before shaking and after 1971 San Fernando Earthquake.

Deformation failures develop incrementally during the earthquake shaking. Lateral spreading is an example of deformation failure, when shaking is strong and the duration of shaking is long. Deformation failures can produce large displacements and cause significant damage. Lateral spreading often occurs near bridges and the

displacements that are produced by lateral spreading can damage the abutments, foundations and superstructures of bridges.



Figure 2.10. Lateral Spreading Problem After the 1964 Niigata Earthquake
(Source: www.ce.washington.edu)

During the Niigata Earthquake (1964), where foundation of the Showa Bridge moved laterally, and abutment that could not carry the bridge collapsed. Figure 2.10 illustrates the Showa Bridge after the earthquake shaking.

2.3.6 Bearing Capacity

Bearing capacity is the capacity of soil to support the loads applied to the ground. When the soil supporting a building or other structure liquefies and loses strength, large deformations can occur within the soil which may allow the structure and tip. As a result, buried tanks and piles may rise buoyantly through the liquefied soil.



Figure 2.11. Bearing Capacity Problem After 1964 Niigata Earthquake
(Source: www.ce.washington.edu)

Many buildings settled and tipped during the 1964 Niigata earthquake, several buildings tipped as much as 80 degrees (Figure 2.11).

2.4. Factors Known to Influence Liquefaction Potential

Sandy soils and sands are not the only factors controlling liquefaction. Many factors govern soil liquefaction. These factors are soil type, relative density or void ratio, ground water level, earthquake intensity, earthquake duration, historical background, grain size distribution, grain shape, depositional environment, age of deposits, initial confining pressure, drainage conditions and soil profile. In this section, all factors will be studied.

2.4.1. Soil Type

Clean sandy soils with few fines are affected easily by a seismic shaking and liquefaction occurs (Tezcan & Özdemir, 2004). To determine the liquefaction potential of silty soils and also of coarser and gravelly soils and rock fills is controversial and complex process. The cyclic behavior of coarse and gravelly soils is different from the cyclic behavior of sandy soils. Coarse, gravelly soils can generate cyclic pore pressures and liquefaction.

Coarse, gravelly soils are different from, sandy soils in two ways:

1. Sandy soils can be much more pervious than finer sandy soil. Sandy soils can rapidly dissipate cyclically generated pore pressures.

2. Because of the mass of larger particles present in coarse and gravelly soils, gravelly soils are deposited seldomly and gently. Cyclic pore pressure generation and liquefaction may not occur in very loose states, compared to sandy soils (R. B. Seed et al., 2001).

Ishihara defined the liquefaction for cohesionless soils in 1996 as follows:

For loose sand, a state of softening is produced suddenly with complete loss of strength during or immediately after strong pore water pressure response develops. Large deformation may occur.

For medium-dense to dense sand the state of softening, produced with the 100% pore water pressure build-up but the deformation does not grow indefinitely large and complete loss of strength does not take place.

In silty sands or sandy silts, the plasticity of fines has a determining role in liquefaction potential. Silty soils with non-plastic fines are as susceptible to liquefaction as clean sands. Cohesive fines generally increase the cyclic resistance of silty soils.

For clayey cohesive soils, if their plasticity index and liquid limit values are greater than a certain threshold limit and if they are saturated, then they may not lose their (effective) strength. Their undrained (effective) strength is generally higher than static strength under dynamic loading. Under cyclic loading, the behavior of clayey materials is defined by the decline of strength with the number of cycles and with the corresponding accumulated strain. The clayey material is easily liquefiable, if the natural water content is higher than 70% of the liquid limit.

2.4.2. Relative Density

Loose sands can liquefy during some earthquake shaking, but the same sand in a denser condition (Idriss, Seed, & Serff, 1974). If sand is placed without compaction, this soil deposit is likely to be susceptible to liquefy. Table 2.1. illustrates liquefaction potential with respect to relative density of fine sands. The stability of hydraulic fill dams and mine tailing piles pose big risks for seismic hazards because soil particles are settled through water like hydraulic filling and are deposited loosely.

Table 2.1. Liquefaction Potential with Respect to Relative Density of Fine Sands
(Source:Tezcan & Özdemir, 2004)

Maximum Surface Acceleration	Liquefaction Risk			
	Very High	High	Moderate	Low
0.10g	$D_r < 17\%$	$17\% \leq D_r < 33\%$	$33\% \leq D_r < 54\%$	$D_r > 54\%$
0.15g	$D_r < 22\%$	$22\% \leq D_r < 48\%$	$48\% \leq D_r < 73\%$	$D_r > 73\%$
0.20g	$D_r < 28\%$	$28\% \leq D_r < 60\%$	$60\% \leq D_r < 85\%$	$D_r > 85\%$
0.25g	$D_r < 37\%$	$37\% \leq D_r < 70\%$	$70\% \leq D_r < 92\%$	$D_r > 92\%$

2.4.3. Void Ratio

Casagrande (1936) proposed a method to determine the critical void ratio. This method helps to decide if sand in the field would liquefy or not. According to this calculation (Eq 2.1), if the sand deposits have a void ratio smaller than the critical void ratio, then the sand deposits will not liquefy in undrained condition.

$$e_{cr} = e_{min} + (e_{max} - e_{min})e^{(-0.75a_{max}/g)} \quad (2.1)$$

Where; e = void ratio, e_{min} = minimum void ratio, e_{max} = maximum void ratio, a_{max} = maximum acceleration amplitude of the applied ground acceleration, g = acceleration due to gravity

2.4.4. Ground Water Level

Liquefaction phenomenon develops in saturated soils. Groundwater level affects the liquefaction potential of soils. If groundwater depth increases, liquefaction potential decreases. Generally, the effects of liquefaction are observed in areas where groundwater depth is shallow (i.e. within a few meters of the ground surface).

2.4.5. Earthquake Magnitude and Distances

The liquefaction potential during an earthquake depends on the magnitude of the stresses or strains induced by the earthquake, which is related to the intensity of ground shaking (H. B. Seed & Idriss, 1971).

Figure 2.12 displays the relationship between the epicentral distance (R_e) and the moment magnitude (M_w) (Steven Lawrence Kramer, 1996). Ambraseys (1988) collected the data which is related to shallow earthquakes where liquefaction phenomena was not observed at different magnitudes and estimated the limiting epicentral distance (R_e) and fault distance (R_f). Curve was generated according to the post-earthquake field investigations.

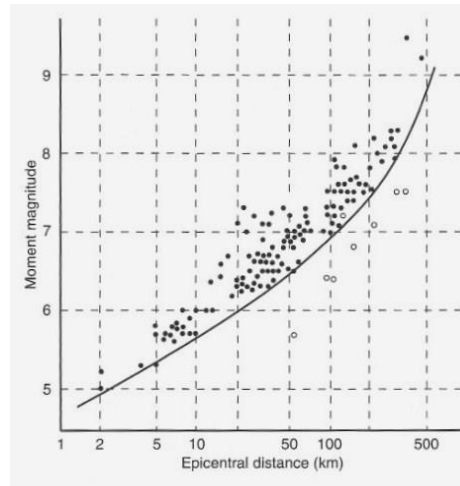


Figure 2.12. Relationship between the Epicentral Distance (R_e) and the Moment Magnitude (Source: Kramer S.L. , 1996)

The expected diffusion area of liquefaction increases dramatically with the increasing magnitude. During deep earthquakes (focal depth $> 50\text{km}$), liquefaction is observed in greater diffusion area.

2.4.6. Earthquake Duration

The duration of the shaking is also a significant factor. The number of significant stress or strain cycles, which are induced the soil, helps to determine the liquefaction potential. Figure 2.13 illustrates the variation between the number of equivalent stress cycles and the earthquake magnitude.

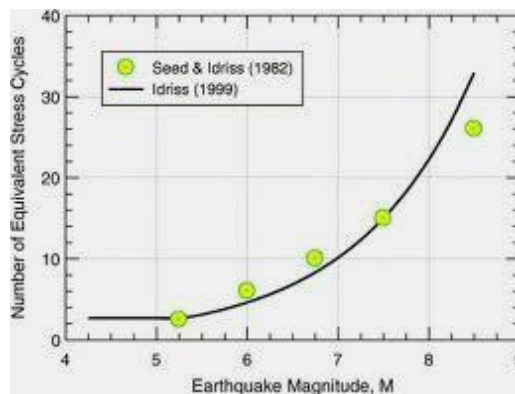


Figure 2.13. Number of Equivalent Stress Cycles versus Earthquake Magnitude (Source: Seed and Idriss 1982, Idriss 1999)

2.4.7. Historical Evidence

Post-earthquake field investigations, where liquefaction often recurs at the same location, give a great deal of information related to liquefaction behavior. Thus, liquefaction phenomena history helps to identify specific sites or more general site conditions. These investigations give information about the possibility of earthquake occurrence and potential of liquefaction.

2.4.8. Grain Size Distribution

Gradation is also a significant factor influencing liquefaction susceptibility. Poorly graded soils are more susceptible to liquefaction than well graded soils. Small particles are placed between large particles in well graded soils. Thus, lower volume change occurs under undrained conditions in well graded soils. Field evidences taken from some post-earthquake field investigations indicates that liquefaction failures occur mostly in uniformly poorly graded soils (Steven Lawrence Kramer, 1996).

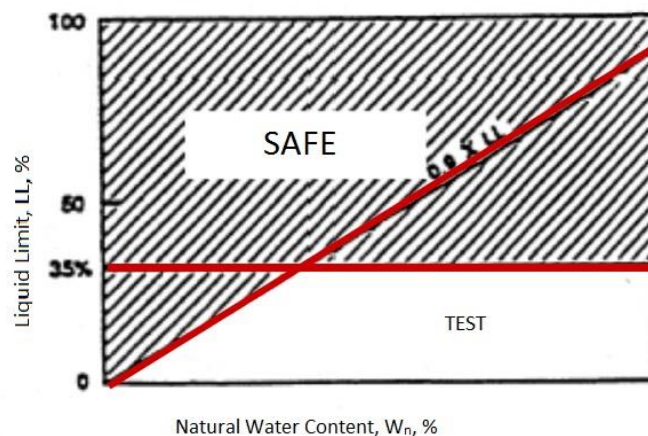


Figure 2.14. The 1st Chinese Criteria

Wang (1979) proposed the 1st Chinese criteria. According to this criteria, fine cohesive soils are potentially liquefiable type and character if

1. they include less than 15% clay fines with weight of grains having sizes smaller than the diameter $0.005\text{mm} \leq 0.15$,
2. liquid limit (LL) is less than or equal to 35%,

3. current in-situ water content greater than or equal to 90% of the liquid limit (Figure 2.14).

Wang (1981) identified three new categories of liquefiable soils. This criterion is called 2nd Chinese criteria. According to this criteria;

1. for saturated sand, at certain levels of earthquake intensity and at low values of effective overburden pressure, if Standard Penetration Test (SPT) blow counts is lower than a critical value.

2. Saturated slightly cohesive silty soils with a water content higher than 90% of its liquid limit and having a liquidity index smaller than 0.75,

3. The unconfined compressive strength is less than 50 kPa, meaning a SPT blow count to be 4 and less than and having a sensitivity in excess of 4.

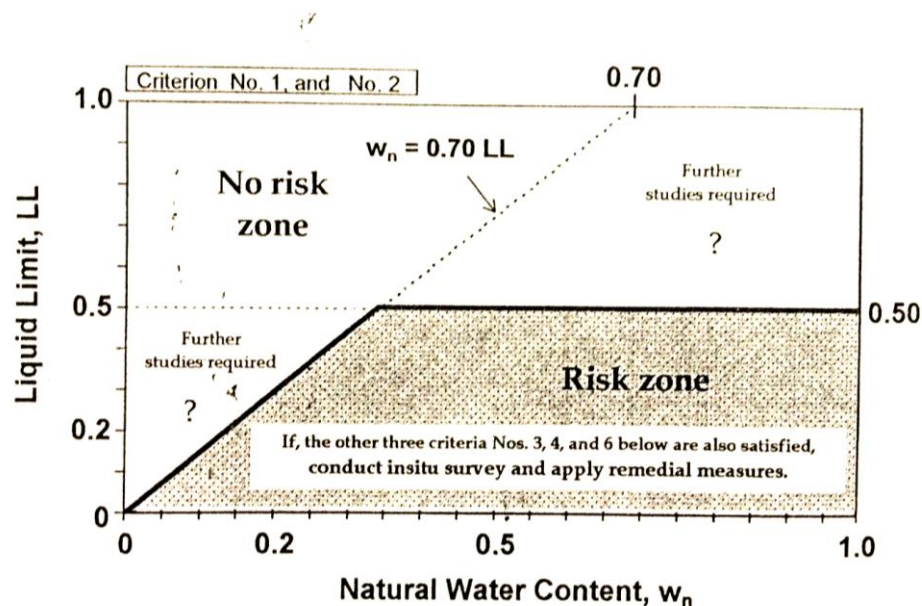


Figure 2.15. The 1st and the 2nd Chinese Criteria (Source: Tezcan & Özdemir, 2004)

Andrews and Martin (2000) developed another criteria called the Chinese criteria or the Modified Chinese Criteria. They recommended that:

1. If a soil has less than 10% clay fines (<0.002mm) and a liquid limit (LL) of the minus #40 sieve is less than 32%, it will be considered potentially liquefiable.

2. Soils having more than 10% clay fines and $LL \geq 32\%$ are unlikely to be liquefaction susceptible.

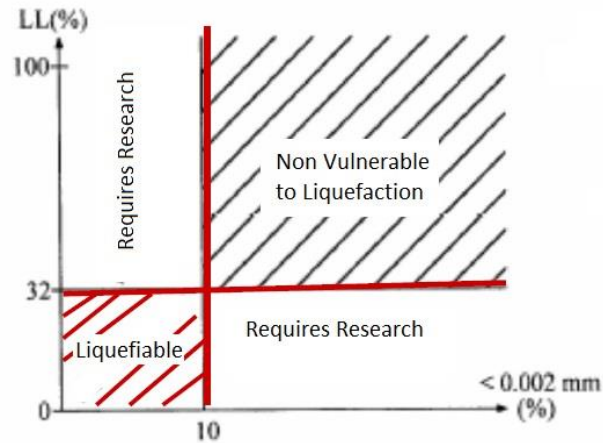


Figure 2.16 Modified Chinese Criteria

2.4.9. Grain Shape

Particle shape can also influence liquefaction susceptibility. Soils with rounded particles are more susceptible to densify than soils with angular grains. Therefore, soils with rounded particle shapes are usually more susceptible to liquefaction than angular-grained soils. Soils with rounded particles mostly occur in the fluvial and alluvial environments, where loosely deposited saturated soils, liquefaction susceptibility is often high in those areas.

2.4.10. Depositional Environment

Soil deposits which are susceptible to liquefaction are formed within a relatively narrow range of geological environments. (T. Youd, 1991). The depositional environment, hydrological environment and age of a soil deposits factors induce to soil deposit's potential (T. L. Youd & Hoose, 1977).

The size, shape and arrangement of grains, hydraulic conductivity and lateral continuity of deposits induce the environment of the deposited soil (Arulmoli, Arulanandan, & Seed, 1985).

Geologic processes which produce high liquefaction potential soil deposits are divided into two groups; 1) uniform grain size distributions and 2) deposit them in loose states. Thus, fluvial deposits and colluvial and aeolian deposits are susceptible to

liquefaction in saturated condition. Liquefaction also is observed in alluvial fan, alluvial plain, brach terrace, playa and estuarine deposits.

2.4.11. Age of Deposits

The age of deposits is another factor to influence liquefaction potential. The age of deposits is related to its density, degree of cementation, ability to transmit, earthquake energy and hydraulic conductivity. New soil deposits are more susceptible to liquefaction than older deposits.

2.4.12. Initial Confining Pressure

The liquefaction potential of a soil deposits reduces when confining pressure increases. The stress required to initiate liquefaction under cyclic load conditions increases with the increase in initial confining pressure. In Niigata earthquake (1964), soil which is less than 2.7 meters fill remained stable. The same soils surrounding the fill liquefied extensively (H. B. Seed & Idriss, 1971).

2.4.13. Drainage Conditions

If the soil is under drained conditions, where pore water dissipates quickly, liquefaction may not be observed, unless;

- 1) Coarse, gravelly soils are surrounded and encapsulated by finer and less pervious materials.
- 2) Drainage is prevented by finer soils which fill-in the void spaces between the coarser particles.
- 3) Depth of the layer or stratum of coarse soil is too large.

In these three cases, the potential of liquefaction in coarse soils increases and risk should be carefully evaluated accordingly (R. B. Seed et al., 2001).

CHAPTER 3

LITERATURE REVIEW FOR MODEL TESTS

3.1. Introduction

Model tests are divided into two groups, one of them is centrifuge test and the other one is shake table test. Centrifuge test performs under higher gravitational acceleration; 1-g model test performs under the gravitational field of the earth. Shake table tests and centrifuge tests are essential to understand the behavior of geotechnical facilities during shaking.

In this chapter, model tests; shake table tests and centrifuge tests will be presented in details. Disadvantages and advantages of shake table tests and centrifuge tests will be presented. Shake table tests which were conducted by many researchers; Pathak (2001), Ueng (2006), Jafarzedeh (2004), Prasad (2004), Yegian (2007), Chau (2007), Thenavanayam (2009), Moss (2010) and Yue (2011) are also illustrated.

3.2. Model Tests

Model tests try to reproduce the boundary conditions for a particular problem and subject to a small-scale physical model of full-scale prototype structure to cyclic mobility. Model tests may be used to assess the performance of a prototype or to examine the effects of different parameters on a general problem. At the same time, model tests are also used to identify the important phenomena and verify predictive theories.

The behavior of soils is sensitive to stress level. Soils may exhibit contractive behavior under high normal stresses. At lower stress levels, soils may exhibit dilative behavior. Model tests have challenges. The most significant one is the problem of testing models, when stress dependency matches that of the full-scale prototype. Matching the stress dependency is very difficult under the gravitational fields of the earth. The other approach is testing under higher gravitational accelerations.

Model tests can be divided into two groups. One of them, performs under the gravitational field of the earth and is called 1-g model test. 1-g model tests are usually performed with shake tables. The other one is the centrifuge test, which performs under higher gravitational acceleration.

1-g model tests and centrifuge tests have drawbacks. The most significant disadvantages are similitude and boundary effects. Similitude cannot be assured for all parameters. The metallic bins or boxes that are constructed for the shaking table and the centrifuge models affect boundary conditions. The sidewalls of the bin or the box can prevent soil movements and reflect energy.

3.2.1. Shake Table Tests

Most physical model testing was being conducted on shaking tables in the early years of geotechnical earthquake engineering. Shaking table research has provided insight to the liquefaction phenomena, post-earthquake settlements, foundation response and lateral earth pressure problems. Shaking tables with a single horizontal translation degree of freedom are used in researches. Shake tables with multiple degrees of freedom have also been constructed. In general, servo-hydraulic actuators control the movement of the shaking tables where dynamic loading capacities are controlled by the capacity of the hydraulic pumps. Large pumps and large actuators are required to produce large displacements of heavy models moving at moderate and high frequencies.

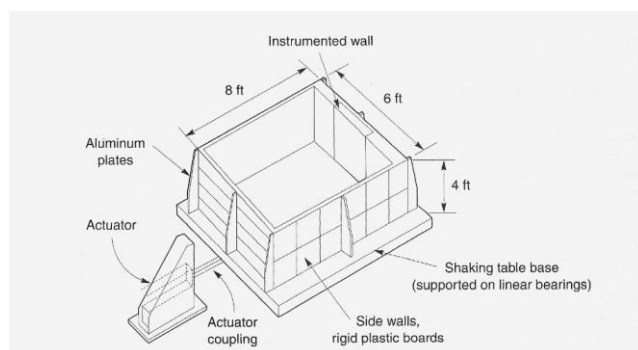


Figure 3.1. Shaking Table with Soil Bin Used for Dynamic Earth Pressure Research
(Source: Sherif et al., 1982)

Some shake tables are small, some shake tables are large with dimensions of several meters. Large metallic boxes can be mounted on large shake tables. Thus, soils can be placed, compacted and instrumented relatively easily inside of large models. The example of shaking table test facility is illustrated in Figure 3.1 (Sherif et al., 1982). Shaking table models can be easily viewed from different perspectives during shaking.

High gravitational stresses cannot be produced in a shaking table test. However contractive behavior related to high normal stresses at significant depths, can be modeled in a shake table test by placing soils very loosely during the model preparation to simulate the contractive behavior. The contribution of factors that produce a cohesive component of strength will be greater in the model than in the prototype at low normal stress levels.

3.2.2. Centrifuge Tests

1/N scale model, which is illustrated in Table 3.1, is used in a centrifuge test. The value, N, refers to the gravitational acceleration used during the centrifuge modeling. Model is located at a distance, r, from the axis of centrifuge and model is rotated at a rotational speed, $\Omega = \sqrt{N/r}$. This rotational speed is enough to raise the acceleration field at the location of the model and rotational speed is equal to N times the acceleration of gravity. The example of a centrifuge test facility is given in Figure 3.2.

Table 3.1. Scaling Factors for Centrifuge Modeling
(Source: Kutter and James, 1989)

Type of Event	Quantity	Model Dimension
		Prototype Dimension
All events	Stress	1
	Strain	1
	Length	1/N
	Mass	1/N ³
	Density	1
	Force	1/N ²
Dynamic events	Gravity	N
	Time	1/N
	Frequency	N
	Acceleration	N
	Strain rate	N
	Time	1/N ²
Diffusion events	Strain rate	N ²

In principle, the stress condition at any point in the model and full-scale prototype should be identical. The overall behavior (displacements and failure mechanism) should also be identical.

Smaller models can be used with the centrifuge tests. The gravitational acceleration at the top of the model is lower than at the bottom of the model, because of the gravitational field increasing with the radial distance. The gravitational field moves in the radial direction. The horizontal plane decreases, when the centrifuge radius increases.

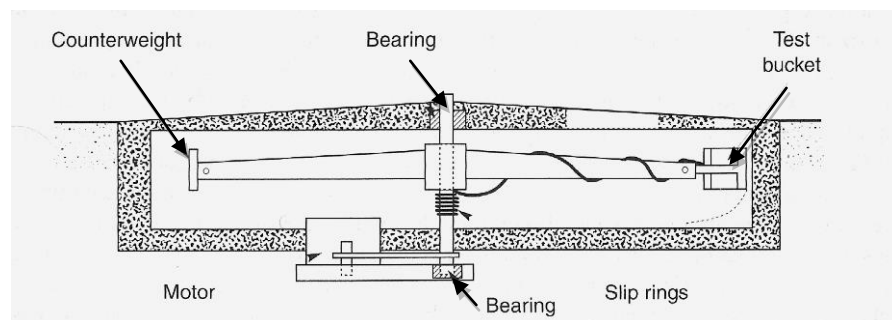


Figure 3.2. Cross Section Through a Geotechnical Centrifuge
(Source: O'Reilly, 1991)

While planning the centrifuge tests, similitude consideration is very important. High speed transducers and data acquisition systems are required to obtain accurate and useful results from the centrifuge tests, but scaling laws do not permit. Miniaturized transducers and cables are required to minimize their influence on the response of the model.

3.2.3. Literature Review of Shake Table Tests

Literature review of some model tests with laminar box, which are conducted by many researchers Pathak (2001), Ueng (2006), Jafarzedeh (2004), Prasad (2004), Yegian (2007), Chau (2007), Thenavanayam (2009), Moss (2010) and Yue (2011) are also explained in the summary (Table 3.2).

Table 3.2. Internal Dimensions and Laminates Number of Laminar Boxes

	Internal Box Dimensions			Laminates Number
	Length(m)	Width(m)	Height(m)	-
College of Engineering,Pune (S.R. Pathak,2001)	0.4	0.4	0.4	N/A
NCREE at Taiwan (Tzou-Shin Ueng et al. ,2006)	1.88	1.88	1.48	15
Sharif University of Technology,SUT(F. Jafarzadeh,2004)	1	1	1	24
University of Tokyo (S.K. Prasad et al.,2004)	0.5	1	1	11
Northeastern University, Boston(M.K. Yegian et al.2007)	0.33	0.22	0.46	N/A
The Hong Kong Polytechnic University(K.T. Chau et al. 2007)	1.4	0.9	1.7	32
NEES at Buffalo, (Thenavanayam et al. ,2009)	5	2.75	6.2	24
California Polytechnic State University(Robb Eric S. Moss,2010)	φ2.27	-	-	16
Shangdong Jianzhu University,China(Qingxia Yue,2011)	3	1.8	1.87	16
Izmir Institute of Technology (IYTE,2011)	1.8	0.65	1.4	24

Some conducted model tests with boxes used in research will be presented briefly and a table, which displays the dimensions of and the most of laminate boxes, will be provided.

3.2.3.1. Shake Table Tests Conducted by S. R. Pathak et al. (2001)

The research conducted by S.R. Pathak et al. (2001) dealt with conducting shake table tests in the laboratory by simulating earthquake conditions on site and comparing the trial tests results, which were conducted for such soil by other researchers. Total of 12 shake table tests were conducted on sand with relative densities of 62%, 67%, 69%, 70%, 72% and 74% at frequencies of 2Hz and 3 Hz.

Square, rigid model box with 40cm x 40cm x 40cm dimension was mounted on the shake table. Potentiometer was connected to the shake table and data, which was taken from the potentiometer were recorded by the data acquisition system. The standpipe was used to measure the pore water pressure. Shakings were continued until pore pressure decreased or stayed a constant value. This phenomenon indicates the initiation of liquefaction.

The results have shown that pore pressure increased with time initially after attaining a peak value, pore pressure decreased or remained constant. Another finding was that time required to reach peak value decreased, when frequency increased. Criterion of the occurrence of liquefaction in the laboratory model and in the field (i.e. the actual field data) was found to be nearly the same.

3.2.3.2. Shake Table Tests Conducted by Tzou-Shin Ueng et al. (2006)

Research was conducted by Ueng et al. (2006) in order to study the behavior of saturated sand, liquefaction occurrence and soil-structure interactions under two-dimensional earthquake shaking. The laminar box, which was constructed for this research was composed of 15 layers. The specimen size 1880mm x 1880mm with 1520mm height. 1-D and 2-D shakings were conducted at different maximum accelerations. Duration of shaking was 10 seconds.

Displacement transducers, accelerometers and velocity transducers were placed on the frames of the laminar box. Miniature piezometers and small-sized piezoresistive accelerometers were placed inside the soil. As a result, more databases for theoretical and numerical analyses of ground responses, liquefaction and soil-structure interaction under earthquake shakings were obtained.

3.2.3.3. Shake Table Tests Conducted by S.K Prasad et al. (2004)

S. K. Prasad et al. (2004) showed that the manual shake table was an alternative method instead of more sophisticated shake table. The external dimension of the laminar box, which mounted on a manual shake table was 1260mm x 560mm. The internal dimension was 1000mm x 500mm with 1000mm height. 2mm thick rubber membrane was used in this laminar box. According to the performance tests results, the membrane did not influence the performance of soil mass. Beside membrane effect, inertia effect, friction effect and wall effect were controlled. All controls showed that tests to understand ground amplification, liquefaction and cyclic mobility phenomena, excess pore water pressure generation and dissipation rates could be conducted with this manual shake table and laminar box.

3.2.3.4. Shake Table Tests Conducted by Thenavanayam et al. (2009)

Shake table tests were conducted to study liquefaction and lateral spreading phenomena. The internal dimensions of the laminar box, which was used in this

research, were 5m x 2.75m with the maximum height of 6.2m. It was composed of 24 laminates.

The first test involved a level ground. The degree of the slope was changed at other tests in order to study liquefaction and to induce lateral spreading of soils during shaking. Accelerometers, pore pressure transducers, potentiometers were used for the instrumentation. During and after the shaking table tests, results were obtained as follows:

- 1) The laminar box system was working well.
- 2) Significant horizontal displacements were observed, when the sloping ground tests were conducted.
- 3) The instrumentation of data was verified by cross-comparison between different types of sensors.

CHAPTER 4

ONE-DIMENSIONAL LAMINAR BOX SYSTEM

4.1. Introduction

In order to understand the performance of the laminar box system and liquefaction of sands, silty sands with different fines content, 1g shake table tests were conducted in this study. The shake table and actuator system were available at the structural laboratory of the Izmir Institute of Technology (IZTECH). 1-D laminar box system and CPTu system were designed to complete the laminar box system. One-dimensional laminar box system is consisted of;

- Strong floor,
- 1-D shake table,
- A hydraulic actuator,
- Computer controlled system (to give shaking to the 1-D shake table),
- A longitudinal laminar box,
- Membrane,
- Hydraulic filling system,
- Instrumentation,
- Data acquisition system,

Strong floor, 1g shake table, design of 1-D laminar box system and its components, design of CPTu system, instrumentation, data acquisition system, preparation of the boxes will be presented. CPTu system was needed to conduct CPTu tests before and after the shaking. Preparations of the boxes were conducted by the hydraulic filling method. The dimensions of these soil preparation boxes are also presented in this section. 1-D laminar box with its components and CPTu system are illustrated in Figures 4.16 to 4.20.

4.2. Strong Floor

The IZTECH – Civil Engineering Department’s structural laboratory was built in 2007 and it is well-equipped for the static and dynamic structural tests. The depth of the strong floor is 1m with heavily reinforced (C25) concrete and reinforced steel (S420). Structural laboratory have a total area of 391m² and housed 51m² strong floors with 4m high reaction frame. The strong floor has extremely high load capacity.

Shake table tests were performed under the gravitational field of the earth. To avoid the effect of the shaking, which was under the gravitational field of the earth, shake table was mounted on the strong floor with giant screws.

4.3. 1-D Shake Table

The aluminum shake table had a length of 2.04m and a width of 0.82m. The thickness of the shake table was 0.008m. Allowable load of the shake table was 3 tons and allowable displacement of the shake table was ± 100 cm, the maximum velocity of the shake table was ± 100 cm/sec and the acceleration capability of the shake table was $\pm 1.2g$. Figure 4.4 displays the base shaking unit with the bottom laminate attached to it.

4.4. Crane

Crane is commonly used for moving heavy materials inside the laboratory. The capacity of the crane was 3 tons. Vertical velocity of the crane was 8.13cm/sec, and the distance between the bottom point of the crane and the strong floor was 4.5m. In this study, the crane was used to carry soil bags, laminates and CPTu system.

4.5. One-Dimensional Laminar Box

To simulate the shear beam conditions that exist during the shaking in free-field, must be satisfied the criteria specified by (Whitman & Lambe, 1986). When designing the laminar box the following factors should be and were taken into consideration.

1. Laminar box with less mass was preferred. Therefore, aluminum was used to reduce the weight of the laminates.
2. Laminar box should have perfectly flexible shear beam at the same time.
3. Laminar box should be perfectly rigid in any horizontal plane. Consequently, laminar box composed of laminates and rollers were placed between two laminates.

Friction between the soil and laminates should be provided. Enough vertical strength in the confining walls supplied the necessary complementary shear stresses.

Laminar box composed of 24 laminates to simulate the earthquake as in the field. Each laminate was 57mm in height and 108mm in width. This feature increased the flexibility of the soil model, which was placed inside the laminar box. Each laminate composed of four pieces of aluminum I-beams. Laminar box size was restricted by the size of the shake table, which was available at IZTECH. Each laminate had a length of 1834mm and had a width of 620mm. Each laminate was composed of;

- Two short edge I-beams
- Two long edge I-beams
- Plate on reinforced welding
- Angle brackets
- Rollers (except top laminate)
- Box stoppers (except top laminate)
- Rubber stoppers (except top laminate).

4.5.1. I-Beam

At the long edge of each laminate, the inner side of I-beam was 1617mm, and the outer side was 1834mm. At the short edge, the inner side of I-beam was 383mm and outer side was 620mm. The inner and outer dimensions of I-beam of laminate are illustrated in Figure 4.1.



Figure 4.1. I-beam

4.5.2. Plate on Reinforced Welding and Angle Brackets

To increase the carrying capacity of welding, plate on reinforced welding and angle brackets were installed on welding. Plates on reinforced welding were inserted on welding at each corner with four $\phi 9$ screws. Dimensions of the plate on reinforced welding were marked in Figure A.8.

50mm x 50mm x 5mm L-profile was used as angle brackets to reinforce the welding at each corner of laminates. The height of the angle brackets, which was at the same height as I-beams was 57mm. Each angle bracket was tied to each corner of the laminate with 4 $\phi 6$ screws (Figure 4.2).

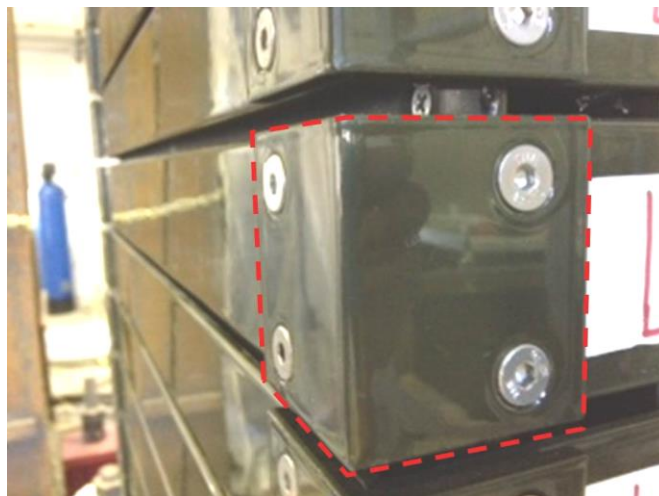


Figure 4.2. Angle Brackets

Plates on reinforced welding and angle brackets were made of aluminum to reduce the weight of the laminar box. The weight of each plate on the reinforced welding was 0.46kg, and the weight of each angle bracket was 0.07kg. Four angle brackets and four plates to reinforce welding were inserted on each laminate. Totally 96 angle brackets and 96 plates were used to reinforce the welding.

4.5.3. Roller Mechanism between Laminates

One of the most essential components of the laminates was roller mechanism. To simulate the shaking as in the free-field, roller mechanisms were placed between the two laminates. Roller mechanism was composed of one roller, one wheel shaft, one plate under roller and two plates near roller.

Laminates slide on each other using low friction high load capacity rollers. Eight roller mechanisms were placed symmetrically inside the top channel of the I-beam at the long side of each laminate (except top laminate). Four roller mechanisms were mounted on the long side, the other four roller mechanisms were mounted on the other long side of the laminate. Totally 184 roller mechanisms were used for the one-dimensional laminar box. The height between the top point and the bottom point of the plate near roller was 42mm, and the length of the plate was 150mm. The plate, which was used under roller, had a length of 150mm, had a width of 85mm and had a thickness of 8mm. The plate under roller and two plates near roller were made of steel and welded to each other. Consequently, a house for the roller was prepared. To place the wheel shaft and the roller, $\phi 18.5$ holes were drilled on the plates near the rollers. Locations of the holes and the diameters of the rollers were adjusted for vertical gap between the laminates. The vertical gap (5mm) was intended to prevent any contact interference between any adjacent laminates during horizontal sliding of the laminates. Figure 4.3 illustrates the all roller mechanism (roller, plates near roller, plate under roller and wheel shaft).

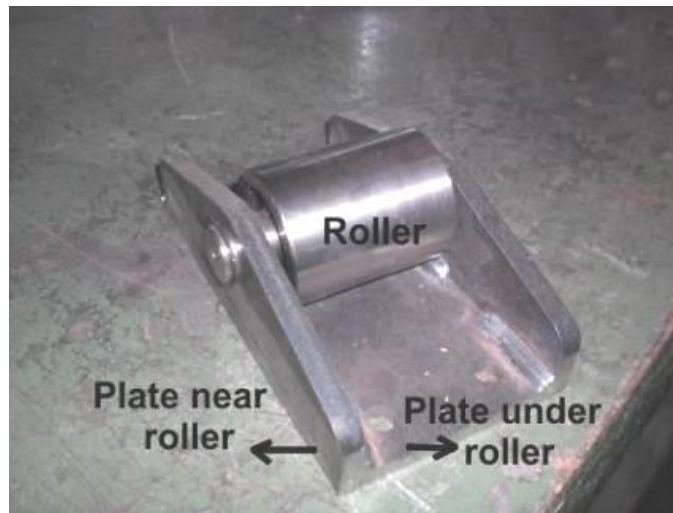


Figure 4.3. Roller Mechanism

The weight of each laminate between the top and the bottom laminate with its components (I-beams, box stoppers, rubber stoppers, roller mechanisms, angle brackets and plates on reinforced welding) was about 34.39kg. The weight of the bottom laminate was 34.37kg, and the weight of the top laminate was 13.23kg. Since roller mechanisms, box stoppers and rubber stoppers were not placed inside the top channel of the I-beams, the top laminate was lighter than the bottom laminate.

4.5.4. Box Stoppers and Rubber Stoppers

In order to limit the horizontal displacement of each laminate, the 50mm x 606mm stoppers were inserted to the two short side of the laminate. Therefore, each laminate was allowed to slide horizontally by a maximum distance of 14mm in the longitudinal direction. The maximum cumulative displacement at the top of the laminar box was 0.32m.

The 50mm x 180mm box stoppers were inserted inside the top channel of the long side to prevent the lateral movement and the rotation. To prevent noise and to reduce damages on the box stoppers during the shaking, 10mm thick rubber stoppers were attached to the back and front of the box stoppers. All components of the bottom laminate, connections of the shake table and the bottom laminate are displayed in Figure 4.4.

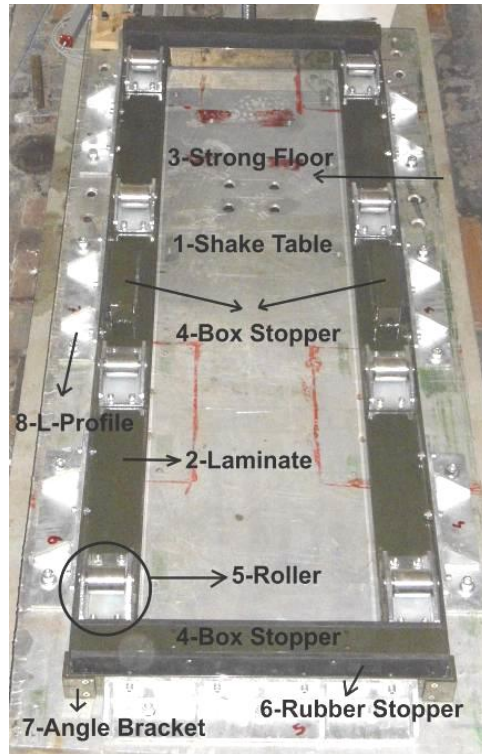


Figure 4.4. Components of Bottom Laminate, Connection of Shake Table and Bottom Laminate (1- Shake Table, 2-Laminate, 3- Strong Floor, 4- Box Stopper, 5- Roller, 6- Rubber Stopper, 7- Angle Bracket, 8- L-Profile)

24 laminates constituted the Iztech's 1-D laminar box. This laminar box was supported on the 1-D shake table. The input motions were applied through high speed actuator.

4.6. Membrane

Membrane was necessary to hold the soil, to avoid water spillage out of the laminar box. Membrane had to be watertight, thin and elastic enough. Membrane should also not to prevent the motion of the laminar box and the performance of the soil model. The study conducted by Prasad et al. (2001) showed that 2mm thick rubber membrane, which was placed inside the 0.5m x 1m x 1m laminar box, did not influence the performance of the soil mass used. Similarly, in the present study 1mm rubber membrane was used inside the laminar box to provide air tightness and water tightness, because shake table tests were conducted under undrained conditions and the membrane did not allow the soil mass to come in direct contact with walls or bearings. The length

of the rubber membrane was 1800mm and width of the rubber membrane was 800 mm. A rubber membrane, which was a little bigger than the laminar box, was used so that the laminar box can process efficiently.

Rubber membrane, which was placed inside the laminar box during the shake table tests, is an EPDM liner. EPDM membrane, which is a refinery product, is a synthetic rubber made of ethylene and propylene materials. Physical properties of the natural rubber (high elasticity, thermal expansion, tensile strength, resistance to cold) cannot be changed in practice. The pre-assembled EPDM membrane stripes are adhered to each other by thermal heat machines and thus a perfect seal is provided. Sidebands which are used for the adhesion of the EPDM membrane stripes to each other ensure the protection of properties at the bonding points, as well as the properties of the material.

Rubber membrane and laminates were carefully placed not to damage the membrane. After the first laminate was mounted on the shake table, the membrane was placed first. Up to the 6th laminate, laminates were moved one by one. The other laminates were placed with the help of the crane. The placement of the membrane is illustrated in Figure 4.5.



Figure 4.5. Placement of the Rubber Membrane

Once the 1-D laminar box was placed entirely, for controlling of the water tightness of the membrane, laminar box was filled with water up to the top. During the shake table tests, top of the membrane should be open for viewing of soil in the laminar box and measuring the settlement.

4.7. Instrumentation

Shake table tests that were conducted in this project, required high density sensor arrays, consisting of accelerometers, pore water pressure transducers and potentiometers. Accelerometers were divided into two groups: 1) submersible accelerometers and 2) traditional accelerometers. Submersible accelerometers were placed inside the soil model, while traditional accelerometers were placed on the laminates and the shake table. Pore water pressure transducers were also placed inside the soil model. Potentiometers were divided into two groups; 1) X-Potentiometers and 2) Z-potentiometers. X-Potentiometers measured the displacement of the laminates, while Z-Potentiometers were placed vertically on the soil model to measure the settlement of the ground.

In the first shake table test, which was conducted with clean sand, three submersible accelerometers and five pore water pressure transducers were placed inside the soil model. Seven X-Potentiometers and five traditional accelerometers were stuck on the laminates. Two Z-Potentiometers measured the settlement of the soil model. One traditional accelerometer was placed on the shake table to measure the acceleration history of the shake table during the shaking. This accelerometer was called bottom accelerometer on the instrumentation plans.

In the second shake table test, which was conducted with 15% fines content, six submersible accelerometers and four pore water pressure transducers were placed inside the soil model. Seven X-Potentiometers measured the displacement of the laminates and eight traditional accelerometers measured the accelerations of the laminates. To measure the settlement of the soil model, two Z-Potentiometers were used. Two bottom accelerometers were placed on the shake table.

In the third shake table test, which was conducted with less than 25% fines content, eight submersible accelerometers and five pore water pressure transducers were placed inside the soil model. Seven X-Potentiometers were attached on the laminates. Two Z-Potentiometers measured the settlement of the soil model. Two traditional accelerometers were placed on the shake table. Instrumentation plan of the shake table tests are illustrated in Chapter 7 (Section 7.3.1.3, Section 7.3.2.3. and Section 7.3.3.2.).

4.7.1. Submersible Accelerometer

Submersible accelerometers (SA), which were manufactured at the Iztech Lab, measured motion of the soil at several different places inside the soil model. Table 4.1 illustrates the properties of the submersible accelerometers. Each submersible accelerometer was coated with silicon to protect the instrumentation from the water causing disturbance effect and hence they were tied on the nets. Half of the submersible accelerometers were placed on one net, while the other submersible accelerometers were placed on the second net to prevent the rotation, due to the weight of the accelerometers. These nets were tied tightly and vertically between the steel plate placed at the bottom of the laminar box and the wood placed on the laminar box, before the filling process started. At the end of the filling process, nets were released on the soil model not to affect the measurement of the submersible accelerometers. Submersible accelerometers on the nets are illustrated in Figure 4.6.



Figure 4.6. Submersible Accelerometer Used in the Shaking Table Test

Submersible accelerometers provide measurements in the x, y and z directions. But in this research only one direction was used to take data from the accelerometers, because of the longitudinal movement of the 1-D laminar box was in the x-direction.

Table 4.1. Properties of Submersible Accelerometer

Natural Frequency	5500 Hz
Linearity Distortion	0.20%
Interaction Between Axis	1%
Time For Activation	1ms
Temperature Range	-40°C – 85°C
Measuring Tape	1600 Hz
Density of Noise	250 $\mu\text{g}/\text{Hz}^{0.5\text{rms}}$
Voltage	5V
Current	1mA
Output Voltage	0.2V-2.8V

In the first shake table test, which was conducted with clean sand, three submersible accelerometers were placed inside the laminar box. In the second shake table test, which were conducted with 15% fines content and the third shake table test, which were conducted with less than 25% fines content, six and eight submersible accelerometers were used, respectively.

4.7.2. Traditional Accelerometers

Traditional accelerometers were attached on the laminates and the shake table. Four traditional accelerometers measured the accelerations in the x, y and z directions, though only one direction is connected to the data acquisition system to measure the acceleration (in the x-direction only) because the movement of the laminar box was one-dimensional.

Traditional accelerometers were placed at the same laminate with potentiometers, to compare the acceleration data recorded by the accelerometer and for the derivative of the potentiometer data. Bottom accelerometers were placed on the shake table to reach the input motion of the shake table in acceleration versus time.

In the first shake table test, 5 traditional accelerometers were attached on the laminates, while only 1 traditional accelerometer was placed on the shake table. In the second shake table test, 8 traditional accelerometers were placed on the laminates lying

on the shake table. In the third shake table test, traditional accelerometers were not attached on the laminates. In the second and third shake table tests, 2 traditional accelerometers were attached (Figure 4.7).

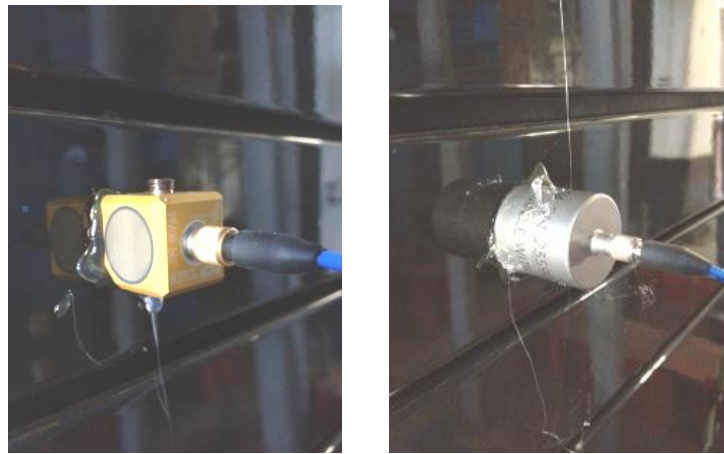


Figure 4.7. Traditional Accelerometer Used in the Shaking Table Tests

4.7.3. Pore Pressure Transducers

The most important instrumentation was related to installation of the pore water pressure transducers to understand the liquefaction phenomena and initiation time of the liquefaction. Pore water pressure transducers were also placed inside the soil model to monitor the data of pore water pressure variation. These data indicated soil liquefaction has occurred.

The type of the pore water pressure transducers are KPC-500KPA and the capacity is 500KPa. They were taken from Tokyo Sokki Kenkyujo Co. Ltd. Connection cable of the pore water pressure transducer is 0.5mm² and its length is 10m. Properties of the pore water pressure transducers are presented in Table 4.2. Before the pore water pressures transducers were placed inside the laminar box, filters (Figure 4.8a), which were kept waiting in water were placed into the pore pressure transducers (Figure 4.8b). Then pore water pressure transducers were tied on nets (Figure 4.8c). Three pore water pressure transducers were placed on one net, and two pore water pressure transducers were placed on the second net (Figure 4.9). These nets were tied vertically between steel plate which was placed at the bottom of the laminar box and wood, which was

placed on the laminar box, before the hydraulic filling process started. 10cm distance was available between the two nets (Figure 4.10).



(a) (b) (c)
Figure 4.8. (a) Filter of the Pore Pressure Transducer, (b) Filter was Placed inside the Pore Pressure Transducer, (c) Pore Pressure Transducer Used in the Shaking Table Tests



Figure 4.9. Submersible Accelerometers and Pore Water Pressure Transducers Tied on Nets

The feature of pore water pressure transducers resisting to high lateral pressure is because of these had dual structures. Therefore, they measure pore pressure changes accurately, even if soil pressure change markedly. Pore water pressure transducers are covered with stainless steel, this feature provides excellent corrosion resistance and they are small to be and handled easily. These pore water pressure transducers can be attached to a pile, a diaphragm wall, a sheet pile, etc. and buried in ground to measure pore water pressure. Pore water pressure transducers can be also buried singly in the soil

to measure pore water pressure. In this research, pore water pressure transducers were tied on the nets and were placed inside the soil model.



(a)

(b)

Figure 4.10. (a) Pore Water Pressure Transducers and Submersible Accelerometers Tied on Nets and Nets are Placed in the Laminar Box, (b) Nets Tied on the Wood to be Tight

Table 4.2. Properties of the Pore Water Pressure Transducers

Type	KPC-500
Capacity	500 KPa
Rated Output	Approximately 1mV/V (2000×10^{-6} strain)
Non Linearity	1% RO
Filter Mesh	40 mm
Temperature Range	0~ +60 ⁰ C (no icing)
Input/Output Resistance	350Ω
Recommended Exciting Voltage	Less than 3V
Allowable Exciting Voltage	10V
Weight	250gr
Cable Length	10m

4.7.4. Potentiometers

X-Potentiometers were used to monitor horizontal displacement of the laminates during the shaking (Figure 4.11a). Z-Potentiometers were placed on the soil surface to measure the settlement of the soil.

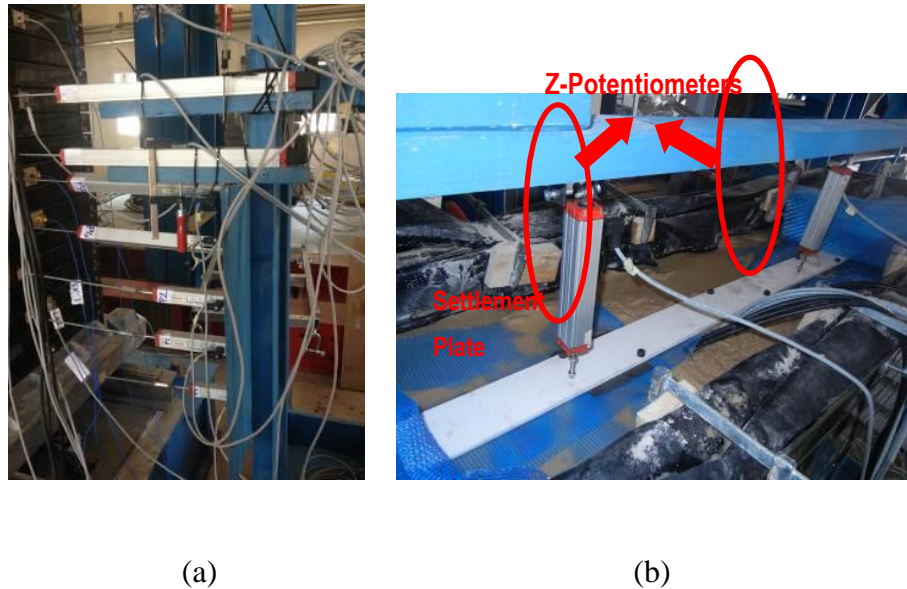


Figure 4.11 : (a) X-Potentiometers Measure the Displacement of Laminates, (b) Z-Potentiometers Measure Settlement

In the first shake table test, seven X-Potentiometers were attached to the laminates. In the second and third shake table tests, six X-Potentiometers were attached to the laminates, 1 X-Potentiometer was used to measure the displacement of the shake table. This potentiometer was important to compare the input motion and displacement of the shake table during the shaking and arranged the offset time of the filtered data. Totally, two LPM 400 potentiometers, four LPM 300 potentiometers and three LPM 100 potentiometers were used in this research. (http://www.opkon.com.tr/UPLOAD/LPM_070308%20TR.pdf)

Up to the thirteenth laminate, X-Potentiometers were attached to the laminates (Figure 4.11b). The last laminate was the thirteenth; because the largest potentiometer (LPM 400) measures up to a maximum of 40cm displacement. Measurable maximum displacement is 20cm in two directions. The maximum displacement is 17.8cm for the 13th laminate. LPM 300 potentiometer measures maximum of 30cm in one direction, and 15cm in both directions. LPM 100 potentiometer measures 10cm in one direction.

Two Z-Potentiometers were placed on the soil model to measure the settlement (Figure 4.11c). To get more accurate results, the piece of smooth mechanism was placed on the soil model. In this study, this smooth mechanism is named settlement plate (Figure 4.11c). Liquefied soil has a density which is less than the density of soil ($\sim 1.95\text{g/cm}^3$), but higher than the density of the water (1g/cm^3). The density of the liquefied soil varies during the test, as the degree of liquefaction changes. In order not to float or sink during the shaking, settlement plate's density must be less than the density of the liquefied soil. ($\sim 1.5\text{gr/cm}^3$).

Instrumentation plan of Test 1, which was conducted with sand, is displayed in Figure 7.9. Instrumentation plan of Test 2, which was conducted with less than 15% fines content, was illustrated in Figure 7.23. Instrumentation plan of Test 3 conducted with less than 25% fines content was shown in Figure 7.33.

4.8. Data Acquisition System

Potentiometers, submersible accelerometers and traditional accelerometers are connected to National Instruments' (NI) SCB-68 connector block for the data acquisition devices (Figure 4.12). The NI SCB-68 is a shielded I/O connector block for interfacing I/O signals to plug-in data acquisition (DAQ) devices with 68-pin connectors. Combined with the shielded cables, the NI SCB-68 provides rugged, very low-noise signal termination service (www.sine.ni.com).

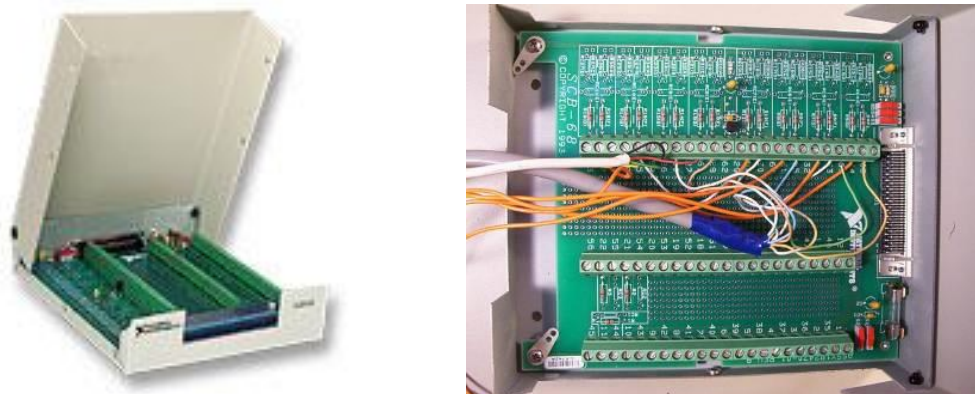


Figure 4.12. NI SCB-68 Connector Block for Data Acquisition Devices
(Source: www.sine.ni.com)

Pore water pressure transducers are connected to NI SCXI-1520 strain gage input module. The NI SCXI-1520 (Figure 4.13) is an 8-channel universal strain gage input module that provides all of the needed features for simple or advanced strain measurements. This single module can read signals from strain, force, torque, and pressure sensors.



Figure 4.13. NI SCXI-1520 Strain Gage Input Module

In the first shake table test, 5 traditional accelerometers connected to NI SCXI-1531 accelerometer input module. The NI SCXI-1531 is a signal conditioning module for serving Integrated Electronic Piezoelectric (IEPE)-compatible accelerometers and microphones (Figure 4.14).



Figure 4.14. NI SCXI-1531 Accelerometer Input Module
(Source : www.sine.ni.com)

Three NI SCB-68 modules, one NI SCXI-1520 module and another NI SCXI-1531 module are connected to the NI PXI-6143 data acquisition unit. All data were collected by the NI PXI-6143 simultaneous sampling multifunction data acquisition unit. Which has 250 ks/s per-channel sampling rates, two 24-bit counter/timers, and eight digital I/O lines The NI PXI-6143 unit was used to collect high-speed, continuous data.

Data acquisition assistant helped to navigate tasks and generated necessary code automatically for instant LabView. All of the devices used can be tested for functionality with the Measurement & Automation Explorer configuration utility. This test informs whether instruments work properly or not.

Using the data acquisition measurements ready for virtual channels, voltage data can be converted into the proper engineering units with chosen list of common sensors and signals by creating own custom scale.

VI Logger Lite is configuration-based software designed specifically for data logging. Features include easy logging and viewing of data, data extraction to Microsoft Excel and code generation in LabVIEW made.

Table 4.3: Connection of Accelerometers and Potentiometers to Module

Name	Box Name	Dimension	Cables							Note
			Green	White	Pink	Brown	Yellow	Ground		
P1	Box 3	100	AI 0	AI 8	-	5 Volt	Connect to screw	Connect to screw	Connect AI 8 to Ground	
P2	Box 3	100	AI 1	AI 9	-	5 Volt	Connect to screw	Connect to screw	Connect AI 9 to Ground	
P3	Box 3	100	AI 2	AI 10	-	5 Volt	Connect to screw	Connect to screw	Connect AI 10 to Ground	
P4	Box 3		AI 3	-	AI 11	5 Volt	Connect to screw	Connect to screw	Connect AI 11 to Ground	
P5	Box 3		AI 4	AI 12	-	5 Volt	Connect to screw	Connect to screw	Connect AI 12 to Ground	
P6	Box 3		AI 5	-	AI 13	5 Volt	Connect to screw	Connect to screw	Connect AI 13 to Ground	
P7	Box 3		AI 6	AI 14	-	5 Volt	Connect to screw	Connect to screw	Connect AI 14 to Ground	
P8	Box 3	300	AI 7	-	AI 15	5 Volt	Connect to screw	Connect to screw	Connect AI 15 to Ground	
P9	Box 1	300	AI 0	-	AI 8	5 Volt	Connect to screw	Connect to screw	Connect AI 8 to Ground	

Name	Box Name	Channel Name	Cable Colour	Bias	Sensitivity	Y-intercept	Slope
SA1	Box 2	AI 1	Purple	1612	190	-8.484	5.263
SA2	Box 2	AI 2	Yellow	1621.6	191.7	-8.459	5.216
SA3	Box 2	AI 3	Blue	1624	192	-8.458	5.208
SA4	Box 2	AI 4	Grey	1618.9	188.7	-8.579	5.299
SA5	Box 2	AI 5	Brown	1630	187	-8.717	5.348
SA6	Box 2	AI 6	Pink	1615	188	-8.590	5.319
SA7	Box 2	AI 7	Green	1625	187	-8.690	5.348
SA8	Box 2	AI 8	White	1239	141	-8.787	7.092

Name	Box Name	Cables							Bias	Sensitivity	Y-intercept	Slope	Note
		Yellow	Green	Black	Red	Pink	Brown	White					
L-A2	Box 1	AI 1		Ground	5 Volt	-	-	-	1636	191.94	-8.523	5.210	Connect AI 9 to Ground
L-A5	Box 1	AI 2		-	-	-	5 Volt	Ground	1616.78	188.47	-8.578	5.306	-
L-A6	Box 1	AI 4		-	-	-	5 Volt	Ground	1624.43	188.28	-8.628	5.311	-
B-A1	Box 1		AI 3				5 Volt	Ground	1525.65	106.85	-14.278	9.359	Connect AI 11 to Ground
B-A2	Box 1		AI 5				Ground	5 Volt					

All National Instruments data acquisition system functions create the waveform data type, which carries acquired data and time information directly into more than 400 LabVIEW built-in analysis routines for display of results in engineering units on a graph. (Source: www.sine.ni.com)

In SCB-68 modules, several channel numbers which are numbered as AI 0, AI 1, AI 2, etc. were placed. Table 4.3 indicates the connection between the instrumentation cable and module's channel. Calibration of the accelerometers, sensitivity and Y-intercept were given to the programme. These properties of the accelerometers are also shown in Table 4.3.

Both data acquisition systems were synchronized to a common clock. This synchronization allowed to compare the data that was taken from instrumentations at the same time.

4.9. Sample Preparation Box

Totally three sample preparation boxes were used during filling process (Figure 4.15). The dimension of the all sample preparation boxes were the same. The length of the boxes was 1260mm, the width of the boxes was 650mm, and their height was 510mm. The volume of the each box was 417.69lt.



Figure 4.15. Preparation Boxes

First, dry sand and dry mixture of sand and silt were prepared in these preparation boxes. Second, the preparation boxes were filled with water. After this process had been completed, hydraulic filling process was started.

During the pouring process, soil was taken from the laminar box and put to preparation boxes. After pouring process of laminar box had been completed, three preparation boxes were filled with saturated soil, which were then used in the shake table tests. To drain the water, a valve was placed at the lower side of each preparation box.

4.10. CPTu System

The pre-shaking and post-shaking CPTu tests were also conducted, beside the shake table tests to determine the relative density of the soil in the model before each shaking test started.

CPT systems were divided into three main groups;

- 1) mechanical cone penetrometers,
- 2) electric cone penetrometers and
- 3) piezocone penetrometers.

In 1948, the municipal engineer Bakker developed the first electrical cone penetrometer in Holland, which was called as the “Rotterdam cone”. In 1974, Schmertmann recognized the importance of pore water pressure measurement for the explanation of CPT data and added this feature in a piezometer probe and started to measure pore water pressures during cone penetrations. (Lunne, Robertson, & Powell, 1997) Cone penetration test with pore pressure measurement is commonly referred as piezocone tests (CPTu). CPTu permits for a continuous measurement of the cone resistance (q_c), local shaft friction (f_s) and pore water pressure (u).

In the late 1970's, Geotech Co. developed the cordless CPT system. The cordless system does not require a cable to transmit the measured data from probes into microphone. This is done acoustically. The cordless CPT is very easy and provides time efficiency. In this research, the cordless CPTu was used during pre-shaking and post-shaking. For the CPTu tests to be done, a special CPT penetration system was developed.

During the CPTu tests, probe should be pushed into the soil at a constant penetration velocity. Hydraulic pump was used to do this process. Hydraulic pump was carried by 1470mm x 750mm beam (Figure 4.16 and Figure 4.17). Six plates were welded perpendicular to the beam for increasing the capacity of the system. The capacity of the system was 5 tons. Four 281cm high U profiles were used as carriers (bearings). Bottom and top points of the U profiles were welded to 160mm x 160mm square plates for connections to U profiles, which are connected to I-beams resting on strong floor (Figure 4.20).

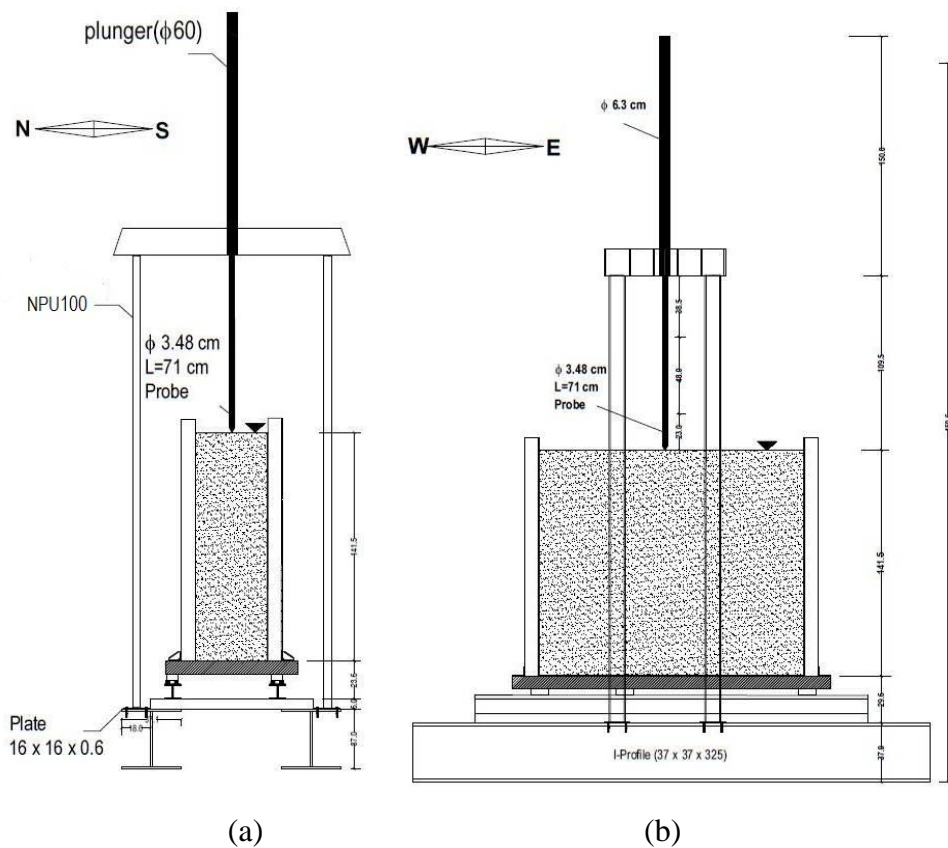


Figure 4.16. (a) Side View of CPTu System (N-S), (b) Figure B.2. Side View of CPTu System (W-E)

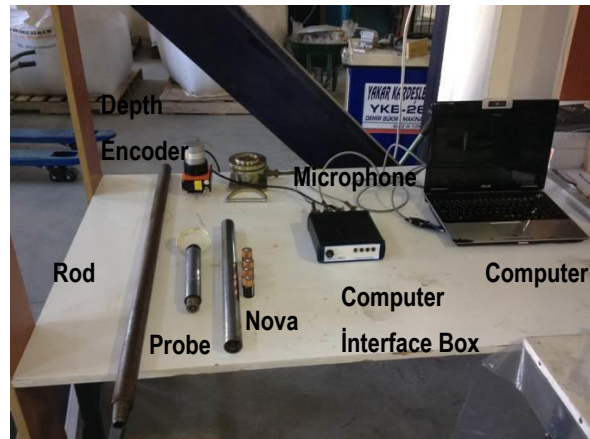


Figure 4.17. Components of the CPTu System

Geotech Co's cordless CPTu system was used to measure cone resistance, local shaft friction and pore water pressure. The CPTu system consisted of

- 1) CPT probe,
- 2) rod,
- 3) microphone,
- 4) depth encoder,
- 5) computer interface box,

Computer components of the CPTu system are illustrated in Figure 4.17.

A cone penetrometer probe with 10 cm^2 base area and apex angle of 60 degrees was used during the CPTu tests (Figure 4.18). Probe consisted of; 1) Point, 2) O-rings, 3) X-rings, 4) filter rings, 5) support rings, 6) friction sleeve and 7) cone body.

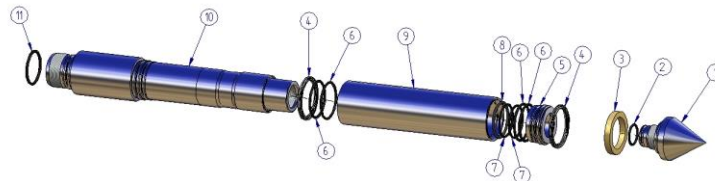
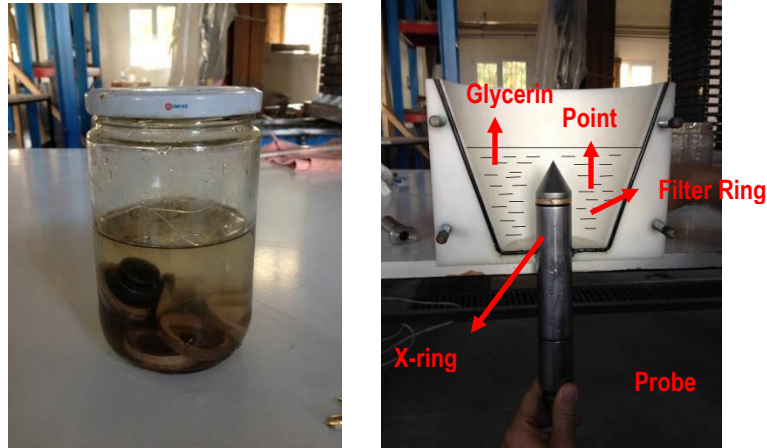


Figure 4.18. CPTu Probe; 1)Point, 10 cm^2 , 2) O-ring, 3) Filter Ring, 4) X-ring, 5) Support Ring, 6) O-ring, 7) O-ring, 8) O-ring, 9) Friction Sleeve, 10) Cone Body, 11) O-ring (Source: Geotech Nova CPT Acoustic Manual)



(a) (b)
 Figure 4.19 (a). Keeping the Rings and Cone Tip Point in Glycerin, (b) Mount of X-ring, Filter Ring and Point in Funnel

The cone tip and the filters should be kept in glycerin until they are used. (Figure 4.19a). The probe was introduced in the funnel. Rings, which were used between the tip point and the friction sleeve and the cone body, prevented soil and water entry. Funnel was filled with glycerin and was mounted with the X-ring on the support ring and then the unit was placed on the top of the probe. Afterwards, the filter ring and the O-ring were placed on top of the probe. Consequently, the point was placed into soil (Figure 4.19b).

The nova is powered by four pieces of alkaline ‘C’ batteries. The batteries were installed in a right way with the positive pole facing the probe. The probe was mounted on the nova. Probe and nova were connected. The total height of the probe and the nova was 710mm, while their diameter is 34.8mm diameter.

The microphone should be mounted under the pushing system. The probe and the nova were placed under the microphone. This process is essential to achieve good sound transmission. The rod, which was added to the cone, is made from the best quality of steel available. The height of this rod was 750mm. A computer interface box and a depth encoder were the components of the CPTu system. Computer interface box collected data from the depth encoder and the microphone, for the purpose of transferring the data to the computer. CPTu test process will be described in Chapter 7.

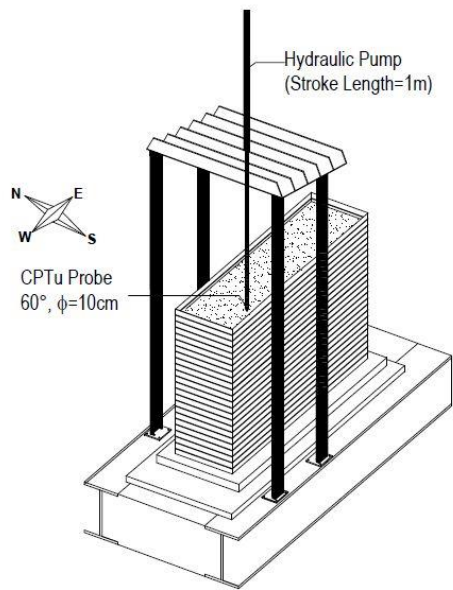


Figure 4.20. CPTu System Used in This Study.

CHAPTER 5

SHAKE TABLE AND INITIAL LAMINAR BOX PERFORMANCE TESTS

5.1. Introduction

Two performance tests were conducted to observe the performance of the shake table and the laminar box, before doing the shake table tests with soils. They were; 1) shake table test with soil bags and 2) pull and push tests. To observe the performance of the shake table, a shake table test was first conducted by loading the shake table with soil bags. Accelerometer was placed on the shake table test, before the tests. The results were taken from the accelerometer to be compared with the input motions.

After completing the 1-D laminar box construction, the laminar box was mounted on the 1-D shake table. As mentioned before, roller mechanisms were placed between laminates and laminates slid on each other using the rollers. In order to investigate whether the roller mechanism affected the movement of the laminar box, the laminar box was placed on the shake table and static loading was applied to each laminate when laminar box is empty. Process and results of the performance tests (shake table test with soil bags and box pull and push tests) are presented in this chapter.

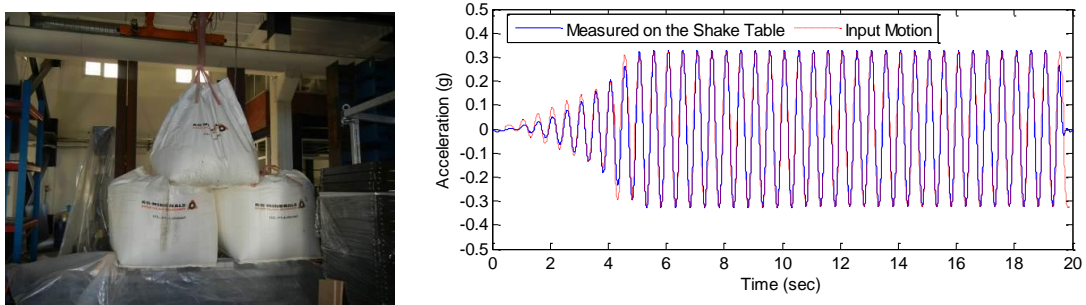
5.2. Shake Table Performance Test

The total weight of the 1-D laminar box with the membrane and the soil bags representing the soil model used, which was placed into the 1-D laminar box, was nearly 2500kg. In order to investigate the effect of the mass on the shaking system, a shake table test was conducted by loading the shake table with the soil bags.

The shake table was shaken with a sinusoidal wave. The level of the shaking was 24 cycles and the frequency was 2 Hz with 0.3g PGA (Peak Ground Acceleration). An accelerometer was placed on the shake table before the shaking. The accelerometer

was connected to the data acquisition system. During shaking, an accelerometer recorded the acceleration data. Figure 5.1a illustrates the test setup.

As shown in Figure 5.1b the acceleration versus time for the input motion and measured data on the shake table were compared to find out that they were nearly same. This result indicates that the shake table works well at high loadings.



(a) (b)
Figure 5.1. (a) Shake Table Test with Soil Bags, (b) Acceleration vs Time of the Input Motion and Accelerometer

5.3. Laminar Box Pull and Push Tests

In order to prevent energy loss, laminar box was composed of 24 laminates and low friction rollers were used between laminates, laminates slide on each other using the rollers. Therefore, the friction between rollers and the laminates is extremely important issue.

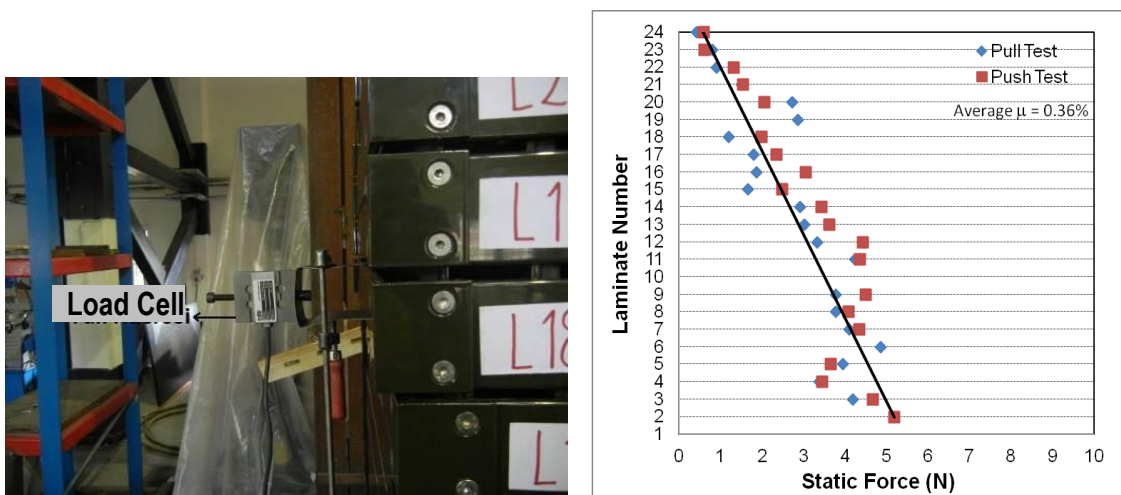
To observe the effect of friction on the performance of the 1-D laminar box, static pull and push tests were conducted on the laminates (Figure 5.2.a). During pull and push tests, membrane were not placed inside the laminar box and the laminar box was not filled with soil.

50kg (500N) capacity load cell was attached to each laminate. Load cell and computer were connected with a cable and then force was applied on the load cell. Applied forces were recorded by the Testlab programme. Coefficient of friction (μ) between the laminate and the rollers were calculated by dividing the measured force on each layer (F_s) by the weight on the roller (W).

$$\mu = \frac{F_s}{W} \quad (5.1)$$

The maximum applied force was 5.2N on the second laminate. Pull and push tests could not be applied on the first laminate because the first laminate was fixed on the shake table. The minimum applied force was 0.51N and occurred on the top laminate.

Applied force has increased with depth. Figure 5.2 (b) displays the applied force on each laminate. Coefficient friction also increased with depth. The average coefficient of friction between the laminate and the roller was found to be around 0.36%. Pull and push test showed that the effect of mass of the frames and the friction between the layers are negligible in the results of the shake table tests.



(a) (b)
Figure 5.2. (a) Load Cell Attached on the Laminate, (b) Static Force per Laminate

CHAPTER 6

SOIL PREPARATION FOR THE SHAKE TABLE TESTS

6.1. Introduction

Laboratory tests were conducted in order to determine the index properties of the soil, which will be used for the liquefaction tests. For shake table tests, soils with different fines' contents were prepared with these soils. After preparation of the soil was completed, hydraulic filling process was used to fill the laminar box. The process of the soil filling method to the laminar box and results of the sieve analysis, hydrometer test, specific gravity, maximum and minimum void ratio tests, falling head permeability test will be presented in this chapter.

6.2. Preparation of Soil Samples

In this research, to conduct shake table tests, ten soil bags were used at IZTECH structural laboratory. Soil bags numbered 1 to 10. Each soil bag was nearly 1 ton. Bag1- Bag5 were silty sand and they were nearly 5 tons. Bag6 - Bag10 were sand and they were also nearly 5 tons.

The first shake table test was conducted with sand. Fines content (FC) was nearly 0%. In the 2nd test fines content was 15%. The 3rd shake table tests were conducted with silty sand and the fines content was less than 25%. Fines content of the soil, which was used for 3rd test wanted to be 25% but it was not uniform. It was important to get information about fines content of the soils, which were kept in soil bags, to arrange the fines content of the soil that were used in shake table tests. To determine the silt percentage and the other properties of the soil, laboratory tests were conducted.

6.2.1. Laboratory Tests

Laboratory tests, which were conducted in the shake table tests were;

- 1) sieve analysis,
- 2) hydrometer tests,
- 3) specific gravity tests and
- 4) maximum and minimum void ratio tests,
- 5) falling head permeability tests.

6.2.1.1. Sieve Analysis

The ASTM D422 standard test method was used in order to calculate the distribution of large sized particles and to determine of the effective size, the uniformity coefficient and the coefficient of gradation. During the sieve analysis; first, sieves and pan were placed on the mechanical shaker and the soil sample was poured on the sieves column (Figure 6.1). Second, sieves column was shaken nearly for 10 minutes, than the weight of each sieve and pan with retained soil on them were recorded. Third, weight of the retained soil was calculated by subtracting the weight of sieve from the weight of the sieve and retained soil.



(a) (b)
Figure 6.1. (a) Ranged the Sieves #4 to #230, (b) Sieves Column were Placed on the Mechanical Shaker

The percentage of the retained soil on each sieve was calculated by dividing the weight of the retained soil to the total weight of the soil sample. Finally, grain size

versus percent passing variation was plotted. C_u (uniformity coefficient) and C_c (Coefficient of gradation) were computed as follows;

$$C_u = \frac{D_{60}}{D_{10}} \quad (6.1)$$

$$C_c = \frac{(D_{30})^2}{D_{60} \cdot D_{10}} \quad (6.2)$$

Where,

D_{10} is the diameter through which 10% of the total soil mass has passed (the effective size),

D_{30} is diameter through which 30% of the total soil mass has passed,

D_{60} is diameter through which 60% of the total soil mass has passed.

6.2.1.2. Hydrometer Test

The ASTM D422 standard test method was used to determine the distribution of the finer particles. The process of the hydrometer test is explained below in details.

- 1) To read zero correction, 125ml dispersing agent (Sodium Hexametaphosphate) and distilled water were mixed in a control cylinder. Hydrometer stem was placed inside (Figure 6.2.).



Figure 6.2. Control Cylinder and Hydraulic Stem

- 2) Fine soils which were passed from #200 sieve, 125ml dispersing agent and distilled water were mixed. The cylinder is turned upside down for 30 times.
- 3) Start time was recorded and hydrometer stem which was taken from the control cylinder was placed to record the first reading. After the first reading, 2, 5, 15, 30, 60, 120, 250, minutes and 24 hours readings were recorded.

6.2.1.3 Specific Gravity Test

The ASTM D 854-00 standard test method was used to determine the specific gravity. Process of the specific gravity is explained below.

1. The pycnometer with distilled water is filled and weighted (W_A). Weight of the empty pycnometer was called (W_P).
2. For 100ml pycnometer, 10gr dry soil sample (W_0) which passed through the #200 sieve were placed inside the pycnometers and filled with distilled water up to 1/3 height. For the 50ml pycnometer, 5gr dry soil sample (W_0) was used.
3. To take the entrapped air, pycnometers were placed inside the dessicator.
4. After pycnometers were taken from dessicator, they are filled with distilled water and weighted again. (W_B)

Figure 6.3 illustrates dessicator, vacuum pump, pycnometer and distilled water. Then specific gravity is computed as follows;

$$G_s = \frac{W_0}{W_0 + (W_A - W_B)} \quad (6.3)$$

Where;

W_0 is weight of dry sample,

W_A is weight of pycnometer with distilled water;

W_B is weight of pycnometer, distilled water and soil sample



(a)



(b)

Figure 6.3. (a) Desiccator and Vacuum Pump, (b) Pycnometer, Distilled Water and Weight (Left to Right)

6.2.1.4. Maximum and Minimum Void Ratio Tests

The ASTM D 4253 standard test method was used to determine the maximum void ratio. The ASTM D 4254 standard test method was used to determine the minimum void ratio.



(a)



(b)

Figure 6.4. (a) Mold and Weight, (b) The Mold Attached to the Vibrating Table

During maximum and minimum void ratio tests, firstly, the volume of the mold (V_m) was calculated, the interior diameter (d) and the height (h) of the mold were

measured and the mold was weighted, (M_m). Secondly, to minimize the particle segregation, during the filling process with loose sand spiraling motion was used. Afterwards, excess soils were taken by a straight case ruler from the surface, the mold and soil was weighted, (M_1). Thirdly, weight (8.79 kg) was placed on the soil sample and mold was attached on the vibrating table, it was vibrated for 8 minutes (Figure 6.4). Finally, the settlement of the soil was measured, (s).

According to these laboratory tests results, Table 6.1. shows the summary of the basic properties of soils inside the soil bags, as found from the labrotory tests performed.

Table 6. 1. Summary of Properties of Soils which were Inside the Soil Bags

Sample Name	Gs	emax	emin	Fines Content (%)
1 (Silty Sand)	2,61	1,68	0,68	63,51
2 (Silty Snad)	2,62	1,69	0,99	54,13
3 (Silty Sand)	2,69	1,67	1,04	75,11
4 (Silty Sand)	2,69	1,70	1,07	75,50
5 (Silty Sand)	2,60	1,64	0,97	67,42
6 (Sand)	2,65	1,00	0,86	3,57
7 (Sand)	2,65	1,03	0,85	2,17
8 (Sand)	2,65	0,94	0,84	0,50
9 (Sand)	2,65	1,03	0,83	4,31
10 (Sand)	2,65	0,97	0,85	3,00

6.2.1.5 Falling Head Permeability Test

The ASTM D 2434 standard test method was used to determine the coefficient of permeability (k) of granular soils (Constant Head Test), was the falling head test method is not standardized. First, the soil sample was filled and until the water level in the funnel was constant, water is allowed to flow through the tunnel. Second, the bottom outlet was opened, water is run through the permeameter, until the sand was saturated and no air bubbles appear to flow out of the discharge pipe. Third, distance between the water surface in the funnel and the bottom outlet of the permeameter was measured and the water is allowed to run through the bottom outlet, opened until water reaches up to a particular height. Then the discharged water during a particular period was calculated and a change in head was noted by adjusting the funnel at different heights. These steps were repeated three times and average k (cm/sec) was calculated. Figure 6.5 illustrates the permeability test setup.



Figure 6.5. Permeability Test Setup

6.3. Hydraulic Filling Method

A robust hydraulic filling method was required in this research to fill the laminar box. An EBARA CMR 1.00M slurry pump was used and the maximum solid particles permeability of the slurry pump is 10mm. Properties of slurry pump is illustrated in Table 6.2. The mixture of sand and water, which was prepared in preparation boxes, was transferred by the slurry pumps' hose. This was an advantage for sensitive electronic equipment, actuators, instrumentations and computer systems. At the end of the hydraulic fill method, sand grains were settled down through water, like natural alluvial deposition of sands in rivers, in lakes and similar to forming man-made post islands.

Table 6.2. Properties of Slurry Pump

Power (HP)	1
Power (Kw)	0.75
Electricity Connection	1 phase/50 Hz
Weight of Pump	12.2 kg
Entrance - Exit	1.5" - 1.5"

A 2cm diameter slurry hose that was attached to a 1-phase 50Hz slurry pump was used to transfer the soil and water mixture from the preparation boxes into laminar box. After sand grains settled down through water, excess water above the sand, which

surfaced inside the laminar box, was taken by the water pump (Figure 6.6 and Figure 6.7). The water level above the sand surface was kept 10.3cm for Test 1, 4.5cm for Test 2 and 2.4cm for Test 3, on average. This phenomenon was repeated many times to fill the laminar box, completely.

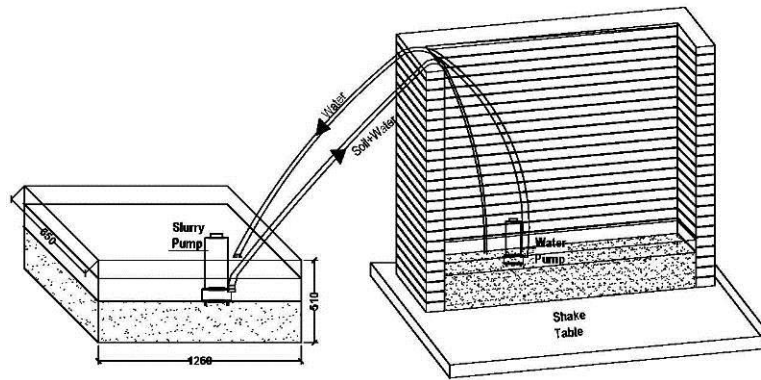


Figure 6.6. Hydraulic Filling Schematic View

Bucket density tests method and CPT-u system, which were presented in Chapter 3, were developed to measure the relative density of the sand poured. The relative density depended on filling velocity, filling direction, discharge velocity, discharge direction, and the waiting time of the settlement of the soil grains.



Figure 6.7. Hydraulic Filling Process

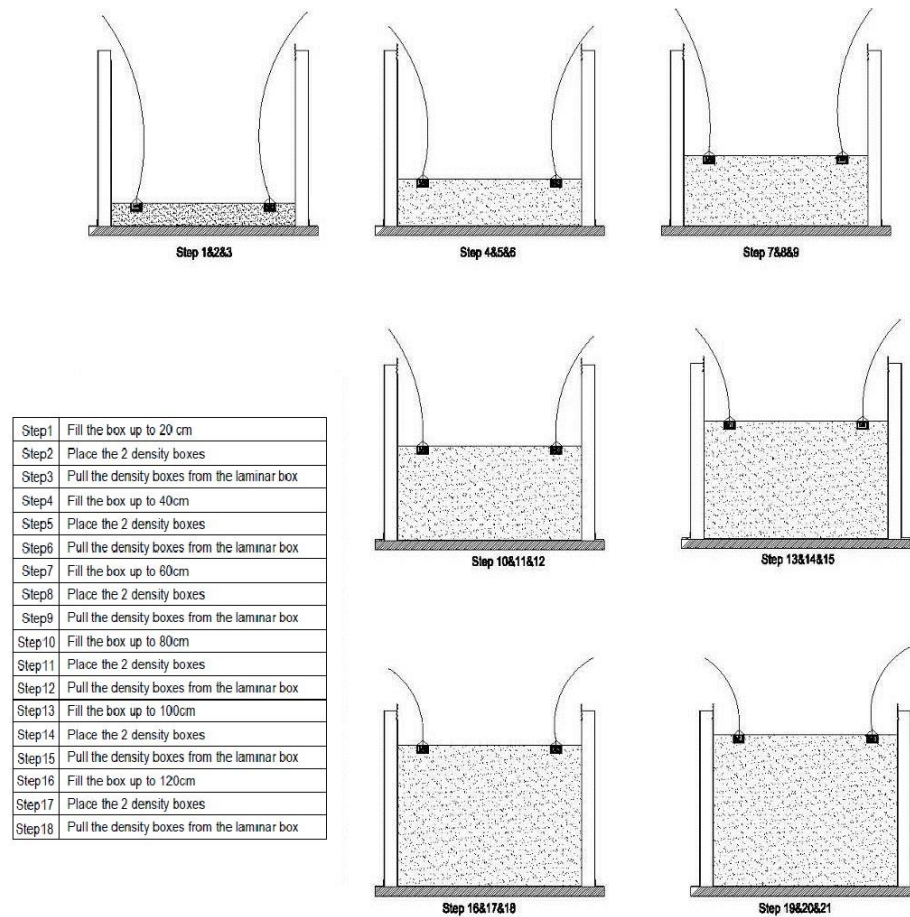


Figure 6.8. Bucket Density Process for Test 1

Diameter of bucket was 5cm and the height of the bucket was 7cm. Two buckets were placed on the soil surface at different depths during the filling process. Buckets were pulled upwards with a rope from the laminar box when buckets were completely filled with soil and then its full weight was measured to estimate the saturated unit weight of the soil (Figure 6.8 and Figure 6.9). Two samples were taken from each bucket to determine the water contents (Table 6.4). Collecting undisturbed soil samples were difficult. Any disturbed soil samples were discarded from the sample pool, due to possible disturbance. The summary of saturated unit weight results were displayed in Table 6.3. Bucket locations for each test are illustrated in Table 6.3. Bucket tests' heights were measured from the bottom of the box upward.

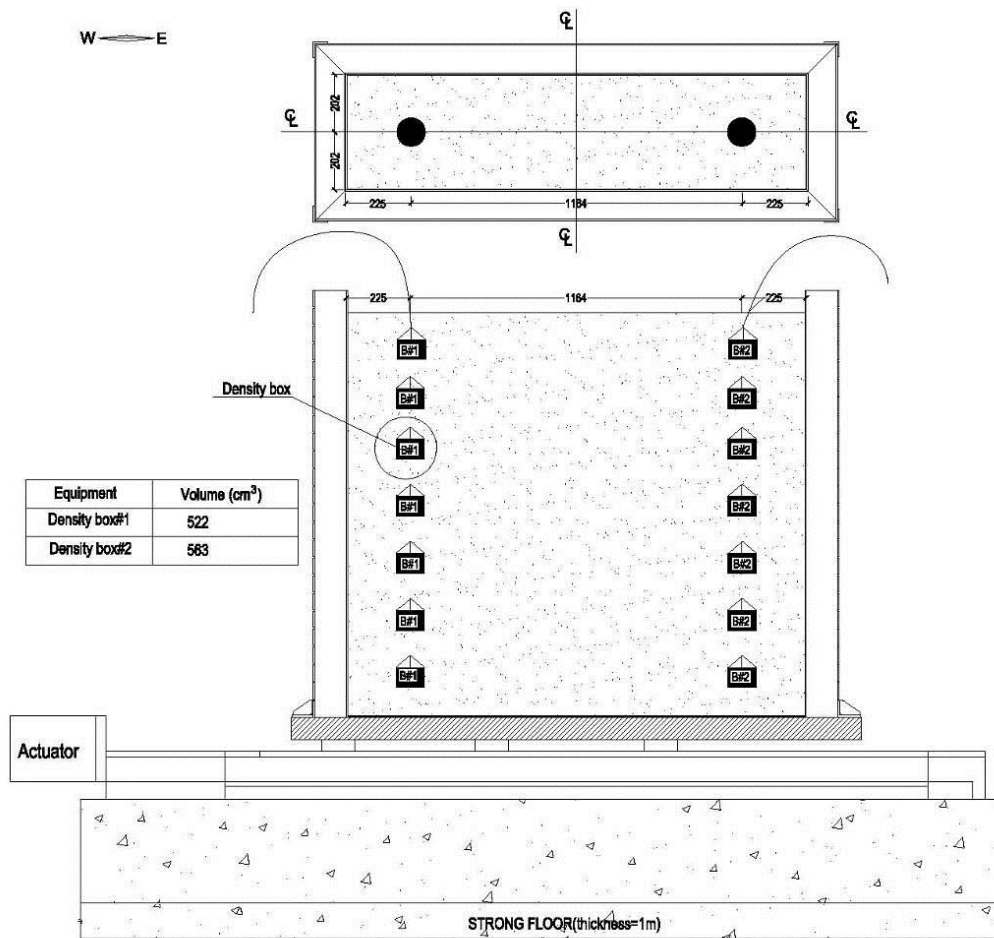


Figure 6.9. Locations of Buckets

Table 6.3. (a) Test 1, (b) Test 2, (c) Test 3 Bucket Density Tests Results

Test 1	
Height	Saturated Unit Weight
cm	KN/m ³
38	17.68
56	18.71
70	17.11
85	19.08
100	16.02
113	19.24
130	16.90

(a)

Test 2	
Height	Saturated Unit Weight
cm	KN/m ³
30	19.19
52	20.00
70	18.41
85	18.86
95	19.38
110	19.18
120	19.85

(b)

Test 3	
Height	Saturated Unit Weight
cm	KN/m ³
13	19.31
45	19.65
57	20.19
72	19.85
76	19.24
101	20.63
129	21.35

(c)

Table 6.4. (a) Test 1, (b) Test 2, (c) Test 3 Water Content

Test 1	
Height	Water Content
cm	%
38	36.00
56	28.00
70	29.70
85	28.10
100	28.90
113	31.40
130	30.35

(a)

Test 2	
Height	Water Content
cm	%
30	26.60
52	27.70
70	31.20
85	30.20
95	27.20
110	31.40
120	27.40

(b)

Test 3	
Height	Water Content
cm	%
13	39.40
45	40.10
57	45.60
72	41.90
76	33.00
101	40.00
129	20.60

(c)

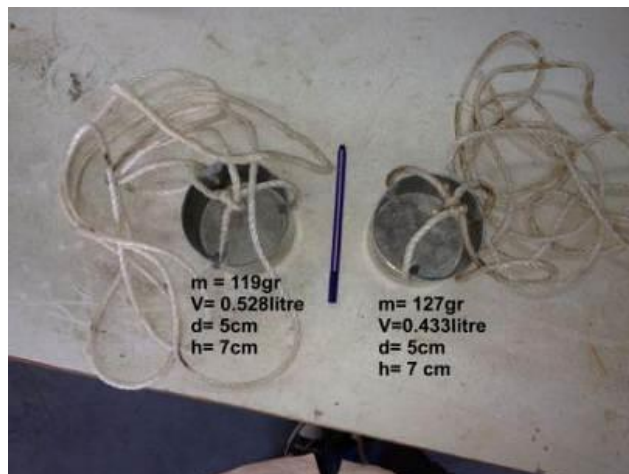
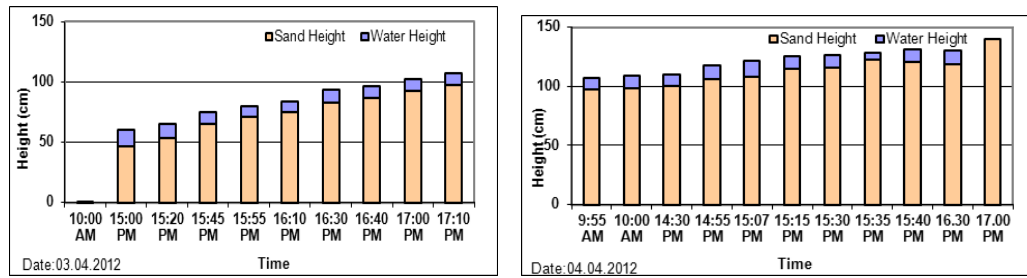
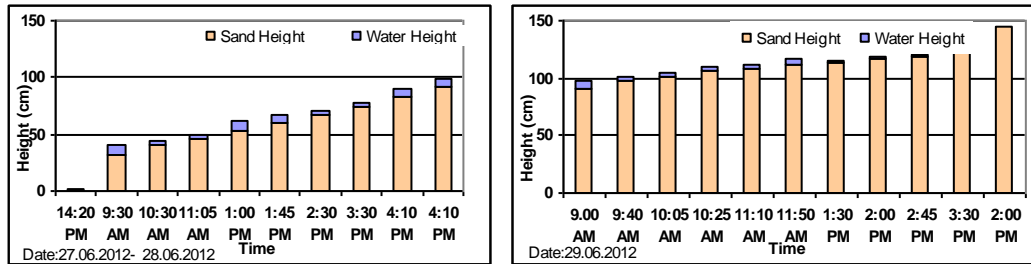


Figure 6.10. Density Buckets Used for Bucket Density Test

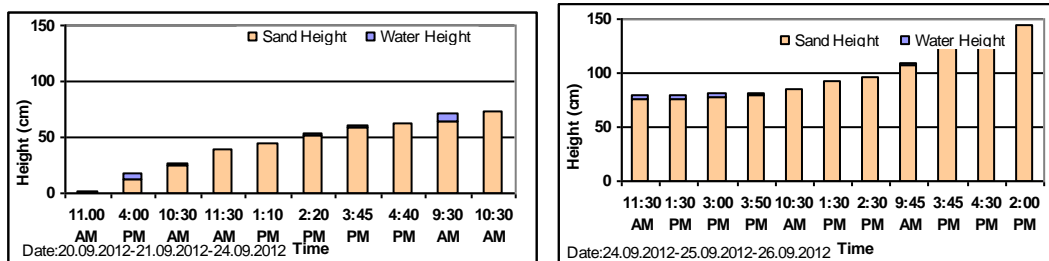
During the filling process, the depth of soil was taken from the soil surface to the top point of the laminar box and it was recorded to determine the filling time. The first and second filling process for the test 1 lasted nearly 2 days, while the third filling process lasted nearly 5.5 days. The time of filling process increased, when percentage of fines content increased. Figure 6.11 (a), (b), and(c) illustrate the height of the water and silt in the laminar box during filling process.



(a)



(b)



(c)

Figure 6.11. (a) Test 1, (b) Test 2 and (c) Test 3 Filling Process

Settlement of the silt in the water takes a long time. The percentage of the silt content of the 3rd test was less than 25. So filling process lasted longer than the 1st and 2nd tests.

CHAPTER 7

CONE PENETRATION TESTS AND SHAKE TABLE TESTS

7.1. Introduction

This chapter presents the details of the piezocone penetration tests (CPTu) which were conducted before each shake table tests (Test 1, Test 2 and Test 3) with the laminar box. One of the main objectives of the CPTu tests was to determine the relative density of the soil model together with initial pore water pressure distribution within soils before each shaking. Total of 15 CPTu tests were conducted in this research.

The shake table tests were intended to simulate liquefaction occurrence in a level ground soil deposit, built on base saturated sand. In this study, total of three shake table tests were conducted. In each shake table test, the soil model was shaken for four times. These tests were named as Shake-1, Shake-2, Shake-3 and Shake-4. Each shake test has lasted for about 12 seconds.

The CPTu system and laminar box system were presented in Chapter 4 in detail. The process and results of the CPTu tests and the shake table tests are presented in this chapter. At the end of the shake table tests, data was collected from the instrumentations. To evaluate the results, these data were filtered by Labview program. Data filtration process is also presented in this chapter.

7.2. CPTu Tests

Laminar box was filled with hydraulic filling method up to 1.4m for Test 1, 1.44m for Test 2 and Test 3. CPTu test was conducted immediately after the completion of placement and after each shaking. Total of five CPTu tests were performed for each shake table test and named as CPT_{ini} , CPT1, CPT2, CPT3 and CPT4.

The primary objective of CPTu was to determine the overall relative density of the soil model. Other objectives were to determine the saturated unit weight and the

pore water pressure distribution. Details of the CPTu system were presented at Chapter 4. CPTu tests were conducted according to ASTM D 3441 (1996) standard. During the CPTu tests, first probe was placed inside the funnel which was filled with glycerin. Firstly, point and filters, which were being kept in the glycerin, were placed on the probe. Secondly, the nova was attached to the end of the probe to transfer the measurements from the probe the surface. Thirdly, depth encoder was placed at a suitable place. Power cable, microphone cable, serial cable and depth encoder cable were connected to the computer interface box. Then, computer interface box was connected to the computer. The microphone should be mounted under the pushing and above the nova. It is essential that good mechanical contact was achieved, in order to guarantee good sound transmission, including sound.

Table 7.1 Technical Specification of Hydraulic Power Unit (BRD-166 ENARPAC Cylinder and PUJ-1401E ENARPAC Pump)

Motor Size	Flow at Rated Pressure	Maximum Pressure	Maximum Force	Maximum Cylinder Speed
<i>kw</i>	<i>lt/min</i>	<i>bar</i>	<i>kg</i>	<i>cm/sec</i>
1.5	11.8	65	5350	2.4

Before each CPTu test, zero load readings of the cone tip and sleeve friction were recorded, while the probe was suspended vertically in the air. These readings indicated the data quality. After zero test, CPTu test started, BRD-166 Enarpac cylinder and PUJ-1401E Enarpac hydraulic pump (50KN capacity) were used to push the probe into the ground at constant speed nearly 70cm because the length of the nova and probe totally was 71cm. Table 7.1 illustrates the technical specification of the hydraulic power unit. The average penetration velocity of all the CPTu tests was 1.2cm/sec. The penetration velocity was different from the ASTM D 3441 (1998) standard (2cm/sec). A pause of few minutes was necessary to add a rod after the probe, and nova was pushed into the ground completely. Hydraulic pump was raised and the microphone was taken. Then, the rod was added on the nova. In this instance, microphone was placed on the end of the rod. The rod and probe was pushed up to the bottom of the soil model. Process of the CPTu test is displayed in Figure 7.1. (a) to (e).



(a) (b) (c) (d) (e)

Figure 7.1. (a) Microphone was Placed on the Probe, (b) Hydraulic Pump was Raised, (c) Rod was Added , (d) Microphone was Placed on the Rod, (e) The Rod and Probe was Penetrated to the Soil

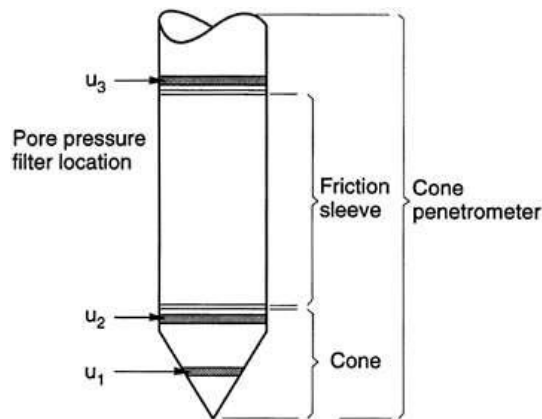


Figure 7.2. Terminology for Cone Penetrometers
(Source: Lunne et al., 1997)

While the probe was penetrated into the soil, the transmitter received the digital multiplexed measured data of cone resistance (q_c), sleeve friction (f_s) and pore water pressure (u) from the probe. Probe amplified the data and converted it into radio waves

that were sent through the hole of the nova and rod to the surface. The results were viewed on the screen on the computer.

To find the cone resistance (q_c), the total force acting on the cone (Q_c) is divided by the projected area of the cone (A_c). To calculate the sleeve friction (f_s), the total force acting on the friction sleeve (F_s) is divided by the surface area of the friction sleeve (A_s). Pore pressure could be measured at one, two and three locations (Figure 7.2) on the cone (u_1), behind the cone before the sleeve (u_2), behind the cone after the sleeve (u_3). In the CPTu tests conducted in this research, pore pressure was measured behind the cone before before the sleeve and not after (u_2). Figure 7.3 displays the location where the CPTu tests were conducted. The location of the CPTu test was important in order not to damage instrumentations which were placed inside the soil model.

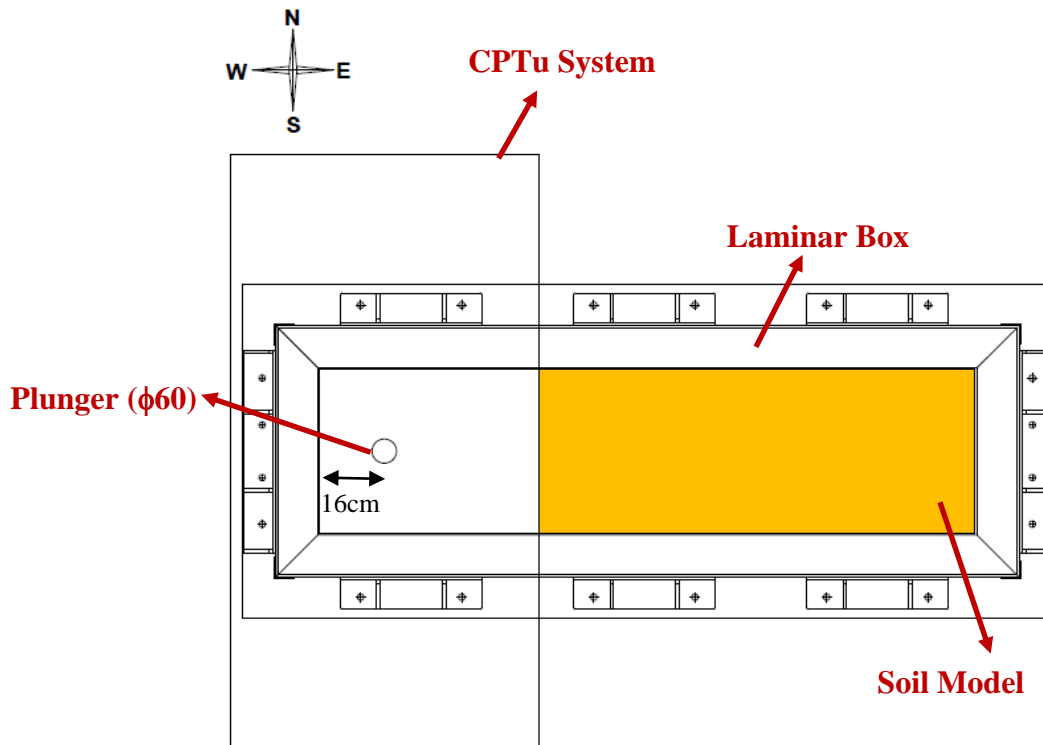


Figure 7.3. Location of CPTu Tests – Top View

Equation 7.1 shows the inferred relative density obtained by CPT correlation's proposed by Robertson and Powell, 1997.

$$D_r = -98 + 66 \log_{10} \left(\frac{q_c}{\sqrt{\sigma_{vo}^1}} \right) \quad (7.1)$$

Where,

D_r = relative density,

σ_{vo}^1 = effective vertical stress,

q_c = cone resistance (σ_{vo}^1 and q_c are in the same units.)

7.2.1. CPTu Tests Results

The profiles of the relative densities were obtained before and after each shaking using the method of Robertson and Powell (1997). As a result of the different settling heights and velocities, the soil at the bottom of the laminar box has been slightly denser than the soil near the surface of the laminar box.

7.2.1.1. Test 1- CPTu

CPT_{ini} was conducted immediately after completion of the placement. CPT1, CPT2, CPT3 and CPT4 were conducted after 1st shake, 2nd shake, 3rd shake and 4th shake, respectively. Figure 7.4 illustrates the CPT test results, which were conducted between subsequent shakings of Test1.

CPTu tests results at 1m height indicated that (These results belong to 1m depth),

- Before first shake D_r was about 29%,
- Before second shake D_r was about 39%,
- Before third shake D_r was about 56%,
- Before fourth shake D_r was about 56%,
- After fourth shake D_r was about 80%.

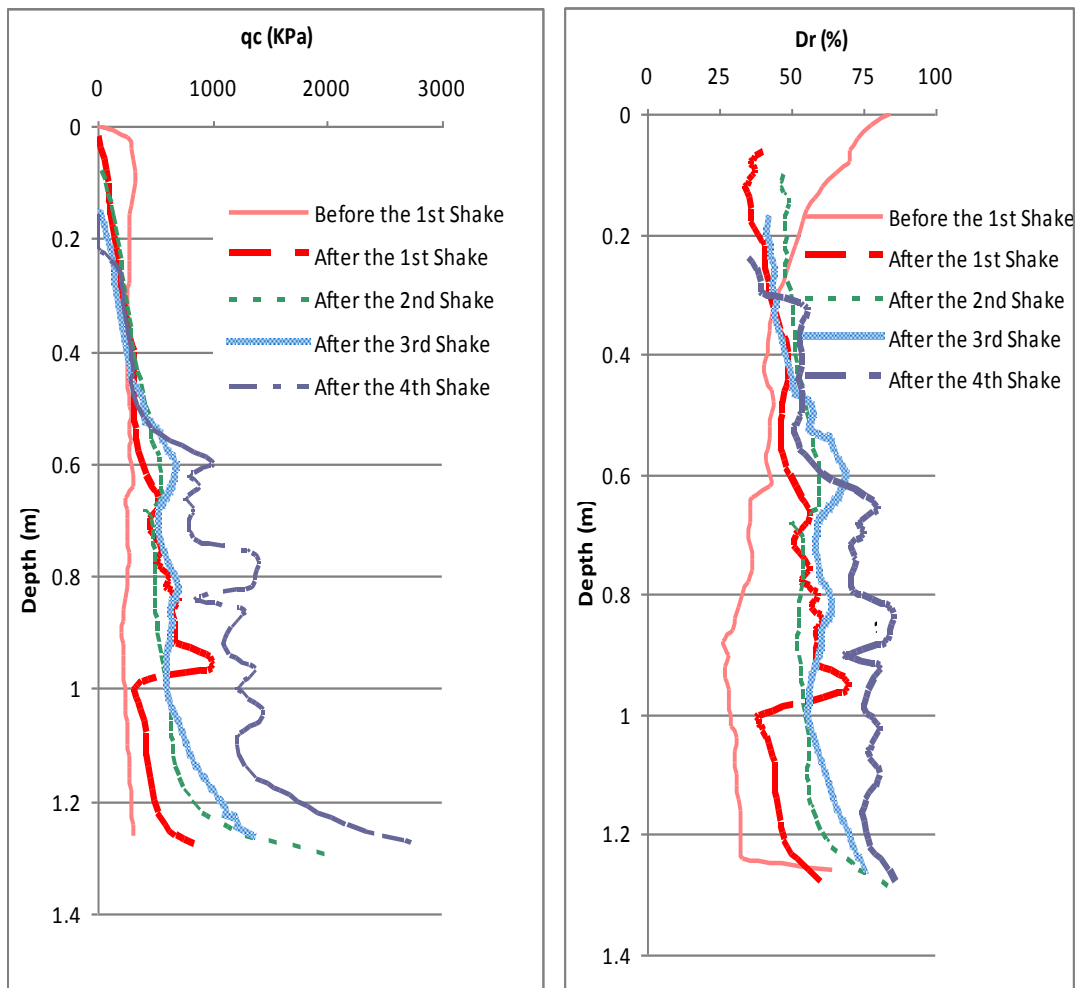


Figure 7.4 Summary of CPT Test Results for Test 1

7.2.1.2. Test 2 - CPTu

Total of 5 CPTu tests were conducted between subsequent shakings of Test1. CPT_{ini} was conducted immediately after completion of filling process. After each shake, additional CPTu tests were conducted to determine the relative density of the soil model (Figure 7.5).

CPTu tests results at 0.5 heights indicated that (These results belong to 0.5m depth),

- Before first shake D_r was about 29% ,
- Before second shake D_r was about 30%,
- Before third shake D_r was about 36%,

- Before fourth shake D_r was about 20%,
- After fifth shake D_r was about 60%,

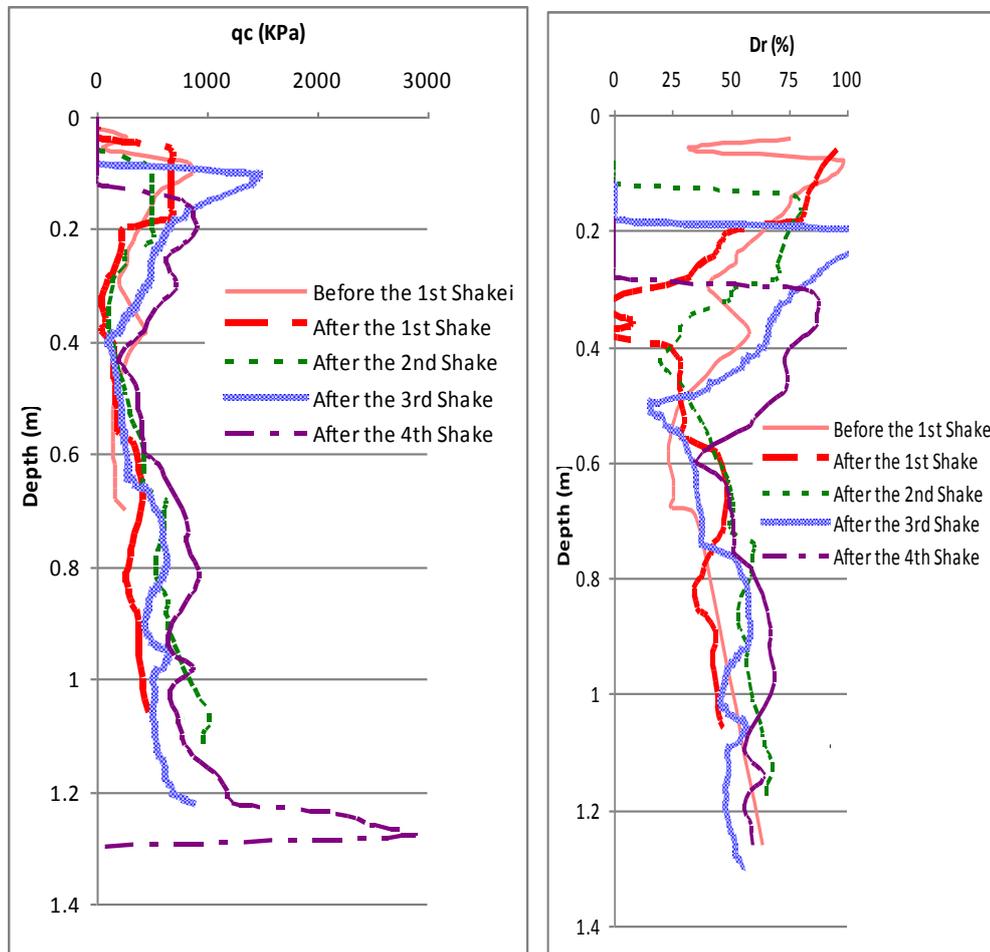


Figure 7.5. Summary of CPTu Test Results for Test 2

7.2.1.3. Test 3 - CPTu

CPT_{ini} was conducted before 1st shake, immediately after filling process was completed. CPT1, CPT2, CPT3 and CPT4 were conducted after each shake. Figure 7.6 illustrates the CPTu tests results.

CPTu tests results at 1m height indicated that (These results belong to 1m depth),

- Before first shake D_r was about 7% ,
- Before second shake D_r was about 8%,

- Before third shake D_r was about 20%,
- Before fourth shake D_r was about 46%,
- After fifth shake D_r was about 58%

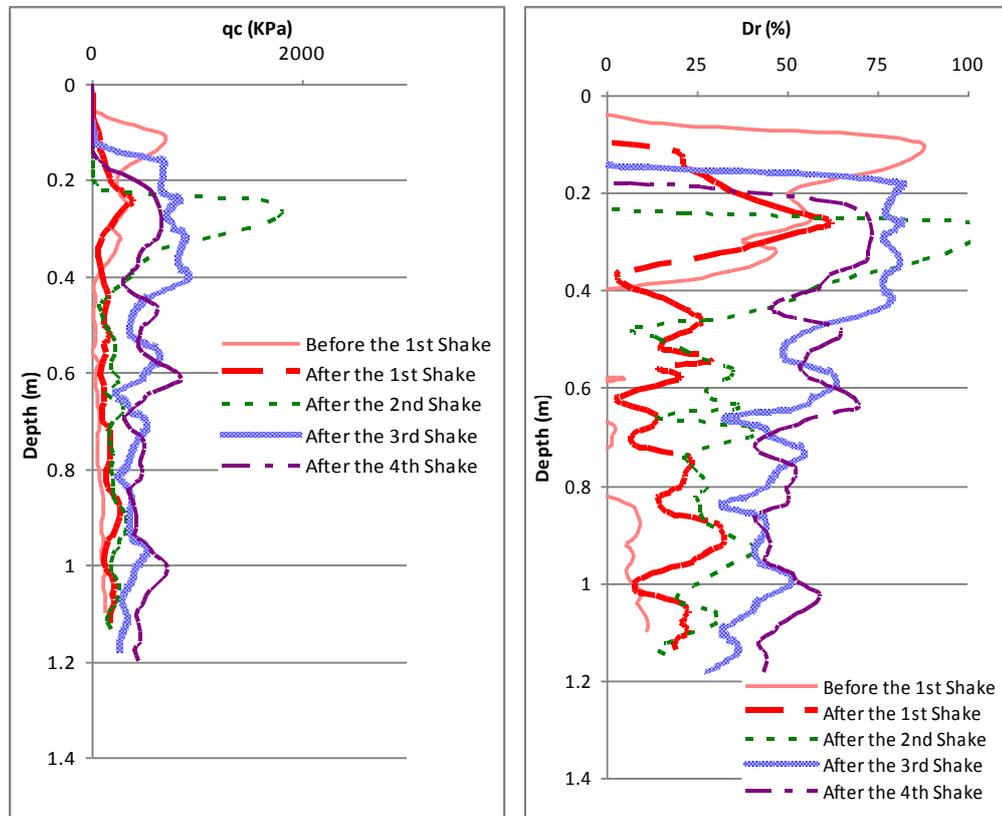


Figure 7.6. Summary of CPTu Test Results for Test 3

7.3. Shake Table Tests

The properties of the soil model, which was placed inside the laminar box for each liquefaction test is presented in this section. Also the input motions which were applied on the shake table and results of shake table tests, which were recorded by instrumentation, are also presented.

Prehistoric liquefaction phenomena illustrate that sand deposits can be liquefied again by a subsequent earthquake after initially liquefying during a previous seismic shaking. It's called reliquefied (Ling et al., 2003). In order to examine the role of silt percentage on reliquefaction three shake table tests were conducted at IZTECH. Each test has consisted of four shakes. After the 1st shake was completed and the excess pore

pressure generated by the 1st shake had entirely dissipated, laminar box was shaken subsequently to evaluate reliquefaction resistance.

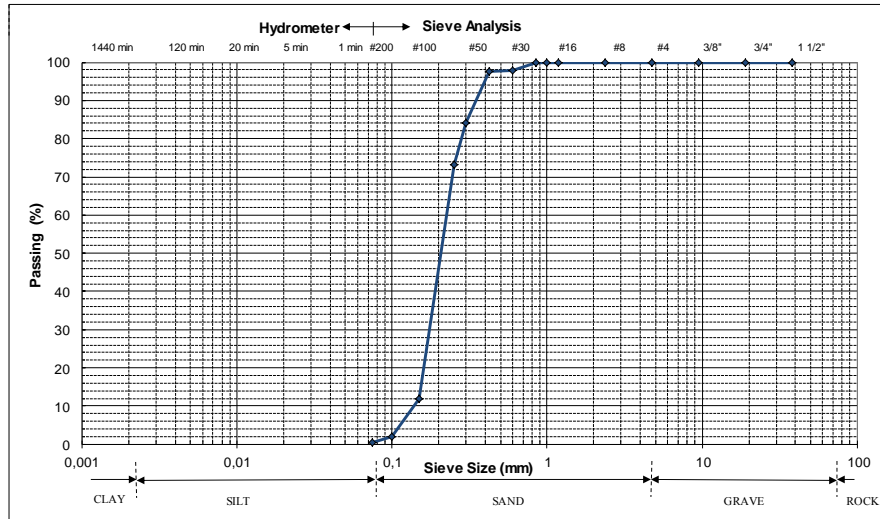
7.3.1. Shake Table Test 1

First shake table test was conducted at IZTECH on April 5th, 2012 with clean sand. Height of the soil model was 1.4m. The main objectives of the first shake table test were;

- To achieve a loose sand deposit using hydraulic filling method.
- To induce liquefaction phenomenon. To study the time for liquefaction triggering status from the pore pressure results.
- To study the soil response during the shaking from the accelerometers and to analyze the laminar box and shake table performance.
- To check the reliability of the instruments.

7.3.1.1. Soil Properties

The soil model with 0% fines content (FC), was placed inside the laminar box for the Test 1 was consisted of 1.40m thick saturated sand deposit built by hydraulic filling method. To calculate the minimum void ratio (e_{min}), maximum void ratio (e_{max}), specific gravity (G_s) and permeability (k), laboratory tests were conducted. Process of the laboratory tests were presented in Chapter 6. Using bucket density tests, saturated unit weight (γ_{sat}) and water content (w) were found. Table 7.2 summarizes the index properties of this sand. Its grain size distribution curve is given in Figure 7.7. SW was the symbol of soil model based on the unified soil classification system (USCS).



D_{10}	D_{30}	D_{60}	C_u	C_c
mm	mm	mm	-	-
0.16	0.18	0.23	1.44	0.88

	e_{min}	e_{max}	G_s	γ_{sat}	w
	-	-	-	KN/m ³	%
Test1	0.84	0.99	2.65	17.82	30.04

Figure 7.7. Grain Size Distribution and Soil Properties for Clean Nearly Uniform Sand

C_u (uniformly coefficient) and C_c (coefficient of gradation) were calculated according to the grain size distribution curve. D_{10} , D_{30} and D_{60} were determined from the grain size distribution curve.

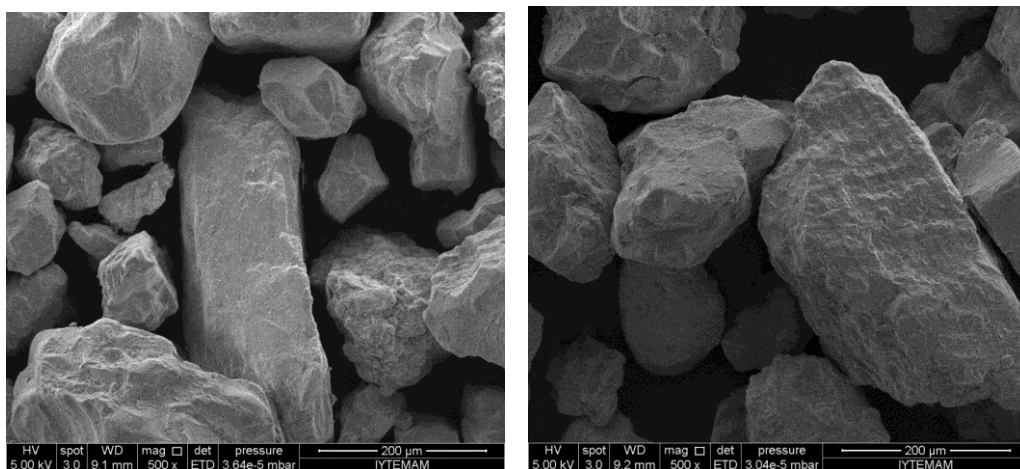
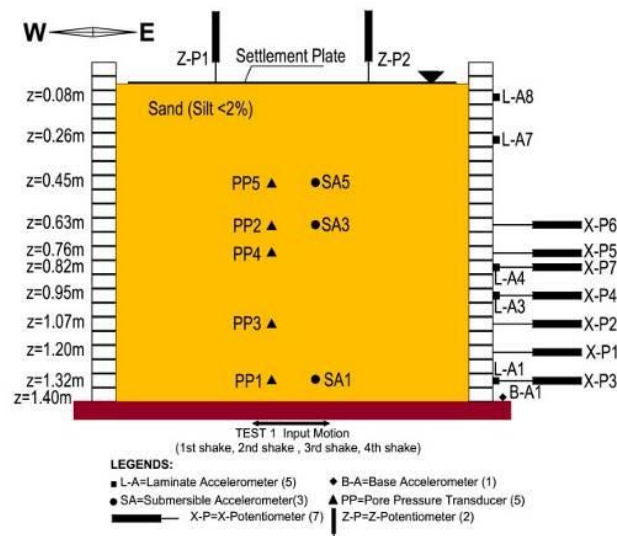


Figure 7.8. SEM images of Soil Sample with 0% Fines Content

A scanning electron microscope (SEM) is a type of electron microscope that produces image of the soil samples used. This SEM images gave information about the grain shapes. Soil samples were magnified 500 times. These images are illustrated in Figure 7.8. As shown in the figure, the soil that is used for the shake table tests have sub-rounded particles. Soils with rounded particles are more susceptible to densify easily than soils with angular grains. Therefore, soils with rounded shapes are usually more susceptible to liquefaction than the angular-grained soils.

7.3.1.2. Instrumentation Plan of Test 1

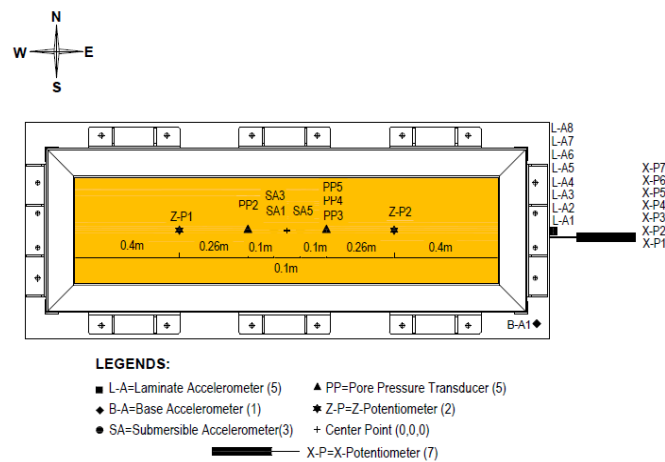
Pore pressure transducers and submersible accelerometers were placed inside the soil model before the hydraulic filling process has started. Laminate accelerometers and X-Potentiometers were attached on the laminates. A bottom laminate was placed on the shake table. After hydraulic filling process was completed, 2 Z-Potentiometers were placed on the ground. Figure 7.9 illustrates the instrumentation plan of Test 1.



(a)

(cont. on next page)

Figure 7.9 (cont.)



(b)

Figure 7.9. (a) Test 1 Side View of Instrumentation Plan, (b) Top View of Instrumentation Plan

7.3.1.3. Input Motions of Shake Table Test 1

To choose the most appropriate and consistent input motions is an important issue to be decided prior to doing shake table tests. The motion had to be large enough to produce liquefaction but not too large to be unsafe in the laboratory. Field evidence and calculations helped to choose the input motions.

- According to threshold strain, for shallower depths than 6m depth with very loose sand and water level at ground surface conditions, porewater pressure measuring starts when maximum acceleration (a_{max}) reaches 0.02-0.07g. (Dorby et al.,1982)
- In centrifuge tests, which were conducted at UC Davis, showed that liquefaction started when maximum acceleration (a_{max}) reached about 0.05g. (Arulanandan et al.,1983,1988)

The soil model was shaken for four times. Each shake has lasted for 12sec. Frequency did not change and it was 2Hz. The maximum displacement was 3.41mm for the first shake, 6.83mm for the second shake, 30mm for the third shake and 35mm for the fourth shake. Figure 7.10 illustrates the input motions of Test 1.

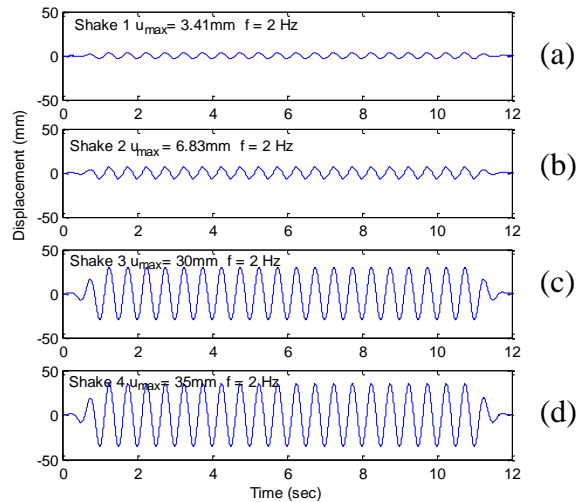


Figure 7.10. Input Motions of Test 1; (a) 1st Shake, (b) 2nd Shake, (c) 3rd Shake and (d) 4th Shake

7.3.1.4. Results of Shake Table Test 1

The instrument results were collected by the data acquisition system. The raw data from instrumentations contained a considerable amount of higher frequency noise. The filtering of these data was an important issue. Before evaluation of the data, filtration was needed.

7.3.1.4.1. Data Filtration

During shaking, data acquisition system collected data from the instruments by the LabView programme. These raw data contained a considerable amount of higher frequency noise. To reach the right results, data should be filtered. LabView filtration programme was used for this process.

LabView filtration programme consisted of two pages; Front panel and block diagram. The process of the filtration is explained below;

1. Data which were collected from instrumentations were read by *read from measurement file* button.
2. Signals were split.

3. *Split signals* button connected to *read from measurement file* button.
4. *Filter* function was constituted for each split signal.
5. Lowpass, highpass, bandpass, bandstop or smoothing are filtering types. One of the filter types was chosen (Figure 7.11). For accelerometers, bandpass filtration type was used. For bandpass filtration, low cut of frequency (Hz) and high cutoff frequency (Hz) were determined. The filtered data was controlled on configure filter page. For pore pressure transducers and potentiometers, lowpass filtration type was chosen. For lowpass filtration, cut of frequency (Hz) was determined.
6. Each split signal was connected to filter function.
7. *Write to measurement file* button was constituted for each instrumentation.
8. *Filter* button and *write to measurements file* button were connected.

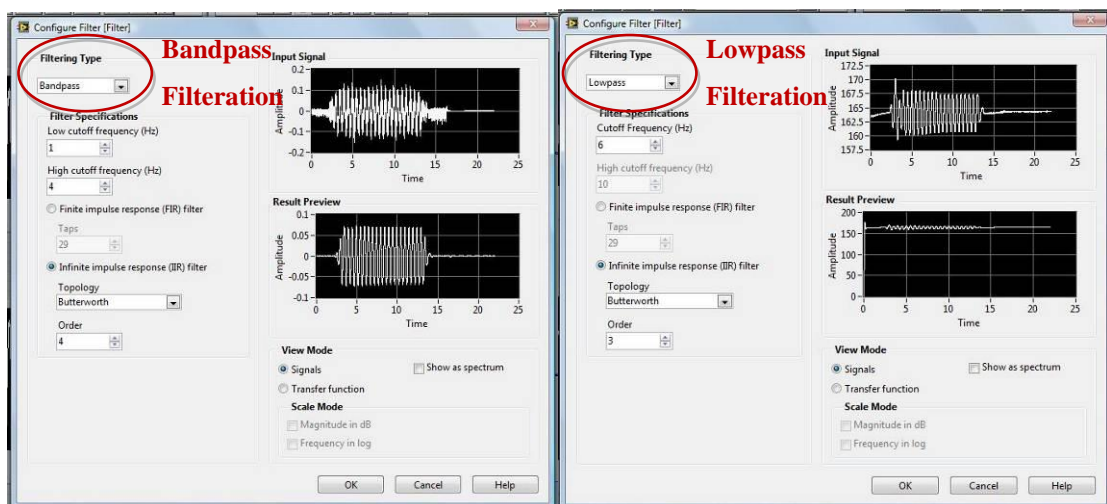


Figure 7.11. Print Screen of the LabVIEW Programme

9. To see the measured data and filter data on graphics, two graphics were created on the front panel for each split signal and the graphic icons appeared on the block diagram. Figure 7.12 illustrates the measured data and filter data on front panel and connection between buttons on the block diagram.
10. One of the graphic icon was tied to connection of split signal and filter icon. On the other hand, the other one was tied to connection of filter icon and write to measurement file.

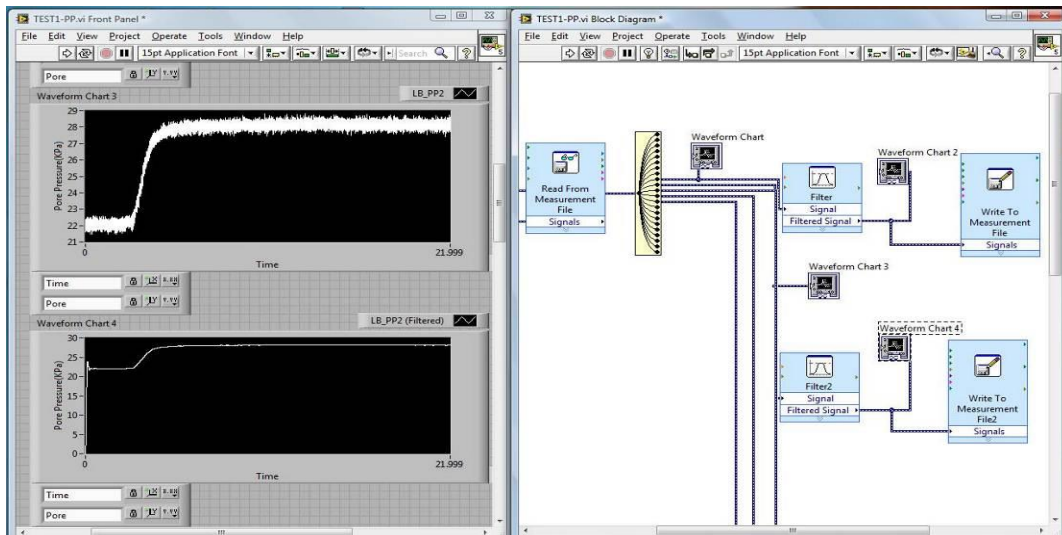


Figure 7.12. Print Screen of the Front Panel and Block Panel on the LabView Programme

The filter type depends primarily on the type of instrumentation. Filter type and values of low cutoff frequency, high cutoff frequency, lowpass frequency and Butterworth are illustrated in Table 7.2.

Table 7.2. Filter Type of Instrumentations

TEST NO	SHAKE NO	INST.	FILTER TYPE	LOW CUTOFF FREQUENCY (Hz)	HIGH CUTOFF FREQUENCY (Hz)	LOWPASS FREQUENCY (Hz)	BUTTERWORTH
Test 1	Shake 1	SA	Bandpass	1	4	-	4
		LA	Bandpass	1	4	-	4
		BA	Bandpass	1	4	-	4
		PP	Lowpass	-	-	6	3
	Shake 2	P	Lowpass	-	-	6	3
		SA	Bandpass	1	4	-	4
		LA	Bandpass	1	4	-	4
		BA	Bandpass	1	4	-	4
	Shake 3	PP	Lowpass	-	-	6	3
		P	Lowpass	-	-	6	3
		SA	Bandpass	0.5	5	-	4
		LA	Bandpass	0.5	5	-	4
	Shake 4	BA	Bandpass	0.5	5	-	4
		PP	Lowpass	-	-	3	3
		P	Lowpass	-	-	3	3
		SA	Bandpass	0.5	4	-	4
Test 2	Shake 1	LA	Bandpass	0.5	4	-	4
		BA	Bandpass	0.5	4	-	4
		PP	Lowpass	-	-	2.5	3
		P	Lowpass	-	-	2.5	3

(cont. on next page)

Table 7.2 (cont.)

		P	Lowpass	-	-	6	3
		SA	Bandpass	1	4	-	4
		LA	Bandpass	1	4	-	4
	Shake 2	BA	Bandpass	1	4	-	4
		PP	Lowpass	-	-	6	3
		P	Lowpass	-	-	6	3
		SA	Bandpass	0.6	4.5	-	4
		LA	Bandpass	0.6	4.5	-	4
	Shake 3	BA	Bandpass	0.6	4.5	-	4
		PP	Lowpass	-	-	4	3
		P	Lowpass	-	-	4	3
		SA	Bandpass	0.5	4	-	4
		LA	Bandpass	0.5	5	-	4
	Shake 4	BA	Bandpass	0.5	5	-	4
		PP	Lowpass	-	-	3	3
		P	Lowpass	-	-	3	3
		BA	Bandpass	1.5	3	-	4
	Shake 1	PP	Lowpass	-	-	6	3
		P	Lowpass	-	-	6	3
		BA	Bandpass	1	4	-	4
	Shake 2	PP	Lowpass	-	-	6	3
		P	Lowpass	-	-	6	3
		BA	Bandpass	0.6	4.5	-	4
	Shake 3	PP	Lowpass	-	-	4	3
		P	Lowpass	-	-	4	3
		BA	Bandpass	0.5	4	-	4
	Shake 4	PP	Lowpass	-	-	3	3
		P	Lowpass	-	-	3	3

Note: SA = Submersible Accelerometers, LA = Laminate Accelerometers, BA = Bottom Accelerometers, PP = Porewater Pressure Transducers, P = Potentiometers. It should be noted that some instrumentations failed during shaking.

7.3.1.4.2. Acceleration Response of the Soil Model

Submersible accelerometers were placed inside the soil model and acceleration histories were recorded at depths, 0.45m, 0.63m and 1.32m. The reading at 1.32m corresponded to that of the 2nd laminate, the reading at 0.63m corresponded to that of the 13th laminate, and the reading at 0.45m corresponded to that the 16th laminate.

Acceleration results, which were collected from the submersible accelerometers, were illustrated in Figure 7.13. SA1 was placed near the bottom. Therefore; SA1 result was closer to the input motion. Once the liquefaction occurs, soil will lose its stiffness. Hence, it is expected for acceleration to reduce. However, we did not see this kind of behavior. There could be two reasons for that 1. Rotation of the accelerometers during the liquefaction and 2. Wrong measure of the accelerometers. Submersible accelerometers were coated with silicon to protect the instrumentation from the pore water. During shake table tests, due to high water pressure inside the laminar box

submersible accelerometers were affected by the water and water infiltrated inside the sensors.

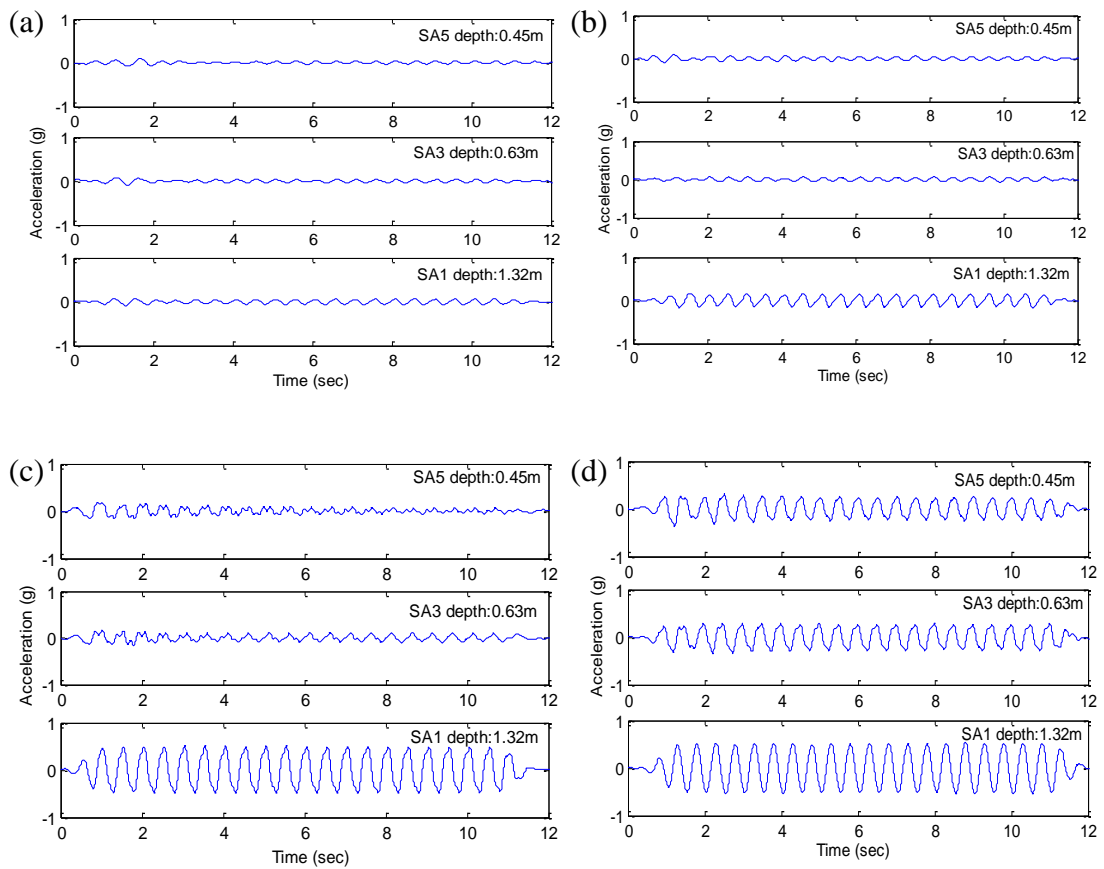


Figure 7.13. Test 1; (a) 1st Shake, (b) 2nd Shake, (c) 3rd Shake, (d) 4th Shake Acceleration Response from Submersible Accelerometers (SA5, SA3, SA1)

7.3.1.4.3. Acceleration Response of Laminates

Traditional accelerometers were attached on laminates to measure the displacement of the laminates during the shaking. Figure 7.14 displays the acceleration versus time graphics, which were recorded by the laminate accelerations.

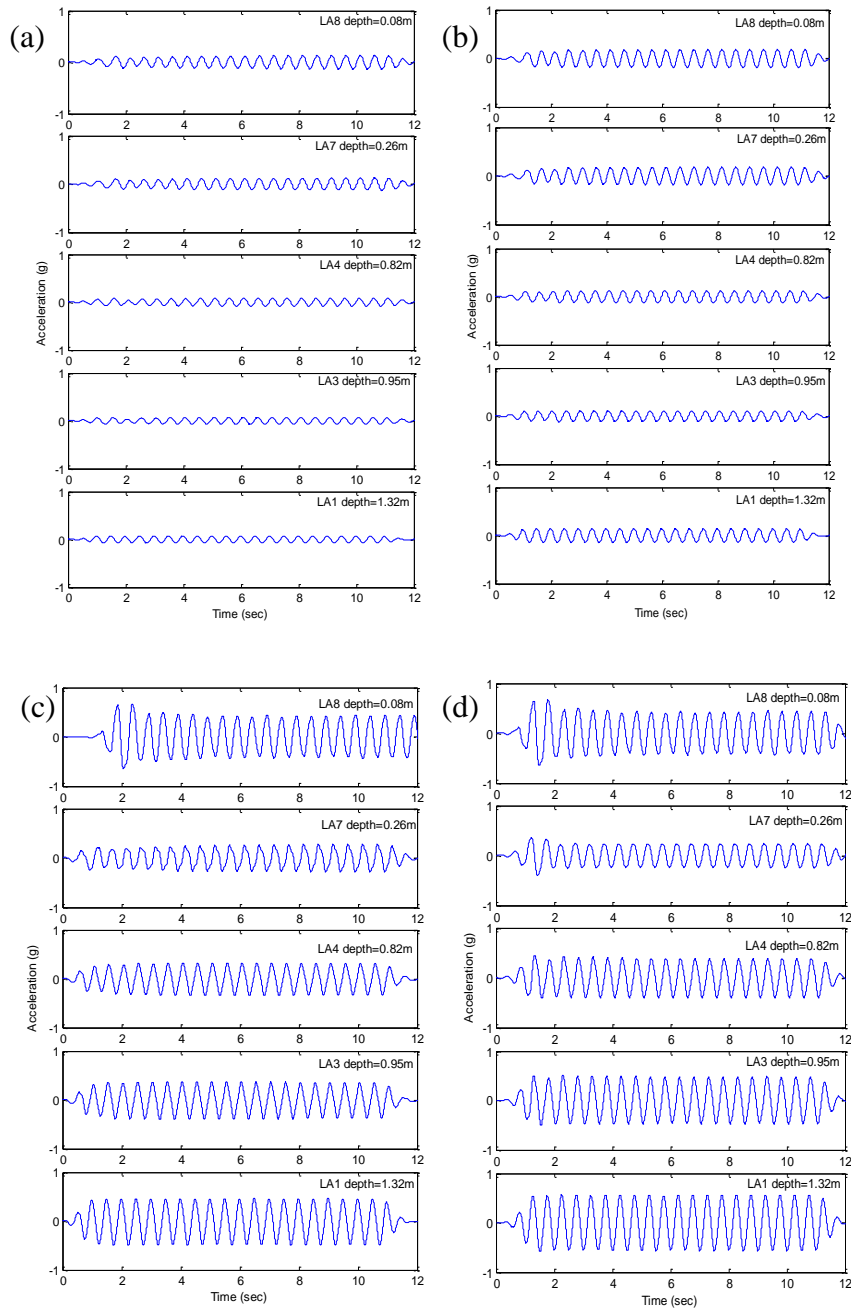


Figure 7.14. Test 1; (a) The 1st Shake, (b) The 2nd Shake, (c) The 3rd Shake, (d) The 4th Shake Acceleration Response from Laminate Accelerometers (LA8, LA7, LA4, LA3,LA)

These accelerometers were attached at the center of the laminates at depths; 0.08m, 0.26m, 0.82m, 0.95m and 1.32m, respectively. The reading at 1.32m depth has corresponded to that of the 2nd laminate. The reading at 0.95m depth has corresponded to that of the 8th laminate. The reading at 0.82m corresponded to that the 10th laminate. The reading at 0.26m depth has corresponded to that the 19th laminate and the reading at 0.08m depth has corresponded to that the 22nd laminate.

7.3.1.4.4. Excess Pore Water Pressure Response

Pore water pressure transducers were placed inside the soil at different depths to measure the excess pore water pressure during the shaking and just after the shaking. Figure 7.15 displays the excess pore water pressure at depths 0.45m, 0.63m, 0.76m, 1.07m and 1.32m in the same figure, during the shaking with the associated dissipation after the shaking.

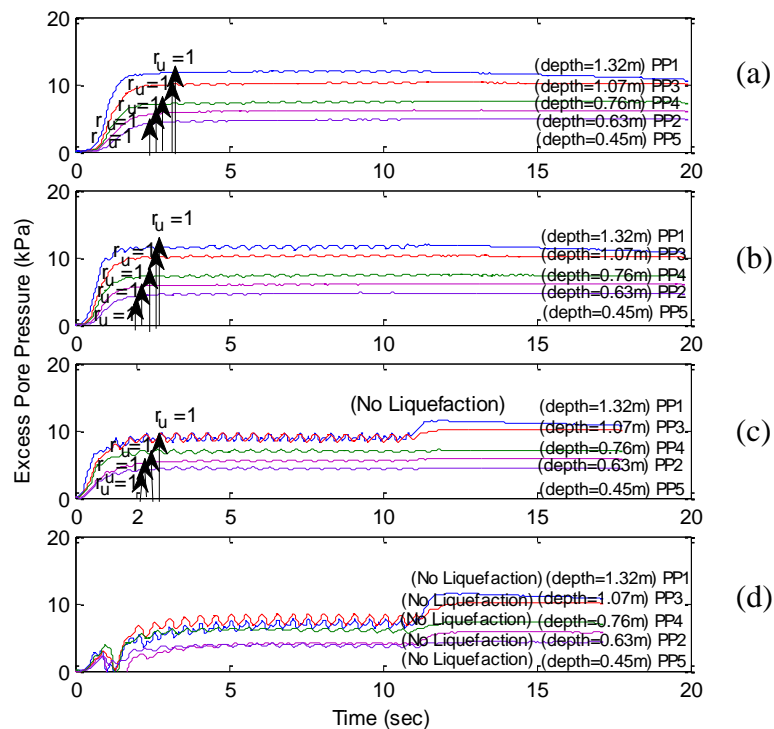


Figure 7.15. Test 1; (a) 1st Shake, (b) 2nd Shake, (c) 3rd Shake, (d) 4th Shake Excess Pore Water Pressure Response

Excess pore water pressures have and pore water pressure ratio has increased with time initially. After reaching a peak value, excess porewater pressure decreased or remained constant at the peak value. When the pore pressure ratio (r_u), reached the nearly 1, liquefaction occurred in the form of sand boils with eruption of ground water during the shaking or just after the shaking, The pore water pressure ratio (r_u) is given by the ratio of excess pore pressure (Δu) to the initial vertical effective stress (σ_{v0}').

$$r_u = \left(\frac{\Delta u}{\sigma'_{vo}} \right) \quad (7.2)$$

Where;

Δu = Excess pore pressure,

σ'_{vo} = Initial vertical effective stress.

The duration of the liquefaction decreased, when depth has increased. Pore pressure ratio ($r_u=1$) has indicated the liquefaction. The arrows in Figure 7.15 are used to illustrate the initiation time of the liquefaction and Table 7.4 illustrates the duration of the liquefaction. As illustrates in Figure 7.15, liquefaction resistance has increases with depth during the shaking event. Liquefaction observed at the bottom of the soil model (PP5) initially then at PP2, PP4, PP3 and PP1, respectively. Table 7.4 also demonstrates that the number of cycles required to trigger liquefaction during the 1st shake was considerably larger than that required to trigger liquefaction during the 2nd shake. The number of cycles required to trigger liquefaction during the 2nd shake was larger than that required to trigger liquefaction during the 3rd shake. During the 4th shake, the soil model did not develop excess pore pressure large enough to liquefy the sand at all depths. If there was not liquefaction, it was noted in Table 7.3 as No-Liq (No Liquefaction) has occurred. This figure illustrates the effectiveness of the laminar box system.

Table 7.3. Summary of Test 1

Fines Content = 0%											
Shaking Number	Pore Pressure Name	Depth	PGA	(PGA) _{eq}	Input max. displacement	Frequency	Duration	Time for liquefaction	N _L	Initial D _r	q _c
-	-	m	g	g	mm	Hz	sec	sec	-	%	
Shake_1	PP-1	1.32	0.05	0.08	3.4	2	12	3.2	6.4	33	315
	PP-3	1.07	0.05	0.08	3.4	2	12	3.1	6.2	31	265
	PP-4	0.76	0.05	0.08	3.4	2	12	3.0	6	36	271
	PP-2	0.63	0.05	0.08	3.4	2	12	2.9	5.8	43	309
	PP-5	0.45	0.05	0.08	3.4	2	12	2.7	5.4	41	264
Shake_2	PP-1	1.32	0.11	0.17	6.83	2	12	2.8	5.6	60	831
	PP-3	1.07	0.11	0.17	6.83	2	12	2.6	5.2	44	424
	PP-4	0.76	0.11	0.17	6.83	2	12	2.4	4.8	59	625
	PP-2	0.63	0.11	0.17	6.83	2	12	2.3	4.6	56	516
	PP-5	0.45	0.11	0.17	6.83	2	12	2.2	4.4	47	319
Shake_3	PP-1	1.32	0.48	0.74	25	2	12	No-Liq	NL	86	2028
	PP-3	1.07	0.48	0.74	25	2	12	2.6	5.2	57	711
	PP-4	0.76	0.48	0.74	25	2	12	2.3	4.6	53	505
	PP-2	0.63	0.48	0.74	25	2	12	2.2	4.4	54	487
	PP-5	0.45	0.48	0.74	25	2	12	2.1	4.2	58	471
Shake_4	PP-1	1.32	0.56	0.86	30	2	12	No-Liq	No-Liq	76	1354
	PP-3	1.07	0.56	0.86	30	2	12	No-Liq	No-Liq	73	1223
	PP-4	0.76	0.56	0.86	30	2	12	No-Liq	No-Liq	58	619
	PP-2	0.63	0.56	0.86	30	2	12	No-Liq	No-Liq	63	661
	PP-5	0.45	0.56	0.86	30	2	12	No-Liq	No-Liq	69	673

Note; PGA=Peak Ground Acceleration, $PGA_{(eq)}$ =Equivalent Peak Ground Acceleration, N_L=Cyclic for Liquefaction, D_r=Relative Density, q_c=Cone Tip Resistance

7.3.1.4.5. Displacement Response of the Laminates

X-Potentiometers were attached on the laminates to measure the lateral displacement of the laminates. Figure 7.16 shows the horizontal displacement histories of the laminates at depths 0.63m, 0.76m, 0.82m, 0.95m, 1.07m, 1.20m and 1.32m.

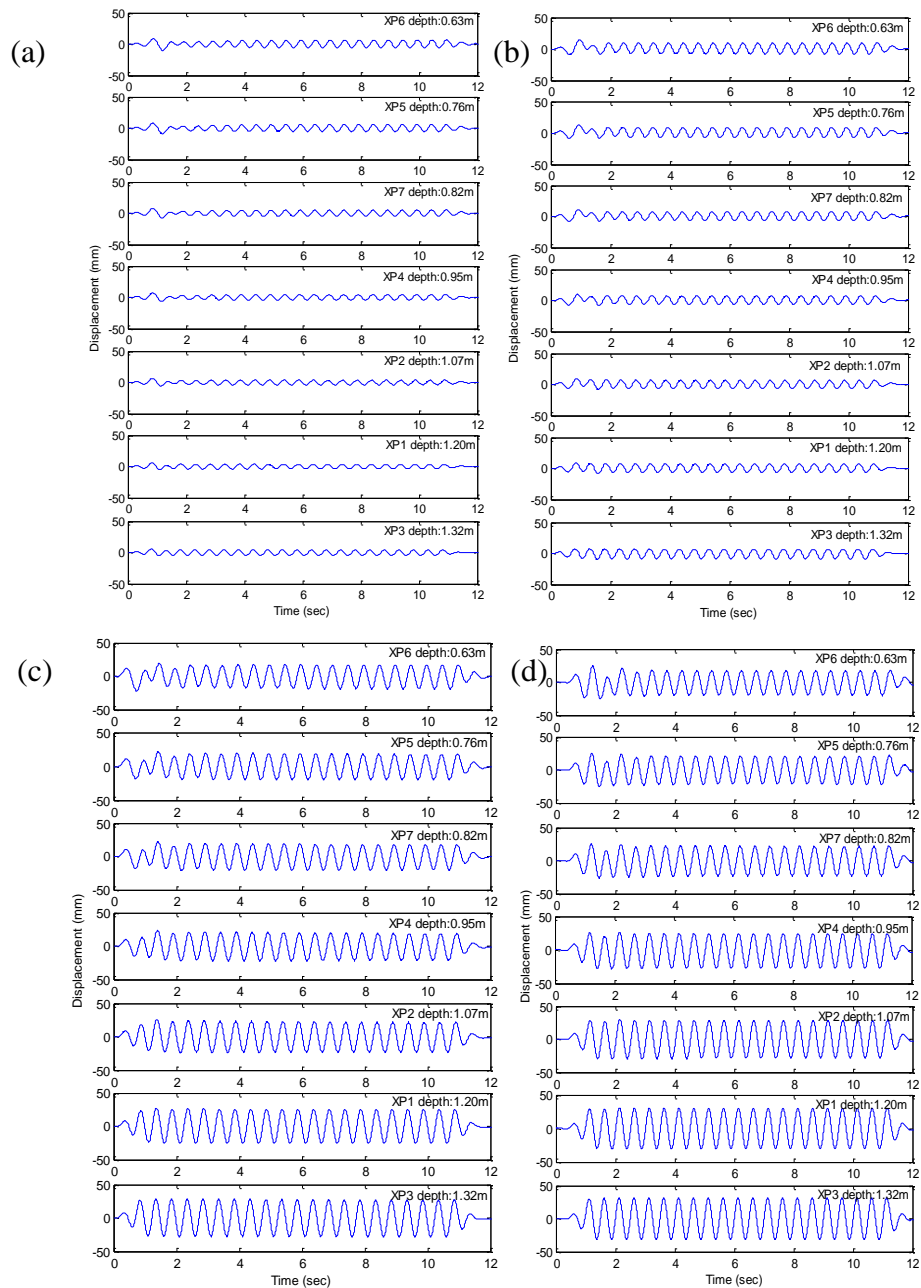


Figure 7.16. Test 1; (a) 1st Shake, (b) 2nd Shake, (c) 3rd Shake, (d) 4th Shake Displacement Responses (XP6 , P5, XP7, XP4, XP2, XP1, XP3)

The readings at 1.32m, 1.20m, 1.07m, 0.95, 0.82m, 0.76m and 0.63m depths corresponded to that of the 2nd, the 4th, the 6th, the 8th, the 10th, the 11th and the 13th laminates, respectively.

7.3.1.4.6. Settlement Response

While shaking or just after shaking, sand boils were observed on the surface of the soil model. Surface settlement is often related to appearance of sand boils. Surface of the soil model was completely submerged and the soil model settled. In this research, settlement of the ground was measured with two methods. 1) Z-Potentiometers placed on the ground surface; 2) Settlement of the ground was measured manually.

Two LPM 100 Z-Potentiometers were placed on the ground surface to measure the settlement during and after the shaking at two different locations. After the shaking has ended, the settlement was continued to be recorded with a new time scale. Figure 7.4 displays the ground surface settlement during and after the shaking at two different locations on the ground surface. The potentiometers can measure a maximum of 10cm settlement. Thus, these potentiometers were not enough to measure the settlement after the first shake. Post shake settlement was greater than the settlement during the prior shaking. Nearly 36% of the total settlement has occurred during the shaking and nearly 64% of the settlement was occurred after the shaking (Table 7.4). These results have showed that after liquefaction, the consolidation of the soil model has increased.

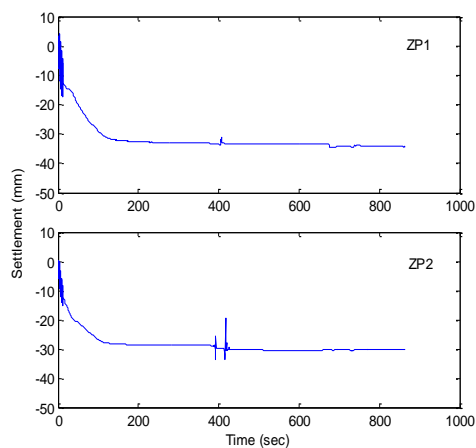


Figure 7.17. Test 1; 1st Shake Settlement Results

Table 7.4. Test 1; Ground Surface Settlement Measured by the Potentiometer

Ground Settlement Measured by Potentiometer			
	During Shake	Post Shake	Total Settlement
	<i>cm</i>	<i>cm</i>	<i>cm</i>
Shake 1	1.31	2.30	3.61
Shake 2	-	-	-
Shake 3	-	-	-
Shake 4	-	-	-

The height of the soil model was measured at three fixed locations (west side, east side and middle side) with a tape measure and the height of the soil model was measured again before the following shake (Figure 7.5). To find the settlement of the ground, the second measurement was subtracted from the first measurement.

Table 7.5. Test 1; Ground Settlement Measured Manually

Ground Settlement Measured Manually					
	West Side	Middle Side	East Side	Average Settlement	Vertical Strain
	<i>cm</i>	<i>cm</i>	<i>cm</i>	<i>cm</i>	<i>%</i>
Shake 1	4.40	6.10	4.90	5.13	4.36
Shake 2	4.60	4.90	3.60	4.37	3.66
Shake 3	4.00	3.10	2.60	3.23	2.40
Shake 4	3.00	2.00	2.50	2.50	1.59

Average settlement was used to determine the vertical strain of the soil model. Thus, after the manual measurement and the measurement by the potentiometer, an average settlement was calculated the average to find the settlement.

The vertical strain (ϵ) of a soil model is given by the ratio of ΔH to the original sample height H_0 .

$$\epsilon = \frac{\Delta H}{H_0} = \frac{s}{H_0} \quad (7.2)$$

Where;

ϵ = Vertical strain,

ΔH = Vertical deformation,

H_0 = Original height of the soil model,

s = Settlement

7.3.1.4.7. Cross Comparison between Instruments

To check the reliability of the instrumentation data, first, the acceleration histories measured by the laminate accelerometer (LA4) and displacement histories measured by the potentiometer (XP7) were compared. LA4 and XP7 were attached on the 10th laminate. A comparison of the acceleration data recorded by LA4 and derivative of the XP7 potentiometer data are shown in Figure 7.18.

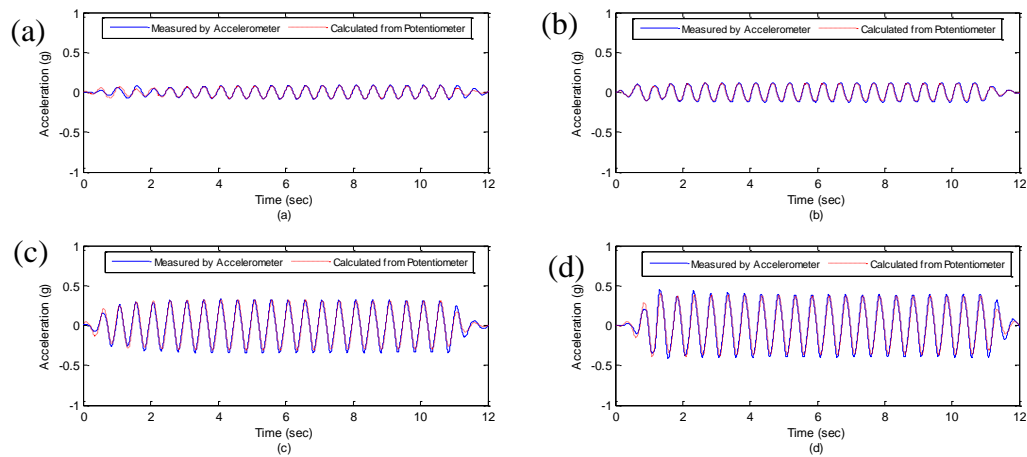


Figure 7.18. (a) The 1st Shake, (b) The 2nd Shake, (c) The 3rd Shake, (d) The 4th Shake, Comparison of LA4 and XP7

Second, the acceleration histories, which were measured by the laminate accelerometer (LA1) and the submersible accelerometer (SA1) and derivative of the displacement histories were measured by potentiometer (XP3) were compared. Comparisons are displayed on Figure 7.19. It's seen that LA1 and XP3 which were attached on the 2nd laminate and SA1 were placed inside the soil model at the same depth with LA1 and XP3 are high quality.

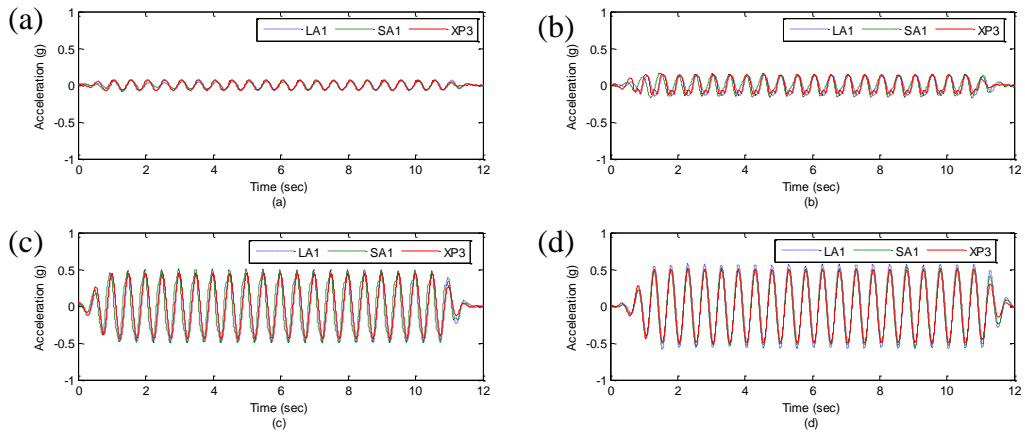


Figure 7.19. Test 1; (a) The 1st Shake, (b) The 2nd Shake, (c) The 3rd Shake, (d) The 4th Shake Comparison of SA1, LA1 and XP3

Third, figure 7.20 displays the comparison of acceleration histories measured by the bottom acceleration (BA1) and input motion, which was given to the shake table. These comparison figures show that; the agreement of histories which were supplied from different type of instrumentations are of high quality.

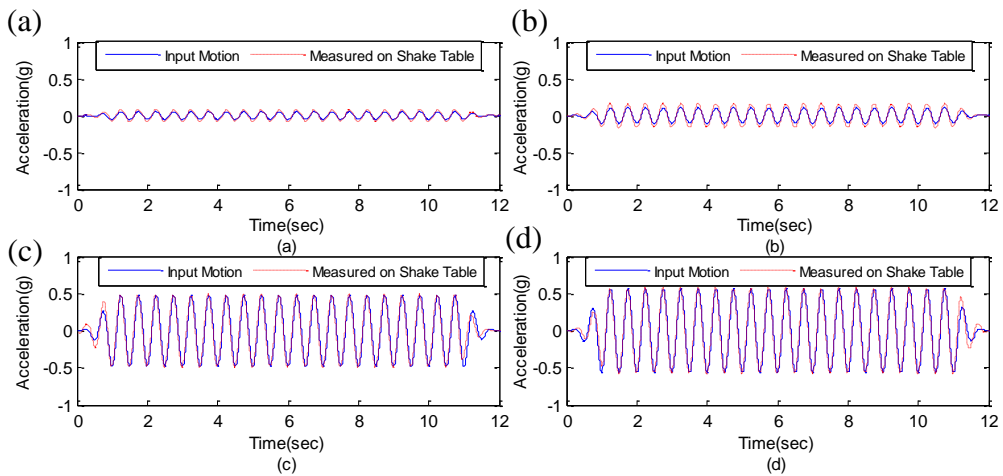


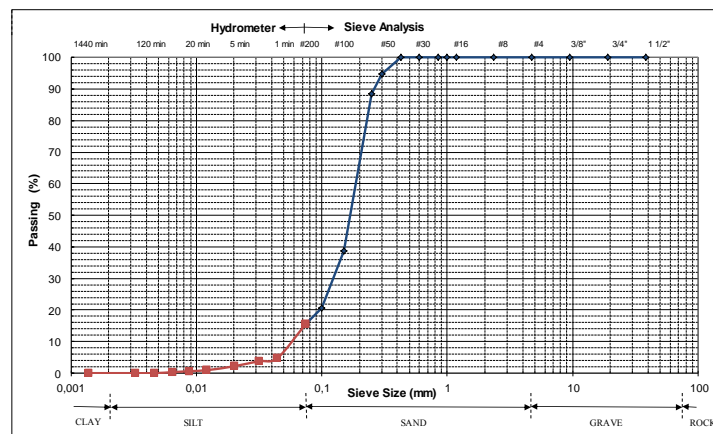
Figure 7.20. Test 1; (a) The 1st Shake, (b) The 2nd Shake, (c) The 3rd Shake, (d) The 4th Shake Comparison of BA1 and Input Motion

7.3.2. Shake Table Test 2

Second shake table tests were conducted at IZTECH on July 10th, 2012 with silty sand. The fines content of the soil model was 15%. Height of the soil model was 1.44m. The soil model was shaken for four times to study the reliquefaction occurrence.

7.3.2.1. Soil Properties

The model consisted of 1.44m thick saturated silty sand deposit built using hydraulic filling model. Test 2 was conducted with 15% silty sand. Figure 7.21 summarizes the index properties of this soil model and its grain size distribution curve. SM was the symbol of soil model based on the unified soil classification system (USCS).



D_{10}	D_{30}	D_{60}	C_u	C_c
mm	mm	mm	-	-
0.06	0.11	0.20	1.82	1.01

	e_{min}	e_{max}	G_s	γ_{sat}	w
	-	-	-	KN/m ³	%
Test2	0.45	0.92	2.59	19.27	28.8

Figure 7.21. Grain Size Distribution for Silty Sand and Soil Properties with 15% Fines Content

C_u (uniformly coefficient) and C_c (coefficient of gradation) were calculated from the grain size distribution curve. Also, D_{10} , D_{30} and D_{60} were determined from the grain size distribution curve.

SEM image, which was taken by scanning electron microscope (SEM), gave information about the grain shape. Soils contain angular particles and rounded particles. Soils with rounded shapes are usually more susceptible to liquefaction than angular grained soils. Soil samples were magnified 100 times; these images are illustrated in Figure 7.22.

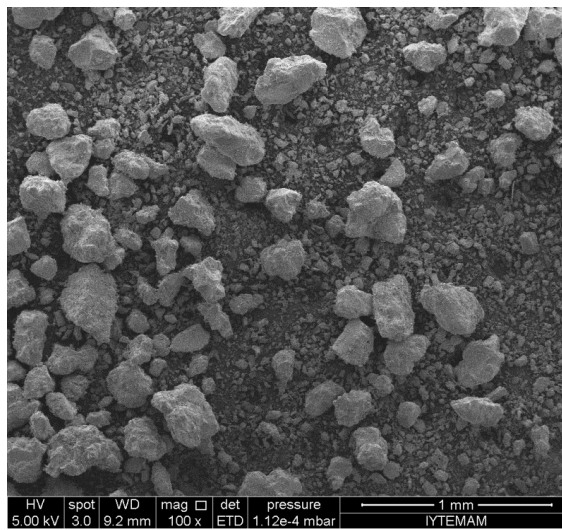
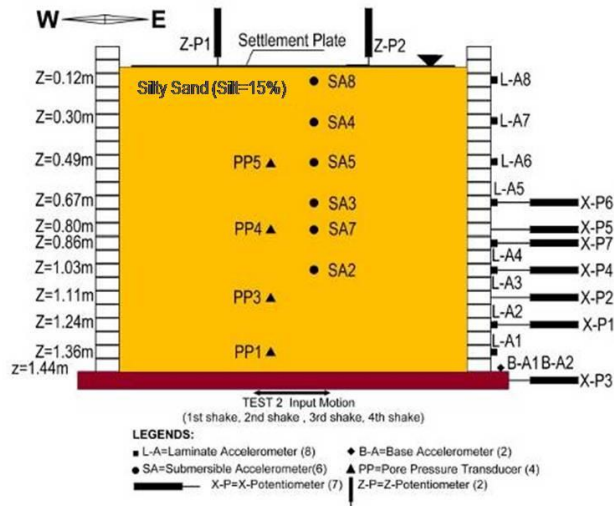


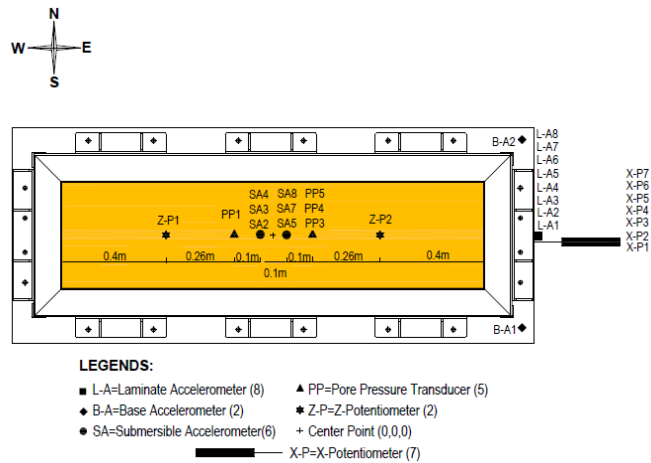
Figure 7.22. SEM Image of Soil Sample with 15% Fines Content

7.3.2.2. Instrumentation Plan of Test 2

Pore pressure transducers and submersible accelerometers were placed inside the soil model before the hydraulic filling process was started. Laminate accelerometers and X-Potentiometers were attached on the laminates. 2 bottom accelerometers were placed on the shake table. After the hydraulic filling process was completed, 2 Z-Potentiometers were placed on the ground to measure the settlement of the ground. Figure 7.23 illustrates instrumentation plan of the 2nd test.



(a)



(b)

Figure 7.23. (a) Test 2 Side View of Instrumentation Plan, (b) Top View of Instrumentation Plan

7.3.2.3. Input Motions of Test 2

The soil model was shaken for 4 times. Each shake lasted for 12 seconds except the second shake. The second shake lasted for 4.3 seconds, due to problem at the shake table. Frequency did not change. It was 2 HZ. The maximum displacement was 2.5mm for the 1st shake, 5mm for the 2nd shake, 20mm for the 3rd shake and 30mm for the 4th shake (Figure 7.24).

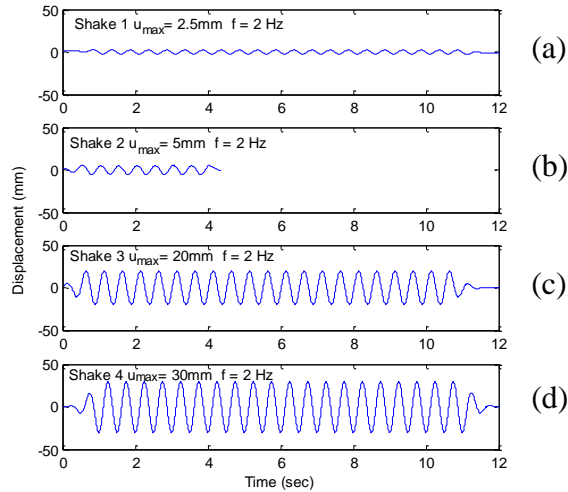


Figure 7.24. Test 2; Input Motion of the (a) 1st Shake, (b) 2nd Shake, (c) 3rd Shake and (d) 4th Shake

7.3.2.4. Results of Test 2

Data was collected by submersible accelerometers, traditional accelerometers, pore pressure transducers and potentiometers, but the raw data contained considerable amount of higher frequency noise. These raw data should be filtered before any the evaluation is made. Filtration process was presented in (Section 7.3).

7.3.2.4.1. Acceleration Response of the Soil Model

Submersible accelerometers were placed inside the soil at different depths. Figure 7.25 illustrates the accelerations at depths, 0.12m, 0.30m, 0.49m, 0.67m, 0.80m and 0.99m. These accelerations data were recorded by the submersible accelerometers which were placed inside the soil. The reading at 0.99m, 0.80m, 0.67m, 0.49m, 0.30m and 0.12m corresponded to that of the 8th laminate, the 11th laminate, the 13th laminate, the 16th laminate, the 19th laminate and the 22nd laminate, respectively.

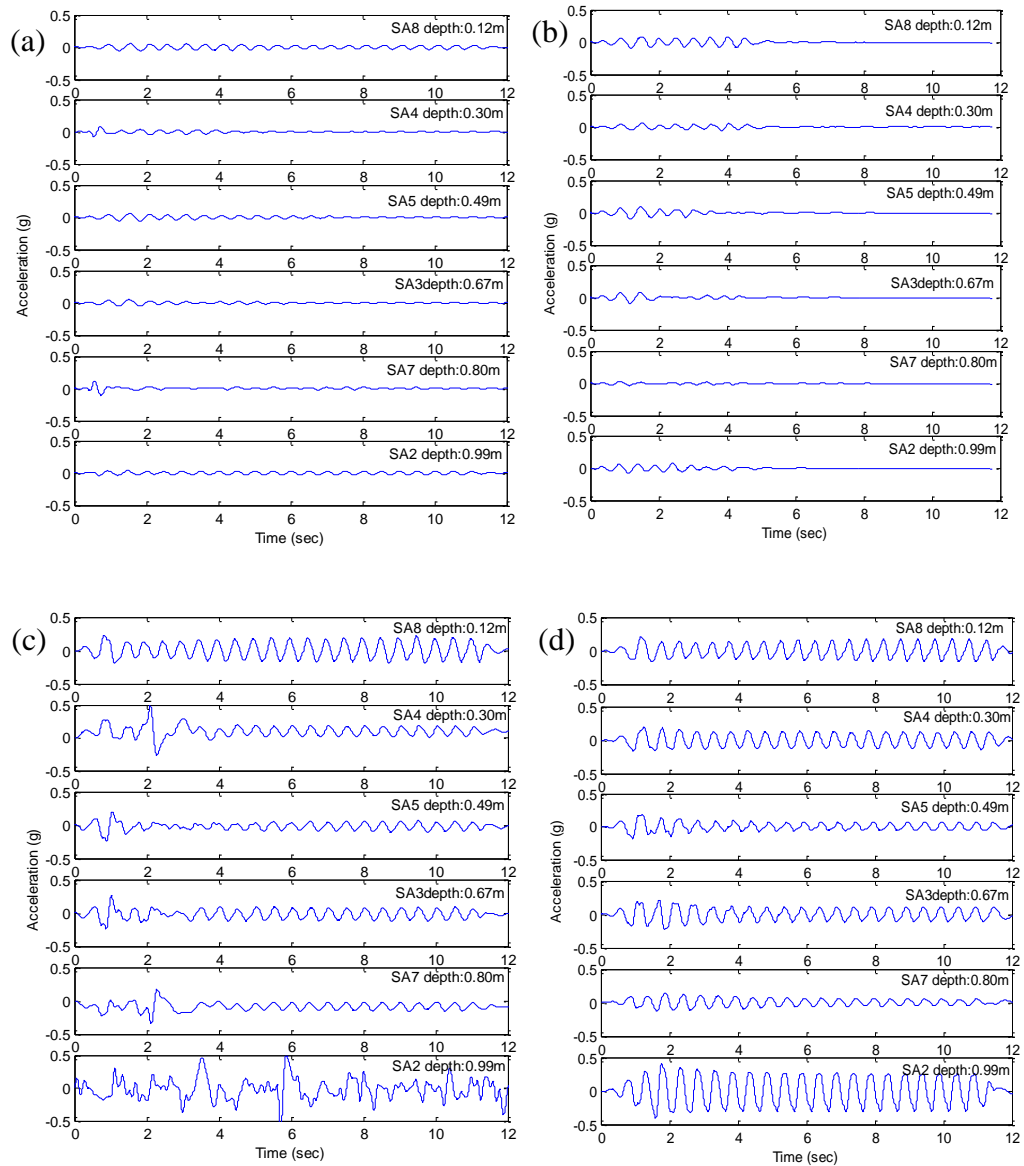


Figure 7.25. Test 2; (a) 1st Shake, (b) 2nd Shake, (c) 3rd Shake, (d) 4th Shake Acceleration Response from Submersible Accelerometers (SA8, SA4, SA3, SA7, SA2)

After initiation of the liquefaction, submersible accelerometers did not give the expected results. Accelerometers might have rotated or measured wrong data.

7.3.2.4.2. Acceleration Response of the Laminates

Traditional accelerometers were attached on the laminates to measure the acceleration response of the laminates during the shaking. Figure 7.26 displays the

acceleration versus time graphics which were recorded by the laminate accelerations. These accelerometers were attached to the center of the laminates at depth, 0.12m, 0.30m, 0.49m, 0.67m, 0.86m, 0.99m, 1.24m and 1.32m.

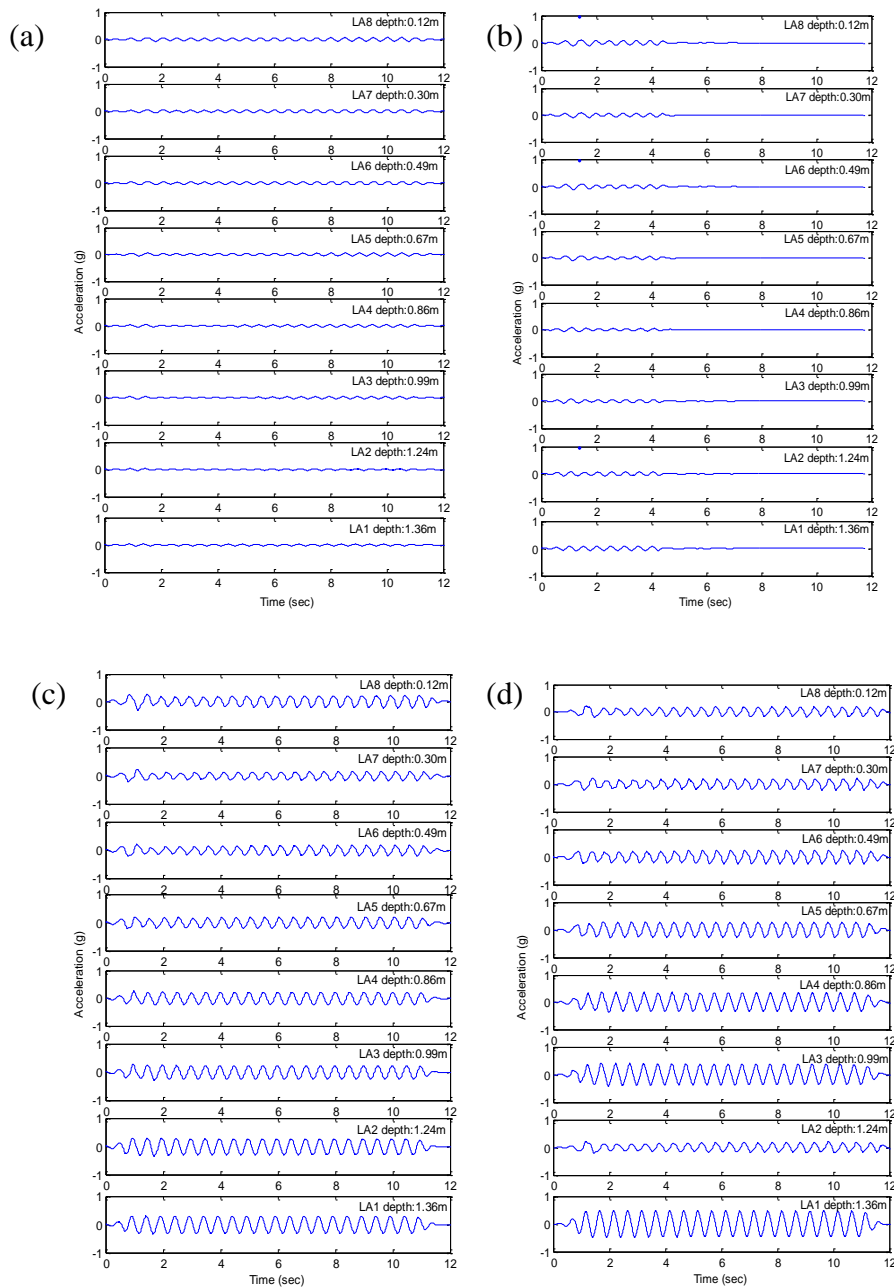


Figure 7.26. Test 2; (a) 1st Shake, (b) 2nd Shake, (c) 3rd Shake, (d) 4th Shake Acceleration Response from Laminate Accelerometers (LA8, LA7, LA6, LA5, LA4, LA3, LA2, LA1)

The reading at 1.32m, 1.24m, 0.99m, 0.86m, 0.67m, 0.49m, 0.30m and 0.12m depths corresponded to that of the 2nd laminate, the 4th laminate, the 8th laminate, the

10th laminate, the 13th laminate, the 16th laminate, the 19th laminate and the 22nd laminate, respectively. Laminate accelerometers were reliable.

7.3.2.4.3. Excess Pore Water Pressure Response

Pore pressure transducers were placed inside the soil at different depths to measure the excess pore water pressures during the shaking and just after the shaking. Figure 7.27 illustrates the excess pore water pressure at depths of 0.49m, 0.80m, 1.11m and 1.36m, during shaking and the associated dissipation after shaking. The reading at 1.36m depths has corresponded to that of the 2nd laminate, the reading at 1.11m corresponded to that of the 6th laminate, the reading at 0.80m depth has corresponded to that of the 11th laminate and the reading at 0.49m depth has corresponded to that of the 16th laminate.

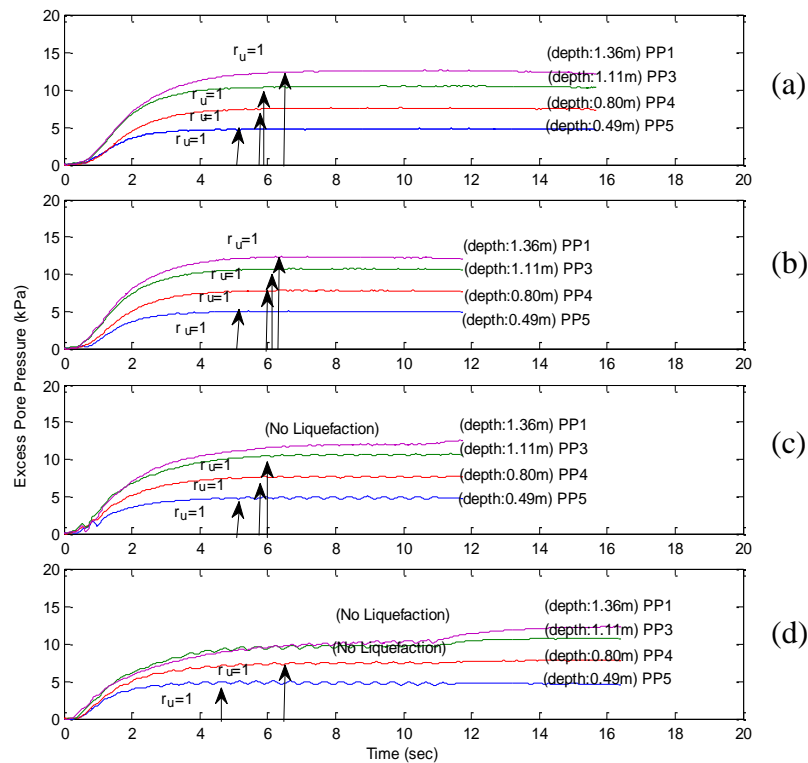


Figure 7.27. Test 2; (a) 1st Shake, (b) 2nd Shake, (c) 3rd Shake and (d) 4th Shake Excess Pore Pressure Response

Excess pore water pressure has increased initially after reaching a peak value and it remained constant. The arrows in Figure 7.27 are used to illustrate the initiation time of the liquefaction event and Table 7.6 illustrates the duration of the liquefaction. As illustrated in Figure 7.27, liquefaction resistance increases with depth during the shaking event. Liquefaction was observed at the bottom of the soil model (PP5) initially then PP4, PP3 and PP1, respectively. The soils, which were closer to bottom, were not weak as much as the above soil. Therefore, the duration of liquefaction has decreased when depth increased Table 7.11 also demonstrates that the number of cycles required to trigger liquefaction during 1st shake was considerably larger than that required to trigger liquefaction during the 2nd shake. The number of cycles required to trigger liquefaction during the 2nd shake was larger than that required to trigger liquefaction during the 3rd shake. During the 4th shake, the soil model did not develop excess pore pressure large enough to liquefy the sand at some depths. If there was not liquefaction, it was noted on Table 7.6 like as No-Liq (No Liquefaction).

Table 7.6. Summary of Test 2

Fines Content = 15%											
Shaking Number	Pore Pressure Name	Depth	PGA	(PGA) _{eq}	Input max. displacement	Frequency	Duration	Time for liquefaction	N _L	Initial D _r	q _c
-	-	m	g	g	mm	Hz	sec	sec	-	%	kPa
Shake_1	PP-1	1.36	0.04	0.06	2.5	2	12	7	14	36	253
	PP-3	1.11	0.04	0.06	2.5	2	12	6.3	12.6	36	253
	PP-4	0.8	0.04	0.06	2.5	2	12	6.2	12.4	36	253
	PP-5	0.49	0.04	0.06	2.5	2	12	5.4	10.8	32	185
Shake_2	PP-1	1.36	0.08	0.12	5	2	4.3	6.4	12.8	47	458
	PP-3	1.11	0.08	0.12	5	2	4.3	6.2	12.4	47	458
	PP-4	0.8	0.08	0.12	5	2	4.3	6	12	34	284
	PP-5	0.49	0.08	0.12	5	2	4.3	5.4	10.8	30	167
Shake_3	PP-1	1.36	0.34	0.52	20	2	12	7.9	15.8	65	957
	PP-3	1.11	0.34	0.52	20	2	12	6.2	12.4	68	957
	PP-4	0.8	0.34	0.52	20	2	12	5.8	11.6	56	530
	PP-5	0.49	0.34	0.52	20	2	12	5.4	10.8	36	276
Shake_4	PP-1	1.36	0.49	0.75	30	2	12	No-Liq	No-Liq	56	881
	PP-3	1.11	0.49	0.75	30	2	12	No-Liq	No-Liq	49	541
	PP-4	0.8	0.49	0.75	30	2	12	6.7	13.4	57	631
	PP-5	0.49	0.49	0.75	30	2	12	4.6	9.2	20	212

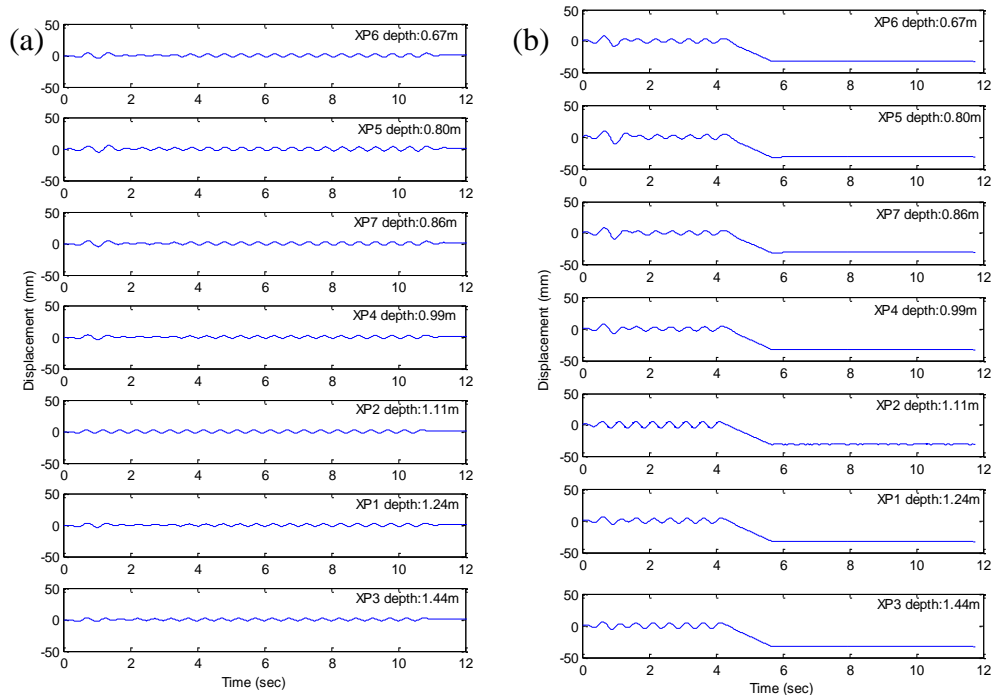
Note; PGA=Peak Ground Acceleration, PGA_(eq)=Equivalent Peak Ground Acceleration, N_L=Cyclic for Liquefaction, D_r=Relative Density, q_c=Cone Tip Resistance

7.3.2.4.4. Potentiometer

Z-Potentiometers and X-Potentiometers were used in Test 2. Z-Potentiometers were measured settlement of the ground. Two LPM 300 Z-Potentiometers were placed on ground surface, their capacity were enough to measure the settlement of the ground because they can measure maximum 30cm. X-Potentiometers measured the displacement of the laminates, horizontally.

7.3.2.4.5. Horizontal Displacement Performance of the Laminates

X-Potentiometers were placed on the laminates to measure the horizontal displacement of the laminates. Figure 7.28 illustrates the horizontal displacement histories of the laminates at depths 1.44m, 1.24m, 1.11m, 1.03m, 0.86m, 0.80m and 0.67m. One of the X-Potentiometer was placed on the shake table to compare the input motions. The readings at 1.24m, 1.11m, 1.03, 0.86, 0.80m and 0.67m depths has corresponded to that of the 4th, the 6th, the 8th, the 10th, the 11th and the 13th laminates, respectively.



(cont. on next page)

Table 7.28 (cont.)

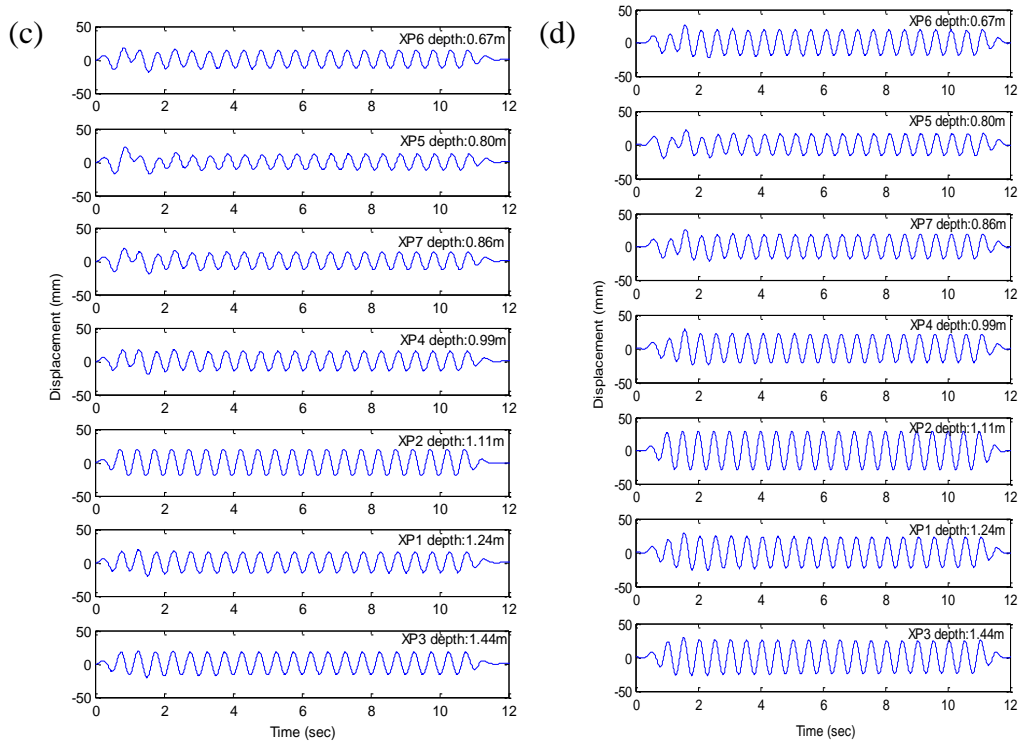


Figure 7.28. Potentiometer Results (a) 1st Shake, (b) 2nd Shake, (c) 3rd Shake, (d) 4th Shake (XP6, XP5, XP7, XP4, XP2, XP1, XP3)

7.3.2.4.6. Ground Surface Settlement Response

Two LPM 300 Z-Potentiometers were placed on the ground surface to measure the settlement at two different locations. Figure 7.29 displays the locations of the potentiometers on the ground surface.



Figure 7.29. Z-Potentiometers

Figure 7.30 displays the ground surface settlement data during and after the shaking at two different locations on the ground surface. After the shaking has ended, the settlements were measured for shortly after, but with a new time scale.

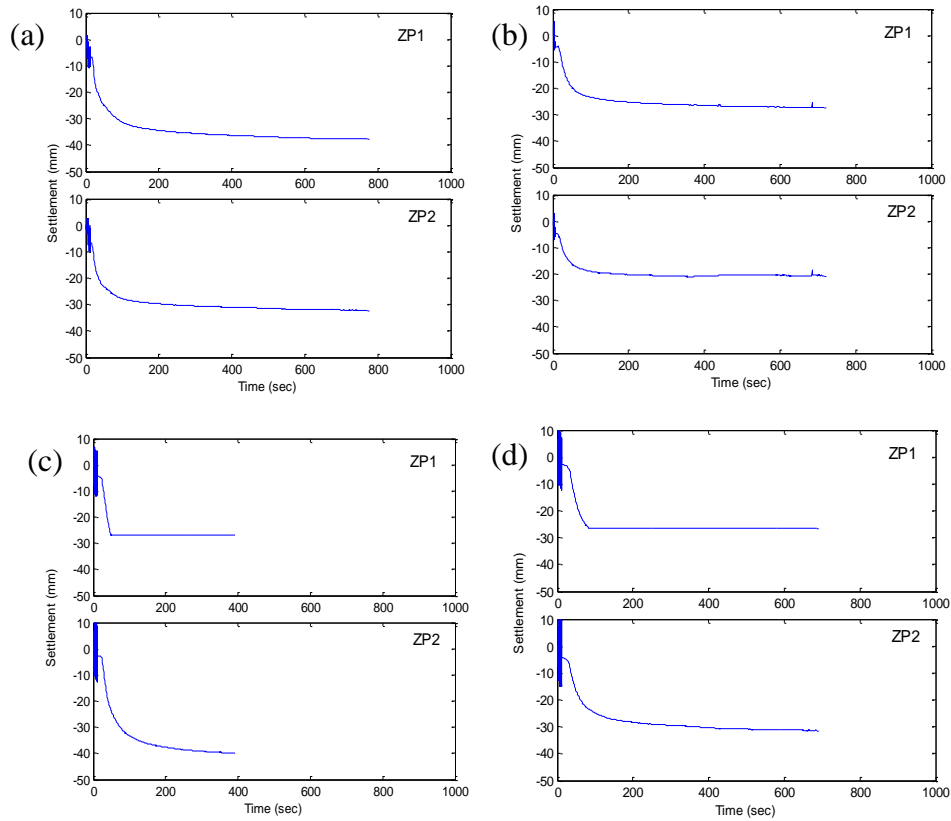


Figure 7.30. Test 2; (a) 1st Shake, (b) 2nd Shake, (c) 3rd Shake, (d) 4th Shake Settlement Response (ZP1, ZP2)

When settlement during a shake and settlement during post shake were compared, settlement post shake was more than the settlement during shaking. Table 7.7 shows the values of settlement during and after the shake. Nearly %16 of the total settlement were occurred during shaking, nearly %84 of the total settlement were occurred after shaking. This result showed that after the liquefaction occurred, the consolidation of the soil model increased.

The manual measurement and the measurement potentiometer were averaged to determine the average ground surface settlement (Table 7.8). The vertical strain (ϵ) of a soil model is displayed in Table 7.8. The ratio of ΔH to the original sample height H_0 gives the vertical strain.

Table 7.7. Ground Settlement Measured by Potentiometer

Ground Settlement Measured by Potentiometer			
	During Shake	Post Shake	Total Settlement
	<i>cm</i>	<i>cm</i>	<i>cm</i>
Shake 1	0.76	2.79	3.55
Shake 2	0.45	1.96	2.41
Shake 3	0.36	2.99	3.35
Shake 4	0.37	2.53	2.90

Table 7.8. Ground Settlement Measured by Potentiometer

Ground Settlement Measured Manually					
	West Side	Middle Side	East Side	Average Settlement	Vertical Strain
	<i>cm</i>	<i>cm</i>	<i>cm</i>	<i>cm</i>	<i>%</i>
Shake 1	4.60	4.70	4.30	4.53	3.26
Shake 2	3.10	2.00	2.00	2.37	1.44
Shake 3	2.60	1.90	1.90	2.13	1.38
Shake 4	2.90	3.20	3.10	3.07	2.36

7.3.3. Shake Table Test 3

Third shake table tests were conducted at IZTECH on September 27th, 2012 with silty sand with less than 25% silt percentage. The height of the soil model was 1.44m. The soil model was not uniform because hydraulic filling method was not suitable for 25% silt content. Test 3 also consisted of four subsequent shakes to evaluate reliquefaction. Input motions were nearly same as Test 1 and Test 2.

7.3.3.1. Soil Properties

The model consisted of 1.44m thick saturated silty sand deposit built by hydraulic filling method. Soil model was prepared with 25% fines content in preparation boxes but fines content was variable in the laminar box. 6 samples were

taken from buckets during bucket density test to conduct sieve analysis. According to these sieve analysis results, the soil model was not uniform, it was variable. Figure 7.31 illustrates the fines content of soil model at 21cm, 49cm, 72cm, 78cm, 93cm and 105cm depths. Average fines content of the Test 3 assumed 25%.

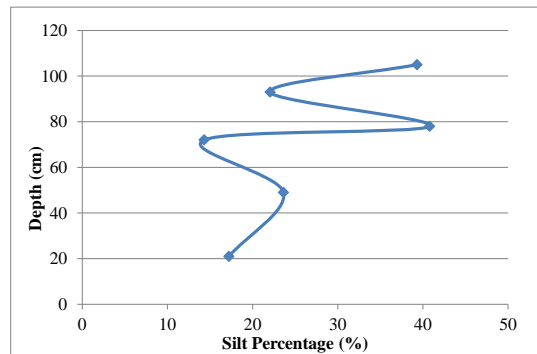
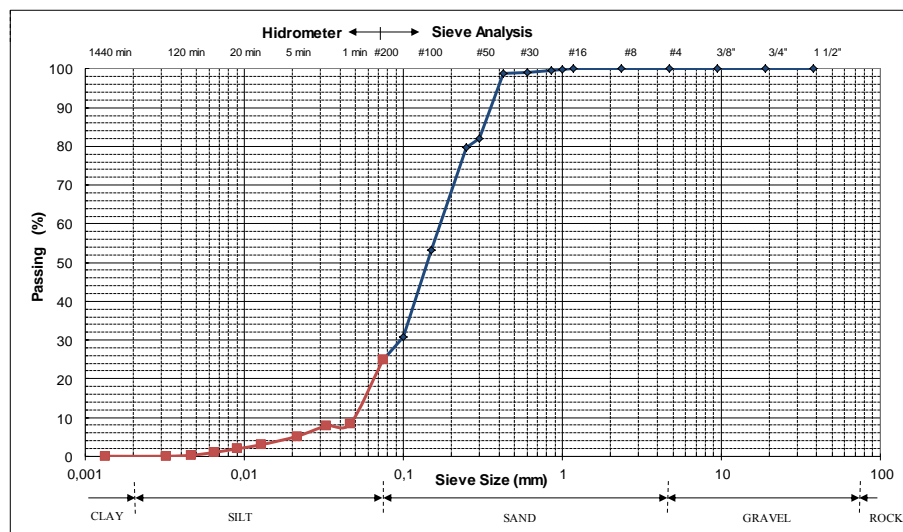


Figure 7.31. Fines Content of the Soil Model in the Laminar Box



D_{10}	D_{30}	D_{60}	C_u	C_c
<i>mm</i>	<i>mm</i>	<i>mm</i>	-	-
0.05	0.10	0.18	1.8	1.11

(cont. on next page)

Table 7.32 (cont.)

	e_{min}	e_{max}	G_s	γ_{sat}	w
	-	-	-	<i>KN/m³</i>	%
Test3	0.76	1.84	2.74	20.03	37.2

Figure 7.32. Grain Size Distribution of Silty Sand and Soil Properties with 25% Fines Content

Table 7.32. summarizes various properties of this sand and its grain size distribution curve. This curve was plotted as a result of sieve analysis. SM was the symbol of soil model based on the unified soil classification system (USCS).

C_u (uniformity coefficient) and C_c (coefficient of gradation) were calculated according to grain size distribution curve. D_{10} , D_{30} and D_{60} were determined from the grain size distribution curve.

SEM image, which was taken by scanning electron microscope (SEM), gave information about the grain shape. Soils contained angular particles and rounded particles but the most of the particles had angular shapes. Soil samples were magnified 100 times. These images are illustrated in Figure 7.33.

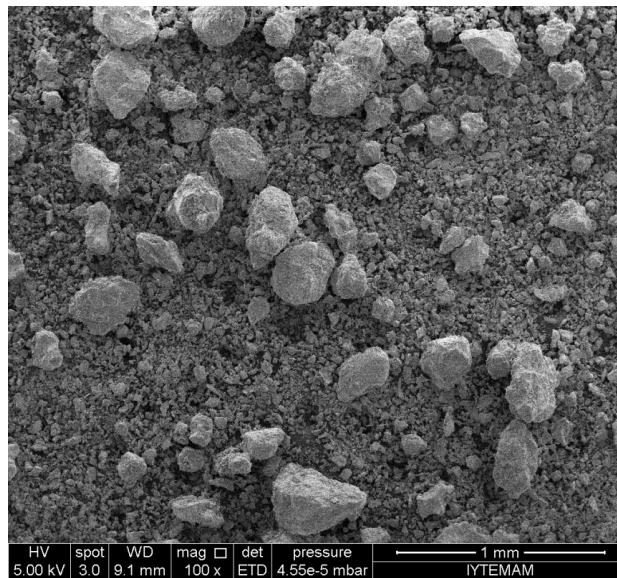


Figure 7.33. SEM Image of Silty Sand with Less Than 25% Fines Content

7.3.3.2. Instrumentation Plan of Test 3

Pore pressure transducers and submersible accelerometers were placed inside the soil model before hydraulic filling process was started.

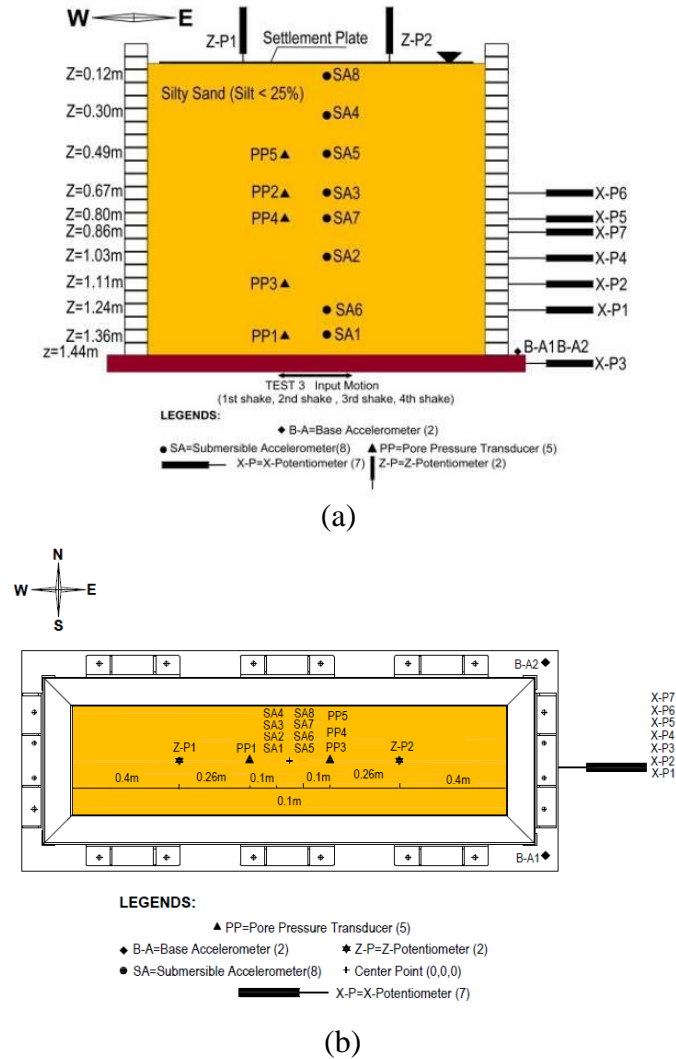


Figure 7.34. (a) Test 2 Side View of Instrumentation Plan, (b) Top View of Instrumentation Plan

X-Potentiometers were attached on the laminates. 2 bottom accelerometers were placed on the shake table. After the hydraulic filling process was completed, 2 Z-Potentiometers were placed on the ground to measure the settlement of the ground. Figure 7.34 displays the instrumentation plan of Test 3.

7.3.3.3. Input Motions of Test 3

Test 3 also consisted of four subsequent shakes to evaluate reliquefaction and each shake lasted for 12 seconds. Frequency did not change, it was 2 HZ. The maximum displacement was 2.36mm for the 1st shake, 10mm for the 2nd shake, 20mm for the 3rd shake and 30mm for the 4th shake. Figure 7.34 illustrates input motions of Test 3. Input motions were nearly the same with Test 1 and Test 2.

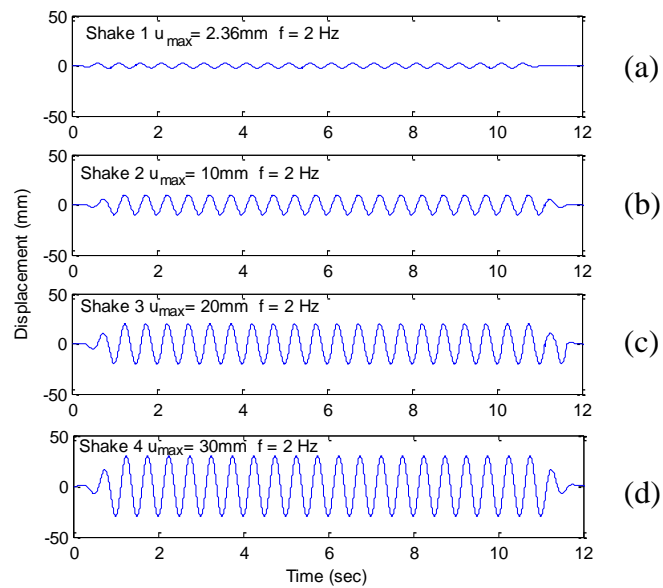


Figure 7.35. Test 3; Input Motion of the (a) 1st Shake, (b) 2nd Shake, (c) 3rd Shake and (d) 4th Shake

7.3.3.4. Results of Test 3

Data was collected by the submersible accelerometers, porewater pressure transducers and potentiometers but the raw data contained considerable amount of higher frequency noise. These raw data should be filtered.

7.3.3.4.1. Excess Pore Water Pressure Response

Porewater pressure transducers were placed inside the soil at different depths to measure the excess pore pressure during the shaking and just after the shaking. Figure 7.36 displays the excess pore pressure at depths 0.49m, 0.80m, 1.11m and 1.36m during shaking and the associated dissipation after the shaking. The reading at 1.36m corresponded to that of the 2nd laminate, the reading at 1.11m corresponded to that of the 6th laminate, the reading at 0.80m corresponded to that of the 11th laminate and the reading at 0.49m corresponded to that of the 16th laminate.

Excess pore water pressure has increased with time initially. After reached a peak value, excess pore pressure remained constant at the peak value. Liquefaction is observed when effective stress corresponded to approximately zero. In other words, pore pressure ratio (r_u) equal to 1. Result of liquefaction phenomenon, upward pore fluid migration observed, post shaking data shows dissipation of excess pore pressure together with the settlement of the soil.

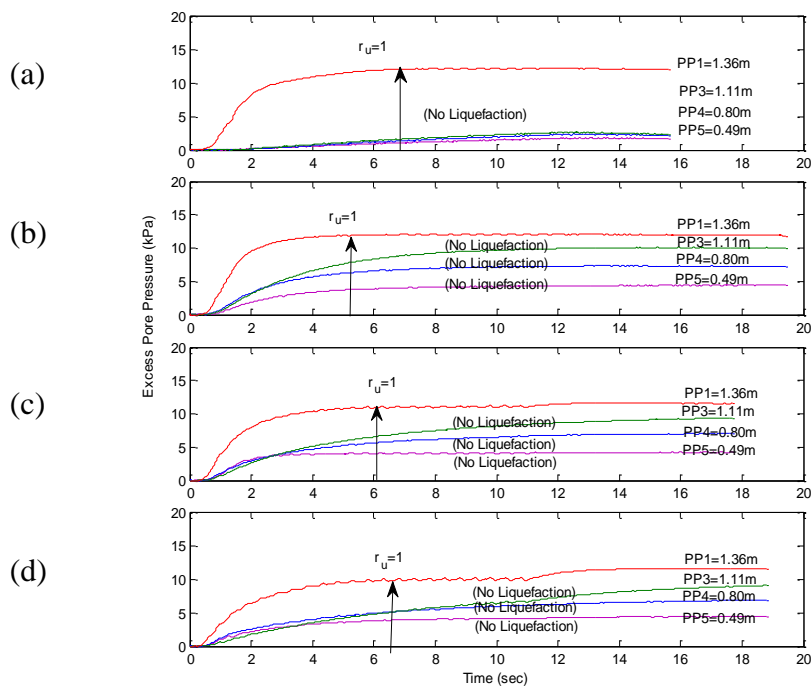


Figure 7.36. Test 3; (a) 1st Shake, (b) 2nd Shake, (c) 3rd Shake and (d) 4th Shake Excess Pore Water Pressure Response

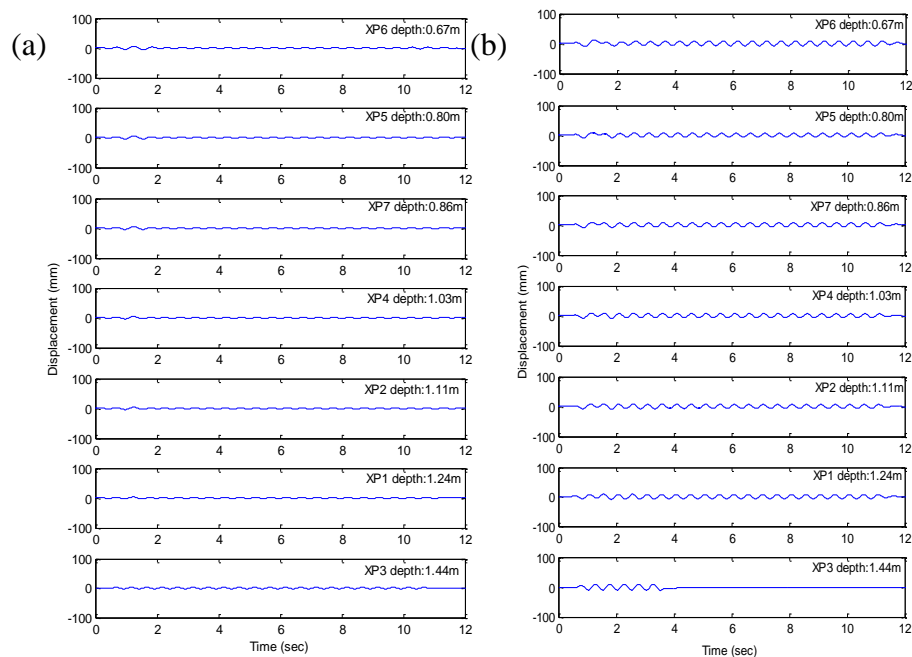
Table 7.9. Summary of Test 3

Fines Content < 25%											
Shaking Number	Pore water pressure trn.name	Depth	PGA	(PGA) _{eq}	Input max. displacement	Frequency	Duration	Time for liquefaction	N _L	Initial D _r	q _c
-	-	m	g	g	mm	Hz	sec	sec	-	%	kPa
Shake_1	PP-1	1,36	0,05	0,08	2,36	2	12	7,1	14,2	11	131
	PP-3	1,11	0,05	0,08	2,36	2	12	No-Liq	No-Liq	11	131
	PP-4	0,8	0,05	0,08	2,36	2	12	No-Liq	No-Liq	-4	67
	PP-5	0,49	0,05	0,08	2,36	2	12	No-Liq	No-Liq	-22	28
Shake_2	PP-1	1,36	0,19	0,29	10	2	12	5,6	11,2	19	175
	PP-3	1,11	0,19	0,29	10	2	12	No-Liq	No-Liq	19	175
	PP-4	0,8	0,19	0,29	10	2	12	No-Liq	No-Liq	15	130
	PP-5	0,49	0,19	0,29	10	2	12	No-Liq	No-Liq	16	107
Shake_3	PP-1	1,36	0,43	0,66	20	2	12	6	12	20	189
	PP-3	1,11	0,43	0,66	20	2	12	No-Liq	No-Liq	18	171
	PP-4	0,8	0,43	0,66	20	2	12	No-Liq	No-Liq	25	185
	PP-5	0,49	0,43	0,66	20	2	12	No-Liq	No-Liq	21	129
Shake_4	PP-1	1,36	0,62	0,95	30	2	12	6,5	13	29	261
	PP-3	1,11	0,62	0,95	30	2	12	No-Liq	No-Liq	36	330
	PP-4	0,8	0,62	0,95	30	2	12	No-Liq	No-Liq	39	310
	PP-5	0,49	0,62	0,95	30	2	12	No-Liq	No-Liq	52	391

Note; PGA=Peak Ground Acceleration, PGA_(eq)=Equivalent Peak Ground Acceleration, N_L=Cyclic for Liquefaction, D_r=Relative Density, q_c=Cone Tip Resistance

7.3.3.4.2. Displacement Response

X-Potentiometers were attached at the center of the laminate to measure the displacement of the laminates.



(cont. on next page)

Figure 7.37 (cont.)

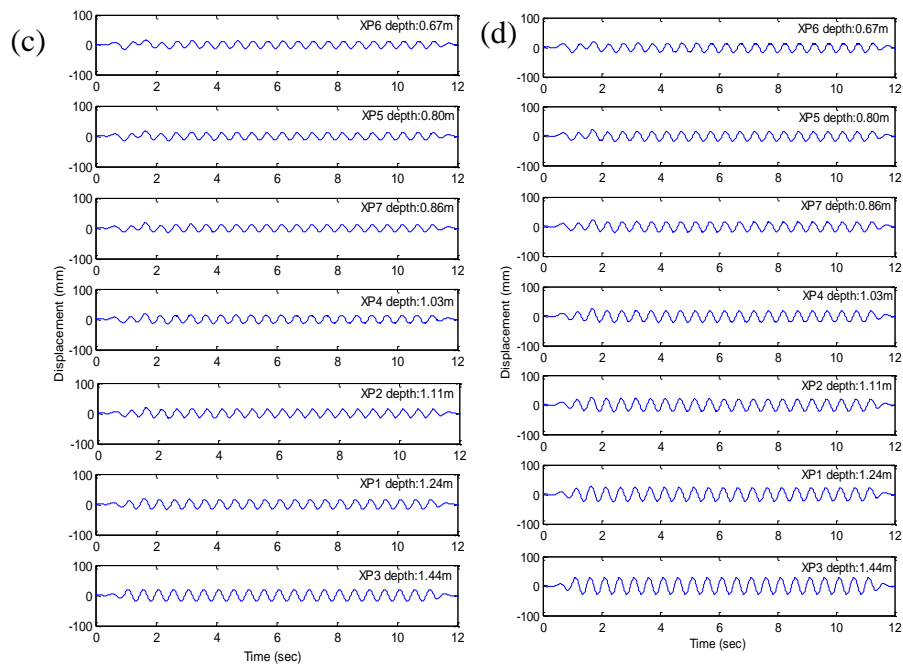


Figure 7.37. Test 3; (a) 1st Shake, (b) 2nd Shake, (c) 3rd Shake, (d) 4th Shake Displacement Response (XP6, XP5, XP7, XP4, XP2, XP1, XP3)

Figure 7.37 displays the horizontal displacement histories of the laminates at depths of 1.44m, 1.24m, 1.11m, 1.03m, 0.86m, 0.80m and 0.67m. One of the X-Potentiometer was placed on shake table to compare the input motions. The readings at 1.24m, 1.11m, 1.03, 0.86, 0.80m and 0.67m depths have corresponded to that of the 4th, the 6th, the 8th, the 10th, the 11th and the 13th laminate, respectively.

7.3.3.4.3. Ground Settlement Response

Total of two LPM 300 Z-Potentiometers were used to measure the total settlement of the ground surface at two different locations and Figure 7.37 illustrates the ground surface settlement data during and after the shaking at two different locations in the ground surface. After the shaking has ended, the settlement was measured shortly after with a new time scale.

Figure 7.38 displays the horizontal displacement histories of the laminates at depths of 1.44m, 1.24m, 1.11m, 1.03m, 0.86m, 0.80m and 0.67m. One of the X-Potentiometer was placed on shake table to compare the input motions. The readings at

1.24m, 1.11m, 1.03, 0.86, 0.80m and 0.67m depths have corresponded to that of the 4th, the 6th, the 8th, the 10th, the 11th and the 13th laminates, respectively.

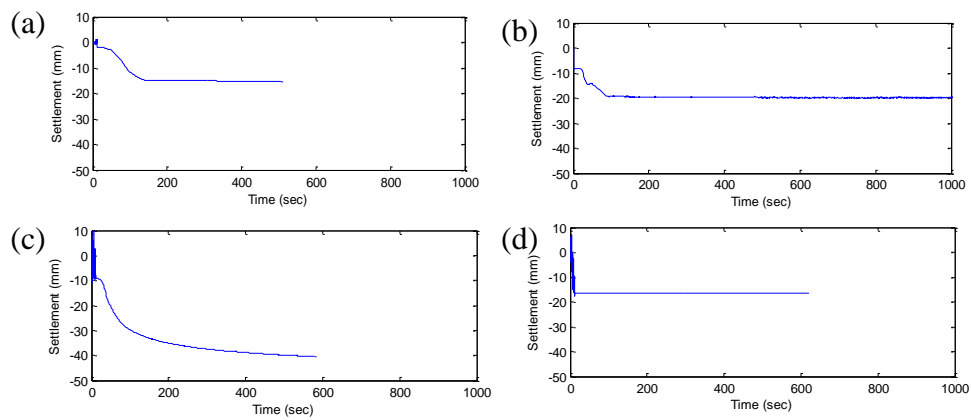


Figure 7.38. Test 3; (a) The 1st Shake, (b) The 2nd Shake, (c) The 3rd Shake, (d) The 4th Shake Settlement Response

Table 7.10 displays the measurements by Potentiometer. Measurements indicated that the settlement post shake was more than the settlement during the shaking. Because, the occurrence of upward pore fluid migration and dissipation of excess porewater pressure along with the settlement of the soil.

Table 7.10. Ground Settlement Measured by Potentiometer

	Ground Settlement Measured by Potentiometer		
	During Shake	Post Shake	Total Settlement
	<i>cm</i>	<i>cm</i>	<i>cm</i>
Shake 1	0.21	1.32	1.53
Shake 2	0.85	1.15	2.00
Shake 3	0.91	3.23	4.14
Shake 4	1.65	0.15	1.80

About 41% of the total settlement of the ground surface has occurred during the shaking. Nearly 59% of the total settlement has occurred after the shaking. Settlement of the ground surface was measured by displacement transducer and also manually by a scale ruler.

The average ground surface settlements were displayed in Table 7.11. Average settlement was necessary to determine the vertical strain of the soil model. Vertical

strain of the soil model was calculated by dividing the settlement with the height of the soil model. Table 7.11 shows the vertical strain of the soil model for each shake.

Table 7.11. Ground Settlement Measured Manually

Ground Settlement Measured Manually					
	West Side	Middle Side	East Side	Average Settlement	Vertical Strain
	<i>cm</i>	<i>cm</i>	<i>cm</i>	<i>cm</i>	<i>%</i>
Shake 1	6,80	6,20	6,70	6,57	4,31
Shake 2	4,00	4,20	5,40	4,53	3,05
Shake 3	3,60	3,90	4,70	4,07	2,92
Shake 4	3,80	3,50	3,00	3,43	2,70

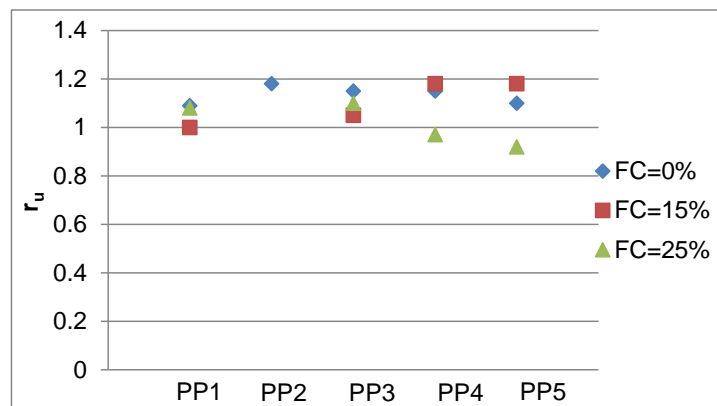
CHAPTER 8

ANALYSES OF THE TEST RESULTS

8.1. Analyses of the Shake Table Tests

In this thesis, the laminar box system and the experimental results of three liquefaction tests performed by using the system were presented. Soil model of the first test consisted of 1.4m saturated clean sand deposit. Soil model of the second test consisted of 1.44m deep saturated silty sand deposit with 15% silt content. Soil model of the third test consisted of 1.44m deep saturated silty sand deposit with less than 25% fines content. Analysis of the test results were as follows;

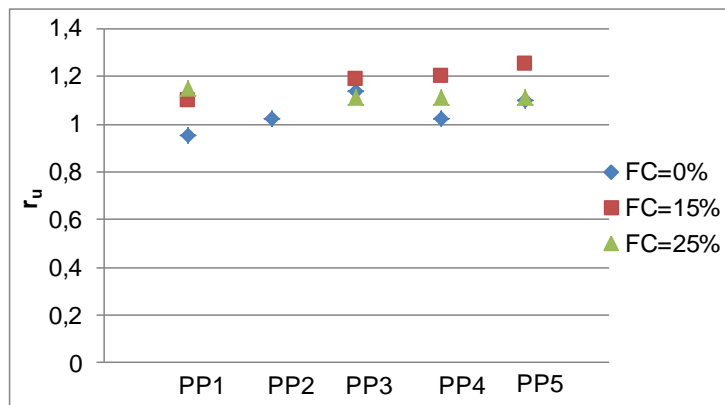
- Pore pressure transducers slid down during shaking. Therefore; pore pressure ratio, r_u was not equal to 1, but equal to nearly 1 at any depth. Hence, initiation time of the liquefaction was taken from where r_u value reached its peak value and remained constant. According to grain size distribution, fines content was 0% and c_u (uniformity coefficient) was 1.44 for the soil profile of the Test 1, while fines content was 15% and c_u was 1.82 for the soil profile of the Test 2. Whereas; fines content was 25%, c_u was 1.80 for the soil profile of the Test 3 Figures 8.1a-8.1d below show variation of pore water pressure ratio, r_u at each excess pore water measurement transducer location per various fines contents, FC.



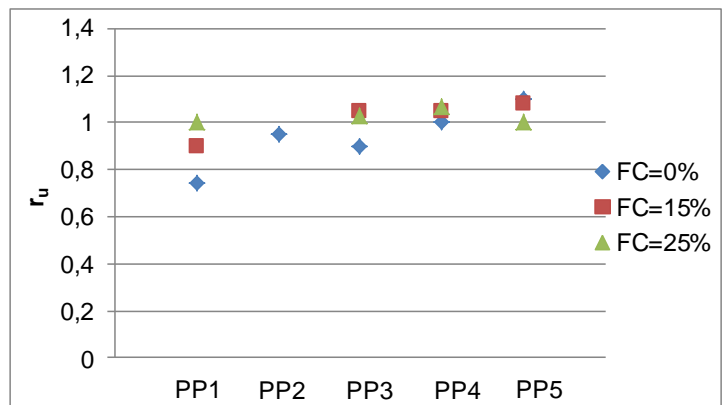
(a)

(cont. on next page)

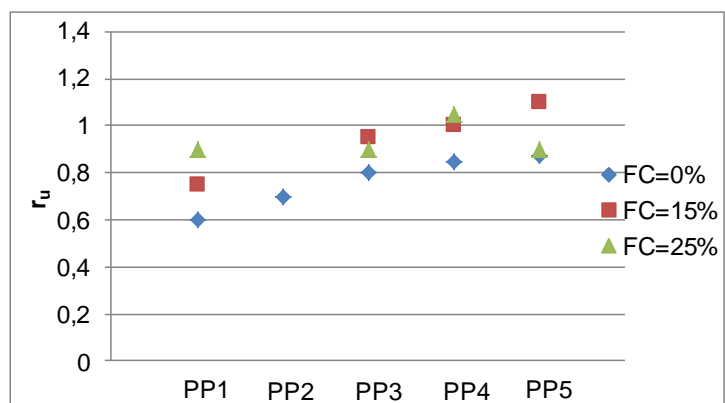
Figure 8.1 (cont)



(b)



(c)

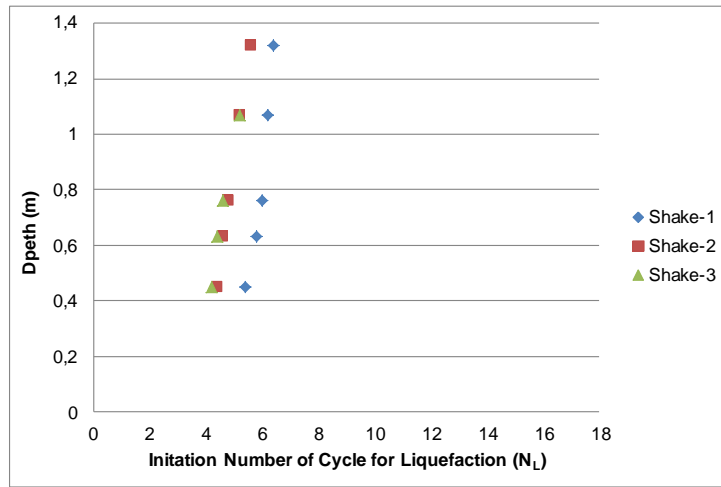


(d)

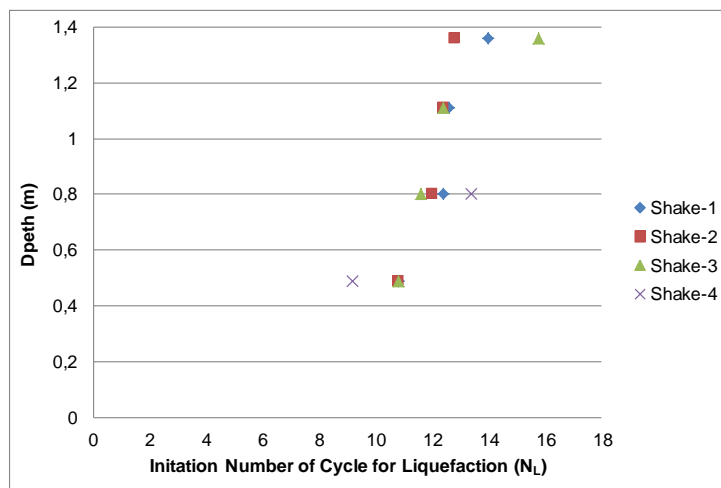
Figure 8.1. r_u values during; (a) Shake-1, (b) Shake-2, (c) Shake-3 and (d) Shake-4

Figure 8.1 indicates that uniformly graded fine sands (or simply called uniform sands) were most vulnerable to liquefaction. Silty soils were found to possess more liquefaction resistance than uniform fine sands. Noted that the soil model for Test 1

contained mostly sub-rounded particles, while soils for Test 2 and Test 3 contained both angular particles and rounded particles, though most of the particles had angular shapes.



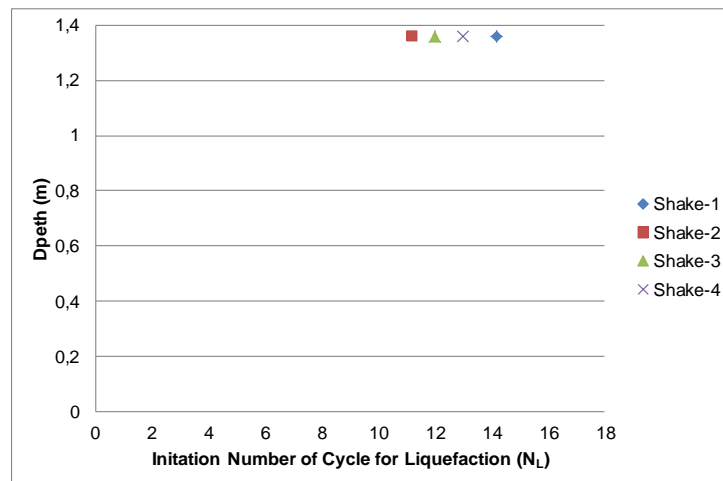
(a)



(b)

(cont. on next page)

Figure 8.2 (cont)



(c)

Figure 8.2. Required Number of Cycles for Initiation of Liquefaction in; (a) Test 1, (b) Test 2, (c) Test 3.

The number of cycles required to trigger liquefaction during the Test 1 was smaller than that required to trigger liquefaction during the Test 2 and Test 3. Liquefaction was observed during all the three shake table tests.

During the Test 1-Shake 3, the test sands did not develop excess pore water pressures large enough to liquefy the sands near the bottom laminate. During the Test 1-Shake 4, the test sands did not liquefy at any depth, despite after 24 cycles.

During the Test 2-Shake 4, the tested silty sands did not develop excess pore water pressures large enough to liquefy at some depths.

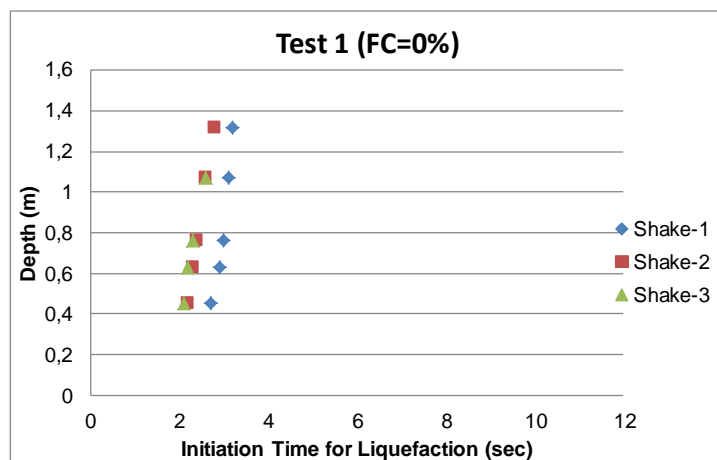
During the Test 3-all shakes, the tested silty sands did not develop excess pore water pressures large enough to liquefy at some depths.

Figure 8.2 indicates that soils with rounded shapes were more susceptible to liquefaction than angular grained soils. Also, following results were obtained;

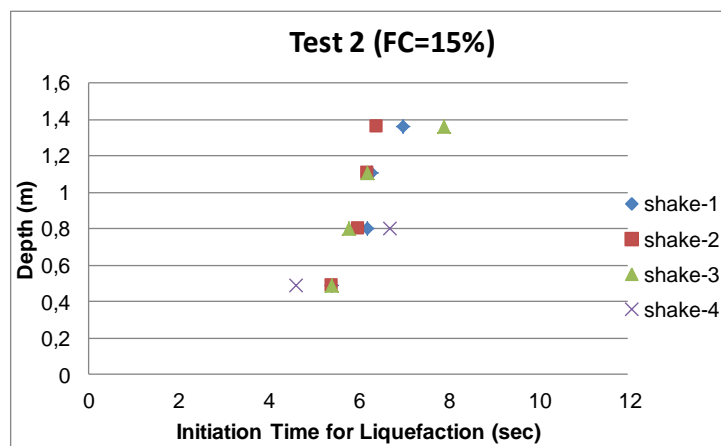
- Soil sedimentation process, which takes place in natural river deposits, could be mimicked by using the hydraulic filling process. Hydraulic filling process usage for clean sands and for silty sands with 15% silt content was suitable. However, silt percentage of the third test's soil model needed to be 25 %, but during the hydraulic filling method, some silt particles have surfaced, suggesting segregation. Because of this problem, the soil model was not uniform. Thus hydraulic filling method has shown

to be unsuitable as a placement method, if fines content exceeds 25%. Thus for the Test 3, fines content was assumed to be nearly 25%.

- More time is required to trigger liquefaction during the Test 2 than that required to trigger liquefaction during the Test 1. Further, more time is required to trigger liquefaction during the Test 3, than that required to trigger liquefaction during the Test 2. Required time to trigger liquefaction increased with fines contents of the soils (Figure 8.2).
- Figure 8.3. illustrates that required time to trigger liquefaction during the 1st shake was larger than that required to trigger liquefaction during the 2nd shake.



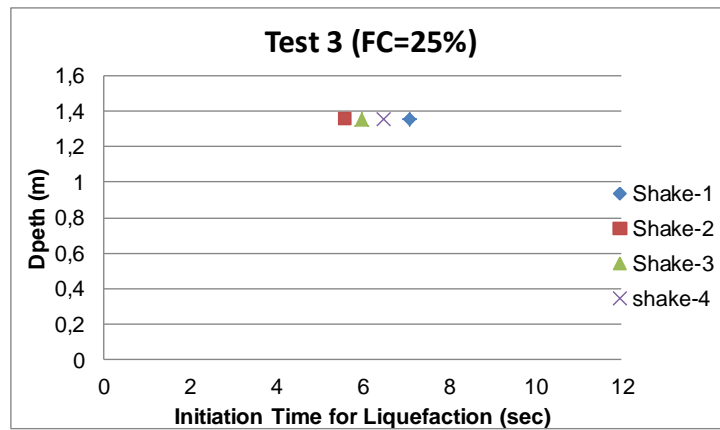
(a)



(b)

(cont. on next page)

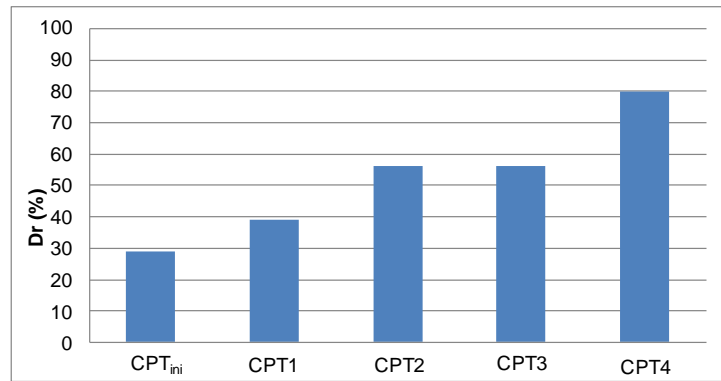
Figure 8.3 (cont)



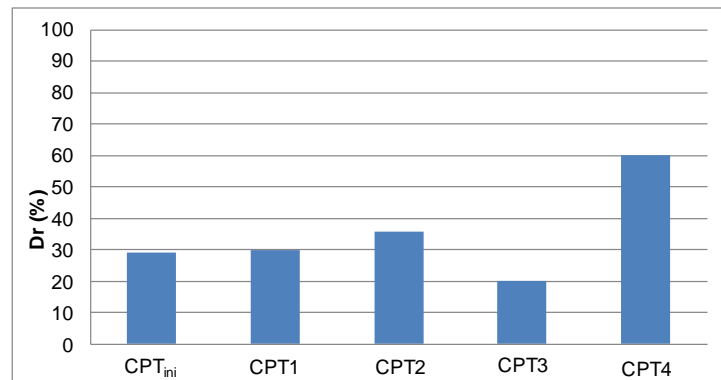
(c)

Figure 8.3. Initiation Time for Liquefaction in; (a) Test 1, (b) Test 2, (c) Test 3

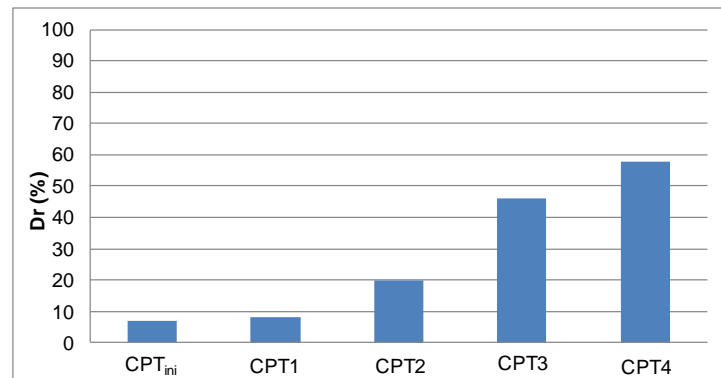
- The soil which was closer to the bottom laminate was not weak as much as the surface soil. So, required time to trigger liquefaction has increased, when depth has increased. Liquefaction has occurred primarily near the top of the sand profile, where the excess pore water pressures that developed may have been augmented by water pressures diffusing from the bottom of the profile, as a result of upward flow occurred during the shaking and reconsolidation of the profile, which has taken place near the bottom laminate (Figure 8.3).
- Figure 8.4. illustrates the relative density for each test. Initial relative densities for the soil model, prior to the 1st shake have ranged from about 7% to 29% at the same depth (depth=1m), and the dissipation of excess pore water pressures induced by shaking led to reconsolidation settlements, resulting increases in relative density to values between about 58% to 80%, after the 4th shake. Liquefaction resistance of each of the tested sands have decreased from 1st shake upto the 2nd shaking, despite some increase in the relative density.



(a)



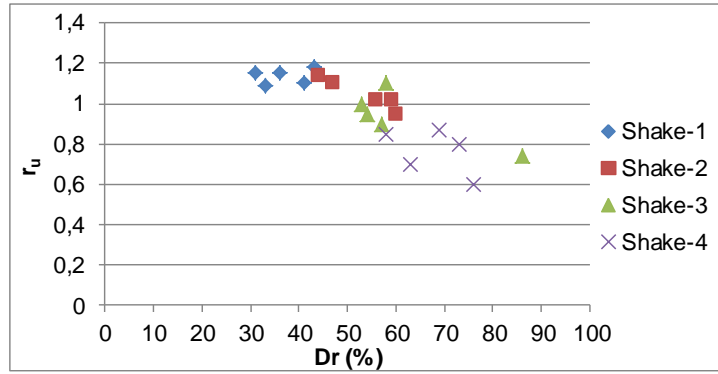
(b)



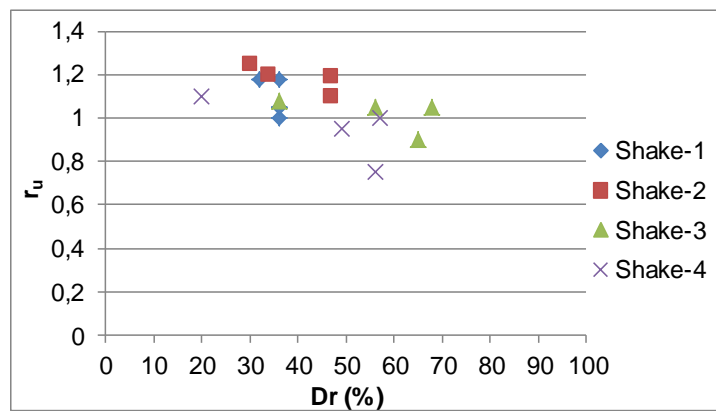
(c)

Figure 8.4. Relative Density (D_r) in; (a) Test 1, (b) Test 2, (c) Test 3.

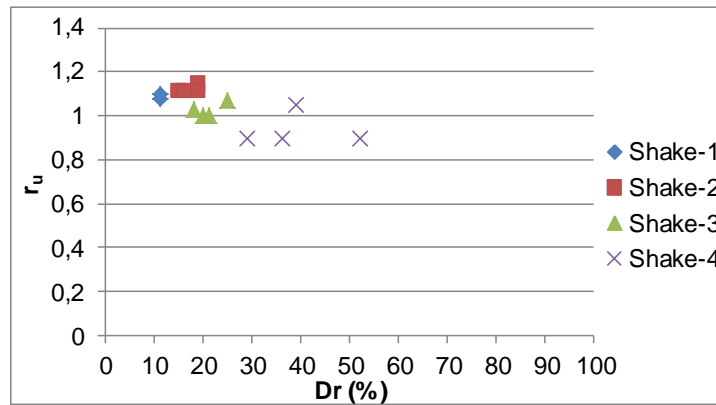
- Figure 8.5. illustrates that the relative density (D_r) values have increased with each shake. Despite the increase in relative density, liquefaction resistance have decreased. Required time to trigger liquefaction during the Shake-1 was more than Shake-2. Relative density values of Test 1 were higher than Test 2 and those for Test 2 were more than Test 3. Despite decreases in relative density, liquefaction resistance values have increased.



(a)



(b)



(c)

Figure 8.5. Relative Density Values to Initiate Liquefaction in; (a) Test 1, (b) Test 2, (c) Test 3.

- Post shaking data confirm that the occurrence of upward pore fluid migration and dissipation of excess pore water pressures together with the ground settlement of the

soil. Thus, ground settlement after the shaking was more than the ground settlement during the shaking (Figure 8.6).

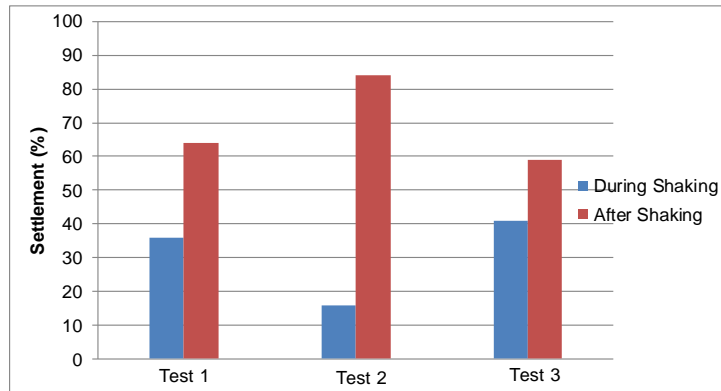


Figure 8.6. Ground Settlement During and After the Shaking in Each Test.

- Figure 8.7. illustrates that; during Test 3; ground settlement of the Test 3 soil model was greater than that in Test 1 and Test 2. Ground settlement values have increased with increasing fines content of the soil model.

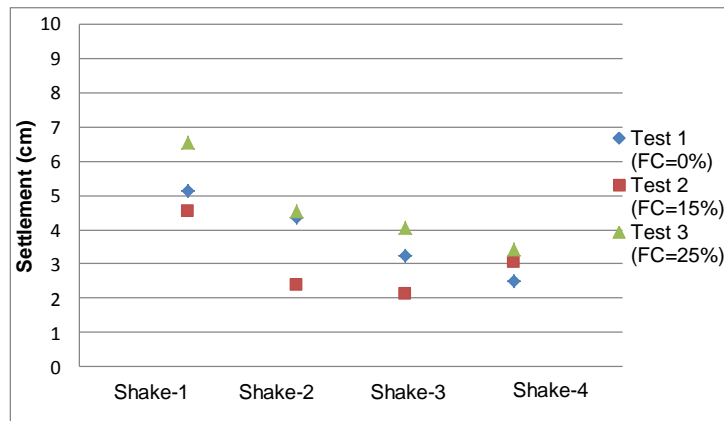


Figure 8.7. Ground Settlement Variation with Fines Content of the Soil Model.

- Test 1, Test 2 and Test 3 have demonstrated the effectiveness of the shake table and the laminar box test set-up with instrumentation and in particular the experimental facilities provided at the structural laboratory of IZTECH.

CHAPTER 9

CONCLUSIONS

9.1. Summary of Findings

Three shake table tests were conducted with sands and silty sands. As a result of comparison between these 3 shake table results, these findings were found;

- Uniform fine sands were most vulnerable to liquefaction. Silty sands were found to possess liquefaction resistance more than uniform fine sands.
- Soils with rounded shapes were more susceptible to liquefaction than angular grained fine sandy soils.
- Required time to trigger liquefaction has increased with increasing fines content and depths of the soil sedimentation. Liquefaction resistance of each of the tested sand has decreased from 1st to the 2nd shaking, despite some increase in the relative density. So; required time to trigger liquefaction during the 1st shake was larger than that required to trigger liquefaction during the 2nd shake.
- Relative density values have increased with each subsequent shake. Despite increase in the relative density, liquefaction resistance have decreased. Relative density have decreased, when fines content have increased. But, despite decreases in relative density values, liquefaction resistance have increased.
- Ground settlement after the shaking was more than that during the shaking.
- Ground settlement of the Test 3 soil model was greater than that in Test 1 and Test 2. Ground settlement values have increased with fines contents of the soil.
- Test 1, Test 2 and Test 3 have demonstrated the effectiveness of the shake table and the laminar box test set-up with instrumentation and in particular the experimental facilities provided at the structural laboratory of IZTECH.

9.2. Suggestions for Future Research

Further research is needed to build on the results of this study to improve screening methods available in the literature. The author would like to propose the followings for future research;

- The shake table tests with 1-D laminar box will be conducted with different fines content in order to examine the role of the silt percentage on liquefaction resistance. However different filling method is needed. During hydraulic filling method, silt particles were gathered at the surface and the uniform soil model with 25 silt percentage may not have been generated. A new technique may be designed using a funnel to put the sand into the box. Filling the laminar box begins with a determined amount of water and sand is added into the box through a funnel, which moves around the box at a constant velocity. Water must be added as required, when adding sand into the box to keep the water height above the sand constant. Having a constant water level above the sand level, allows for the sand to be deposited through the water, a process which decreases its depositing velocity, as it continues through the water.
- In order to understand the lateral spreading effect during the liquefaction tests, some suitable mechanism may be prepared.

REFERENCES

- Ambraseys, NN. (1988). Engineering seismology: Part II. *Earthquake engineering & structural dynamics*, 17(1), 51-105.
- Arulanandan, K., Anandarajah, A., & Abghari, A. (1983). Centrifugal modeling of soil liquefaction susceptibility. *Journal of Geotechnical Engineering*, 109(3), 281-300.
- Arulanandan, K., & Muraleetharan, K.K. (1988). Level ground soil-liquefaction analysis using in situ properties: I. *Journal of Geotechnical Engineering*, 114(7), 753-770.
- Arulmoli, K., Arulanandan, K., & Seed, H.B. (1985). New method for evaluating liquefaction potential. *Journal of Geotechnical Engineering*, 111(1), 95-114.
- Dobry, Ricardo, Ladd, RS, Yokel, Felix Y, Chung, Riley M, & Powell, D. (1982). *Prediction of pore water pressure buildup and liquefaction of sands during earthquakes by the cyclic strain method* (Vol. 138): US Department of Commerce, National Bureau of Standards.
- Eseller-Bayat, Ece, Gokyer, Seda, Yegian, Mishac K, & Alshawabkeh, Akram. (2012). Liquefaction Response of Partially Saturated Sands: Experimental Results. *Journal of Geotechnical and Geoenvironmental Engineering*.
- Eseller-Bayat, Ece, Yegian, Mishac K, & Alshawabkeh, Akram. *Liquefaction Mitigation Using Entrapped Air*. Paper presented at the 2007 NORTHEAST GEOTECHNICAL GRADUATE RESEARCH SYMPOSIUM.
- Idriss, IM, Seed, H.B., & Serff, N. (1974). Seismic response by variable damping finite elements. *Journal of Geotechnical and Geoenvironmental Engineering*, 100(Proc. Paper 10284).
- Ishihara, Kenji. (1996). *Soil Behaviour in Earthquake Geotechnics*: Oxford University Press.
- Jafarzadeh, B. (2004). *Design and evaluation concepts of laminar shear box for 1G shaking table tests*. Paper presented at the Proceedings of the 13th world conference on earthquake engineering, Vancouver, paper.
- Kramer, S.L. (1996). Geotechnical earthquake engineering. *Prentice-Hall Civil Engineering and Engineering Mechanics Series, Upper Saddle River, NJ: Prentice Hall, | c1996, 1.*
- Kramer, S.L., & Seed, H.B. (1988). Initiation of soil liquefaction under static loading conditions. *Journal of Geotechnical Engineering*, 114(4), 412-430.

- Kutter, BL, & James, RG. (1989). Dynamic centrifuge model tests on clay embankments. *Geotechnique*, 39(1), 91-106.
- Ling, Hoe I, Mohri, Yoshiyuki, Kawabata, Toshinori, Liu, Huabei, Burke, Christopher, & Sun, Lixun. (2003). Centrifugal modeling of seismic behavior of large-diameter pipe in liquefiable soil. *Journal of geotechnical and geoenvironmental engineering*, 129(12), 1092-1101.
- Lunne, T, Robertson, PK, & Powell, JJM. (1997). Cone penetration testing. *Geotechnical Practice*.
- Mogami, T., & Kubo, K. (1953). *The behavior of soil during vibration*. Paper presented at the Proc. 3rd Inter. Conf. on Soil Mech. And Found. Engrg.
- Moss, Robb ES, Crosariol, Vic, & Kuo, Steven. (2010). Shake Table Testing to Quantify Seismic Soil Structure Interaction of Underground Structures.
- Prasad, S. K., Towhata, I., Chandradhara, G. P., & Nanjundaswamy, P. (2004). Shaking table tests in earthquake geotechnical engineering. *CURRENT SCIENCE*, 87(10), 1398-1404.
- S.R Pathak, R.S. Dalvi and A.D. Katdare. (2010). EARTHQUAKE INDUCED LIQUEFACTION USING SHAKE TABLE TEST. *Fifth International Conference on Recent Advances in Geotechnical Earthquake Engineering and Soil Dynamics and Symposium in Honor of Proffesor I.M. Idriss*.
- Seed, H. Bolton, & Idriss, I. M. (1982). *Ground motions and soil liquefaction during earthquakes*. Berkeley, Calif.: Earthquake Engineering Research Institute.
- Seed, R.B., Cetin, KO, Moss, RES, Kammerer, AM, Wu, J., Pestana, JM, & Riemer, MF. (2001). *Recent advances in soil liquefaction engineering and seismic site response evaluation*: NISEEE.
- Sherif, Mehmet A, Ishibashi, Isao, & Lee, Chong Do. (1982). Earth pressures against rigid retaining walls. *Journal of the Geotechnical Engineering Division*, 108(5), 679-695.
- Silver, M.L., & Seed, H.B. (1971). Volume changes in sands during cyclic loading. *Journal of Soil Mechanics & Foundations Div*.
- Tezcan, S.S., & Özdemir, Z. (2004). *Liquefaction risk analysis and mapping techniques*: Higher Education Research Foundation.
- Thevanayagam, S., United States. Federal Highway Administration., & Multidisciplinary Center for Earthquake Engineering Research (U.S.). (2006). *Liquefaction remediation in silty soils using dynamic compaction and stone columns*. Buffalo, NY: Multidisciplinary Center for Earthquake Engineering Research.

- Ueng, T. S., Wang, M. H., Chen, M. H., Chen, C. H., & Peng, L. H. (2006). A large biaxial shear box for shaking table test on saturated sand. *GEOTECHNICAL TESTING JOURNAL*, 29(1), 1-8.
- Whitman, RV, & Lambe, PC. (1986). Effect of boundary conditions upon centrifuge experiments using ground motion simulation. *ASTM geotechnical testing journal*, 9(2), 61-71.
- Youd, T.L., & Hoose, SN. (1977). *Liquefaction susceptibility and geologic setting*. Paper presented at the Proc., 6th World Conf. on Earthquake Engineering.
- Youd, TL. (1991). *Mapping of earthquake-induced liquefaction for seismic zonation*. Paper presented at the International Conference on Seismic Zonation, 4th, August.
- Yue, TX, Zhao, N, Du, ZP, Fan, ZM, Wang, CL, Chen, CF, . . . Shi, WJ. A Novel Method for Earth Surface Modelling and Its Applications.

APPENDIX A

DESIGN OF LAMINAR BOX

A-1 Introduction

Design of the laminar box to carry out shake table tests on large scale soil model is presented in this chapter. The main objectives of the laminar box design proposal are:

- To design a safe system, limit excessive displacements,
- Laminates slide each other using rollers and these rollers were low friction high load capacity,
- To prevent damages on welding, plates were used on welding.
- The most affected component was box stoppers by force during shaking. Thus, box stoppers were placed with welding and bolt inside the top channel of the short edge.

Design of laminar box system includes:

- Laminates
- Roller mechanisms
- Box stoppers
- Plates reinforced welding
- Angle brackets

A-2 Shake Table

The aluminum shake table was available at IZTECH structural laboratory. The dimensions of shake table and the properties of actuator are displayed in Figure A.1.

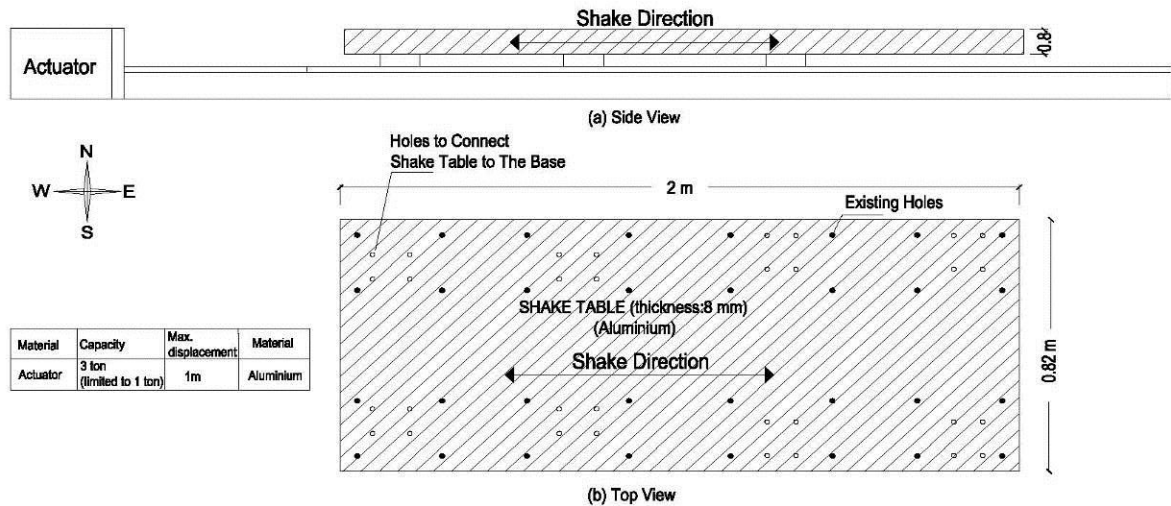


Figure A.1. (a) Side View of Shake Table, (b) Top View of Shake Table

A-2 Components of Laminates

Laminates consisted of 1) I-Beams, 2) Roller Mechanisms, 3) Box Stoppers, 4) Plates reinforced welding and 5) Angle Brackets.

Laminates slid on each other using low friction high load capacity rollers. Eight roller mechanisms were placed inside the top channel of the I-beam at the long side of each laminate (except top laminate). Locations of these roller mechanisms are shown in Figure A.2 and Figure A.3. Figure A.4 displays details of the roller mechanism.

To limit the laminate's displacement and to prevent any over-stressing related to large displacements, box stoppers#2 were placed inside the top channel of I-beam at the short side of each laminate (except top laminate). To prevent the lateral movement and the rotation, box stoppers#1 were inserted inside the top channel of I-beam at the long side of each laminate (except top laminate). To prevent the noise and to reduce damages on the box stoppers during shaking, rubber stoppers were attached on back and front of the box stoppers. Locations of these box stoppers are illustrated in Figure A.3. Allowable maximum displacement for each laminate was 14mm.

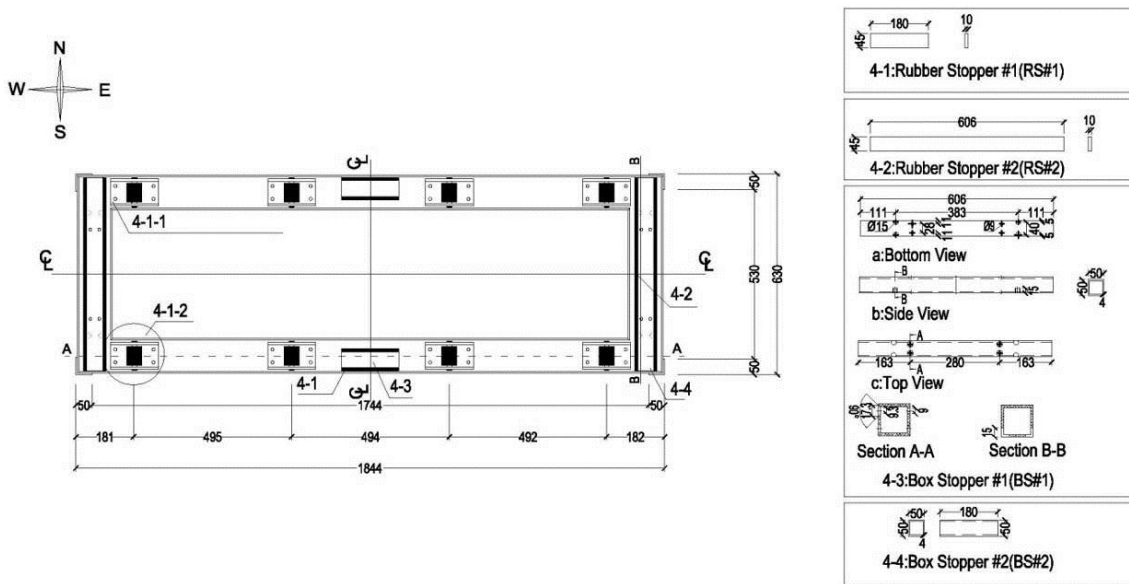


Figure A.2. Details of Laminate L1-L23

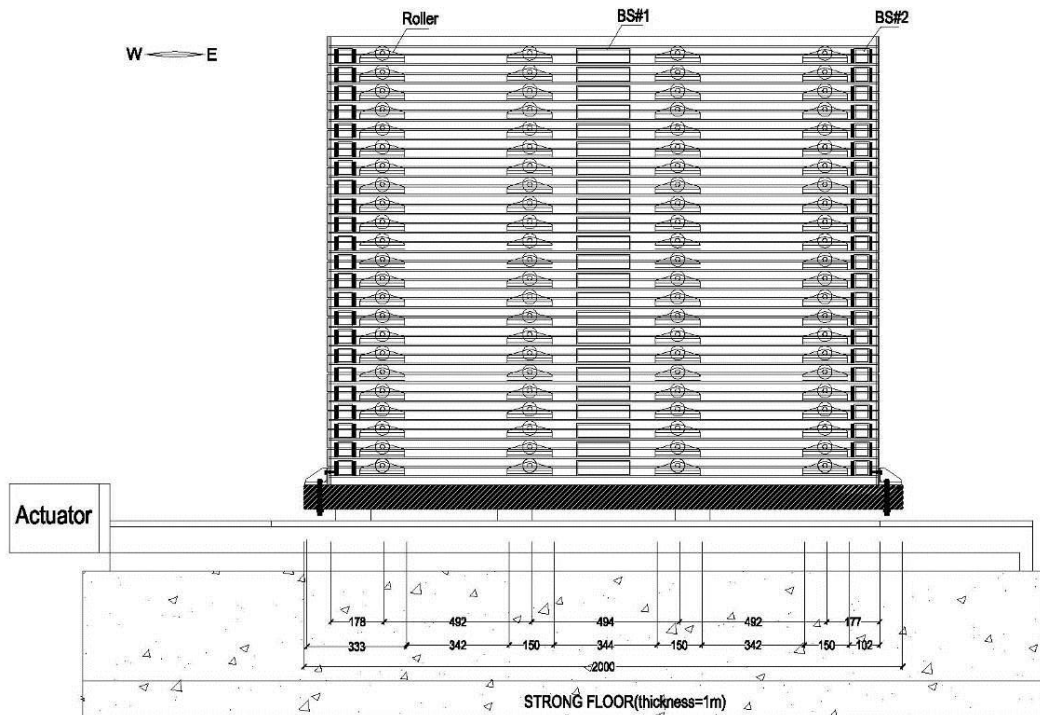


Figure A.3. Section A-A, Locations of Box Stopper#1 and Roller Mechanisms

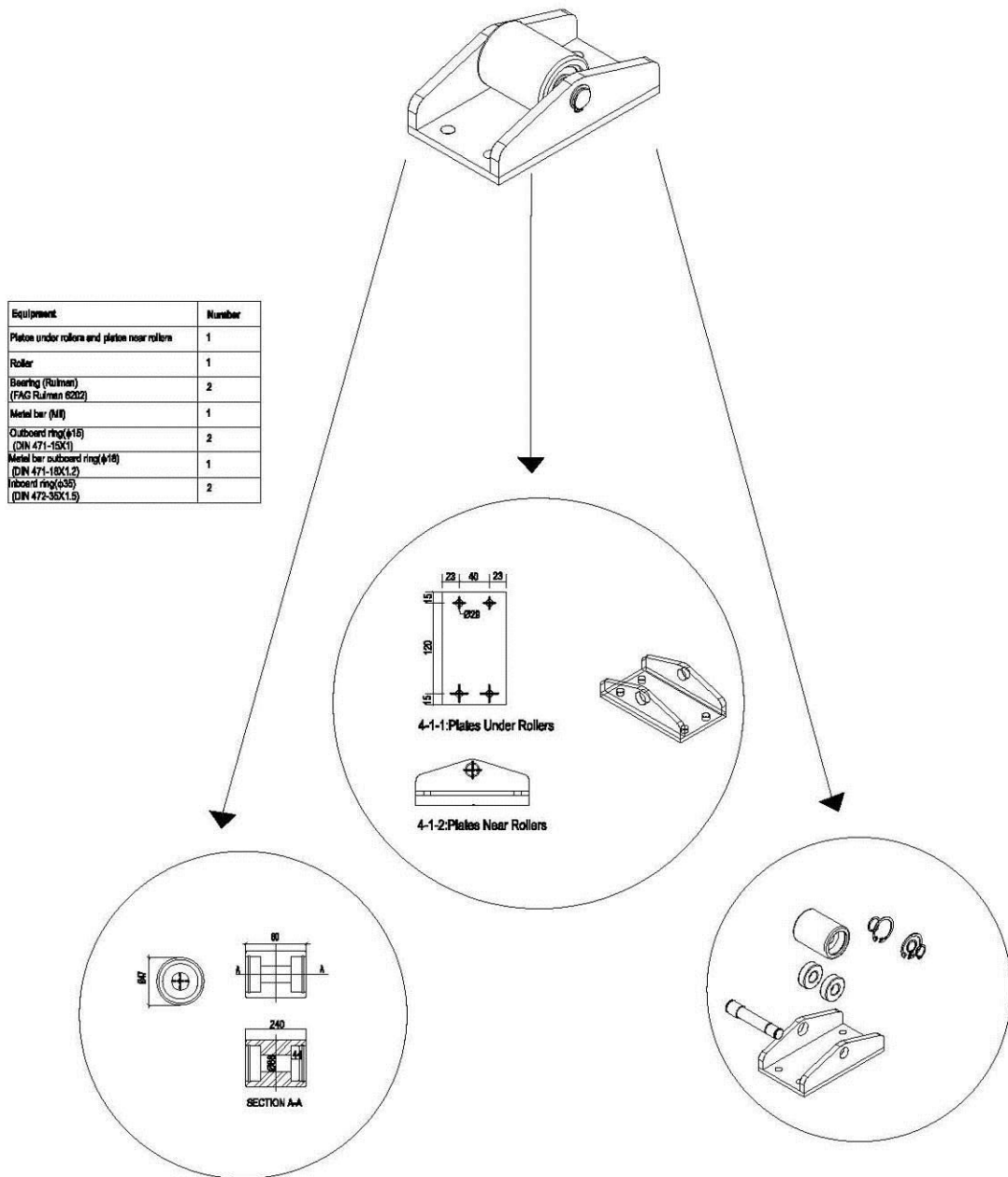


Figure A.4. Detail of Roller Mechanism

The maximum displacement of each laminate was 14mm longitudinal directions; the cumulative displacement was 322mm.

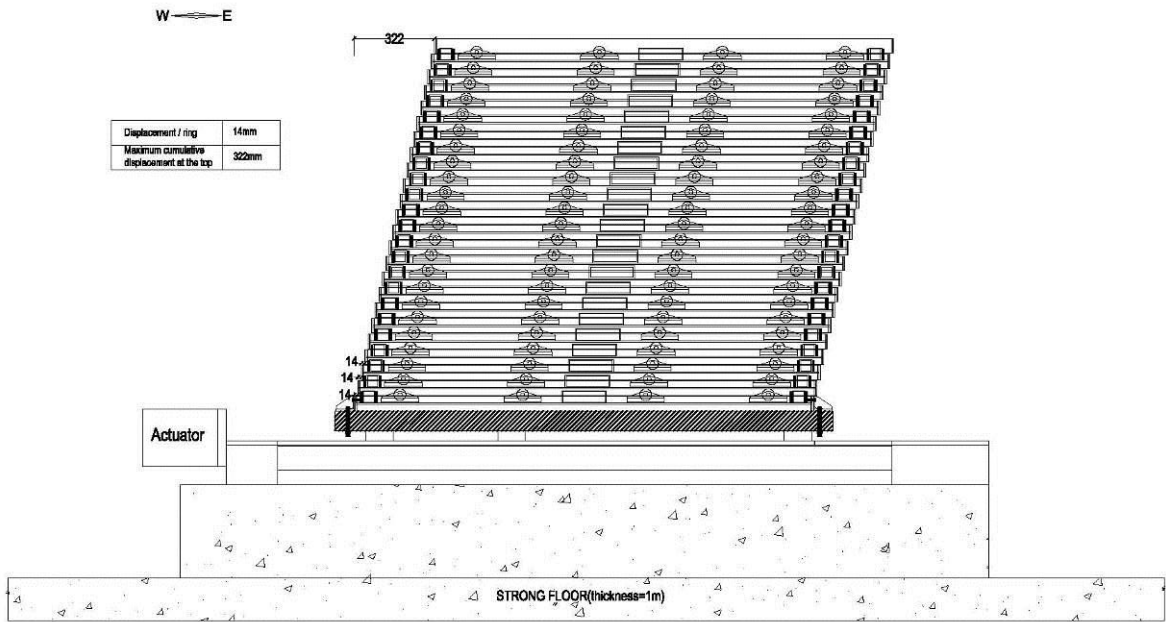


Figure A.5. The Maximum Displacement of Laminate and Cumulative Displacement

Roller mechanisms and box stoppers did not placed inside the top channel of top laminate's I-beam. To reinforce the welding, plates on reinforced welding and angle brackets were placed on top laminate. Dimensions and locations of the plate on reinforced welding are displayed in Figure A.6.

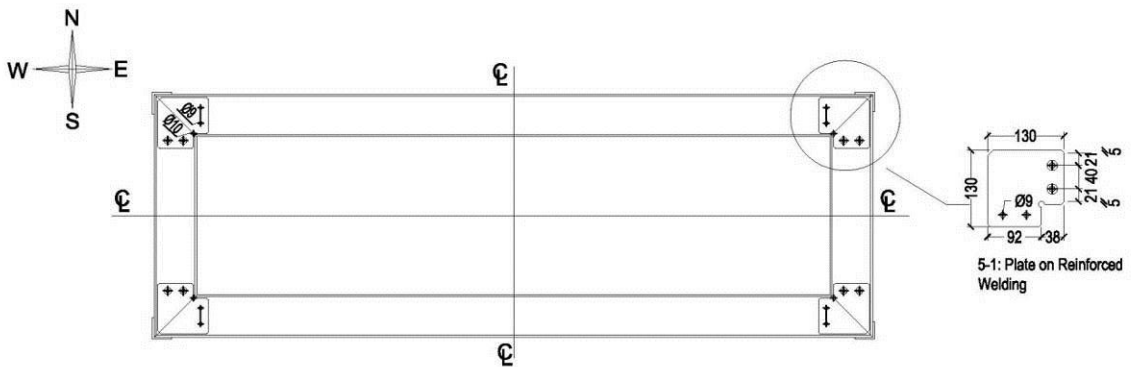


Figure A.6. Details of Laminate L24 (Top Laminate)

The laminar box was carried with 3 tons capacity crane. The laminar box was placed on the shake table. To keep together all laminates, four profiles were tied to the laminates. The crane was available at IZTECH structural laboratory.

Box stoppers were placed inside the top channel of short edges with welding. These box stoppers limit excessive displacements in both longitudinal and lateral directions. Also, box stoppers prevent overturning of the laminates during shaking. Welding was controlled before laminar box was constructed. All calculations are presented in Table A.1.

Table A.1 Calculations

Welding Check				
Gravity, g	9.81	m/sec ²		
Soil+Box+Membrane Weight, W	2545	kg		
Maximum Horizontal Acceleration, a _{max}	2.94	m/sec ²		
Force , F	7491	N		
F/2=	3746	N		Note: Divided by 2 because two side of the laminar box take the force)
Height of Stopper at Long Edge, y	5	cm		
Maximum Moment, M	18728	Ncm		
Weldings dimension, L	60	cm		
Distance from welding line to top of the laminate, a	0.26	cm		
Moment of inertia(I _x)	97.59	m ⁴		
Stress (σ _x)	479.77	N/cm ²	<1000 N/cm ²	Check Satisfy OK
Overturning Check				
Total Stress				
Soil Length, L	1.42	m		
Unit Weight, g=	19.3	KN/m ³		
svo	27.31	KN/m ²		
Horizontal Stress				
Lateral pressure coefficient, Ko=	0.5			
Horizontal Total Stress, sh =	13.65	KN/m ²		
Effective stress, svo' =	13.43	KN/m ²		
Volume of soil, V=	0.92	m ³		
Weight of soil, W=	17.82	KN		
Overturning moment				
Total Weight of laminar box	7.7	KN		
Maximum cumulative displacement at the top	0.33	m		
Overturing Moment	8.4	KN-m	Note: After ground motion,center of gravity of laminar box is within boundaries	Check Satisfy OK

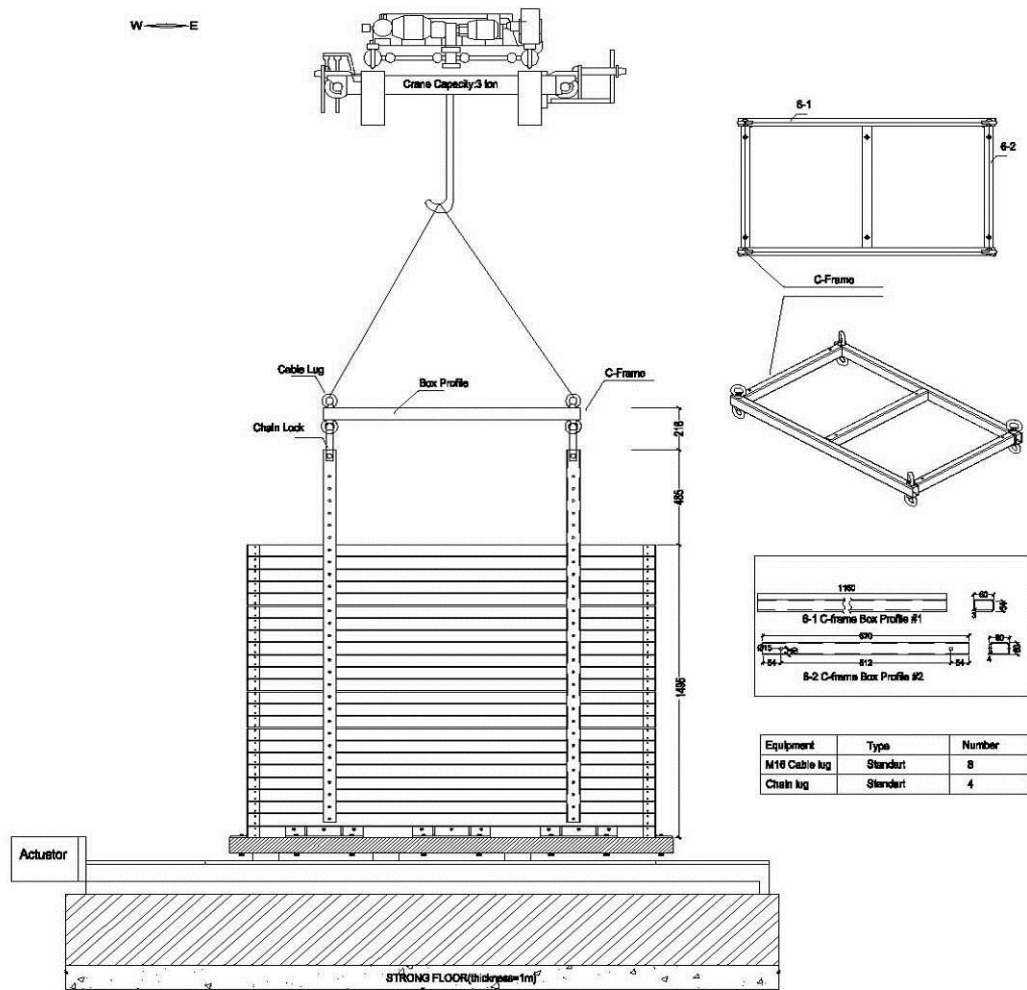


Figure A.7. Side View of Laminar Box (W-E) and C-Frame

A-3 Connection between the Laminar Box and the Shake Table

For shake table tests, 1-D laminar box was constructed. The height of laminar box is 1.5m and has 24 laminates, each 57mm thick. The vertical gap between two adjacent laminates was 5mm to prevent any contact interference between any adjacent laminates during horizontal sliding of the laminates. The bottom laminate connected to shake table by L-Profiles, the connections and L-Profiles are illustrated in Figure A.8 and Figure A.9.

Table A.2 shows various details of the available structural laboratory equipment, laminar box properties and detailed laminar box system components.

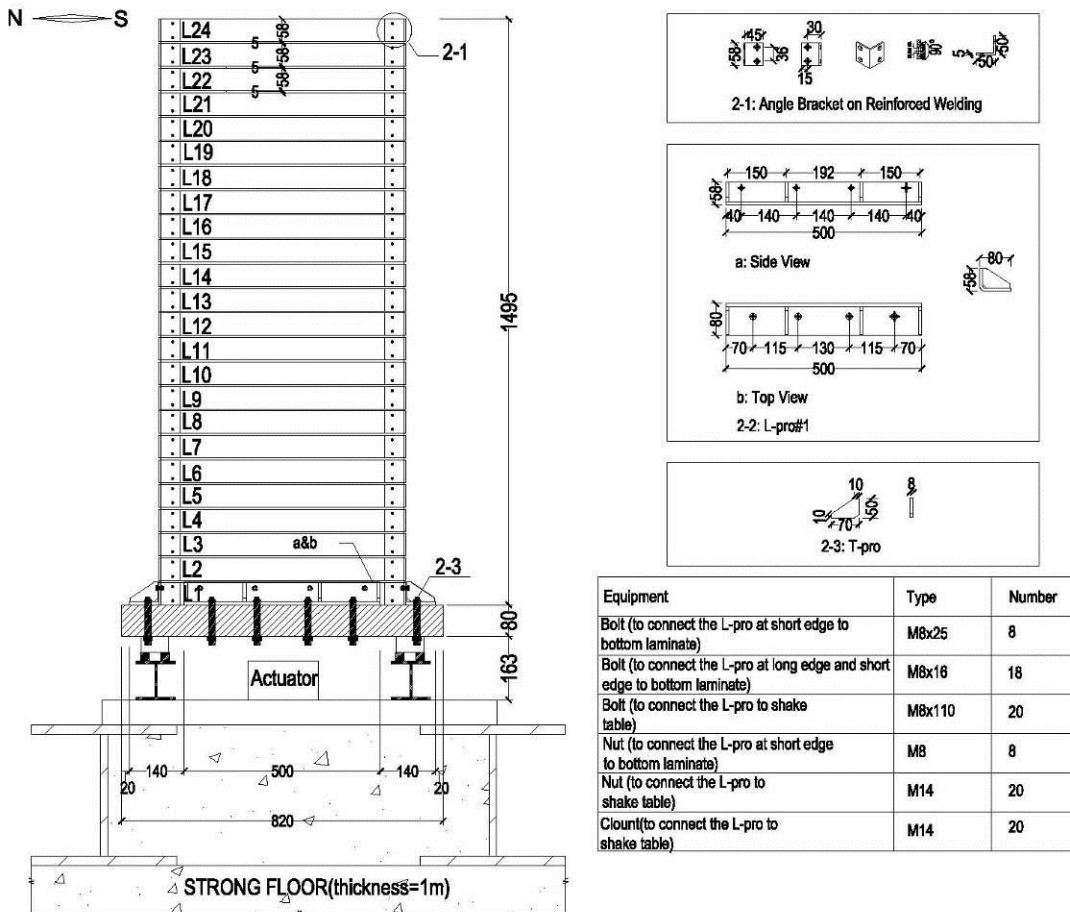


Figure A.8. Side View of Laminar Box (N-S)

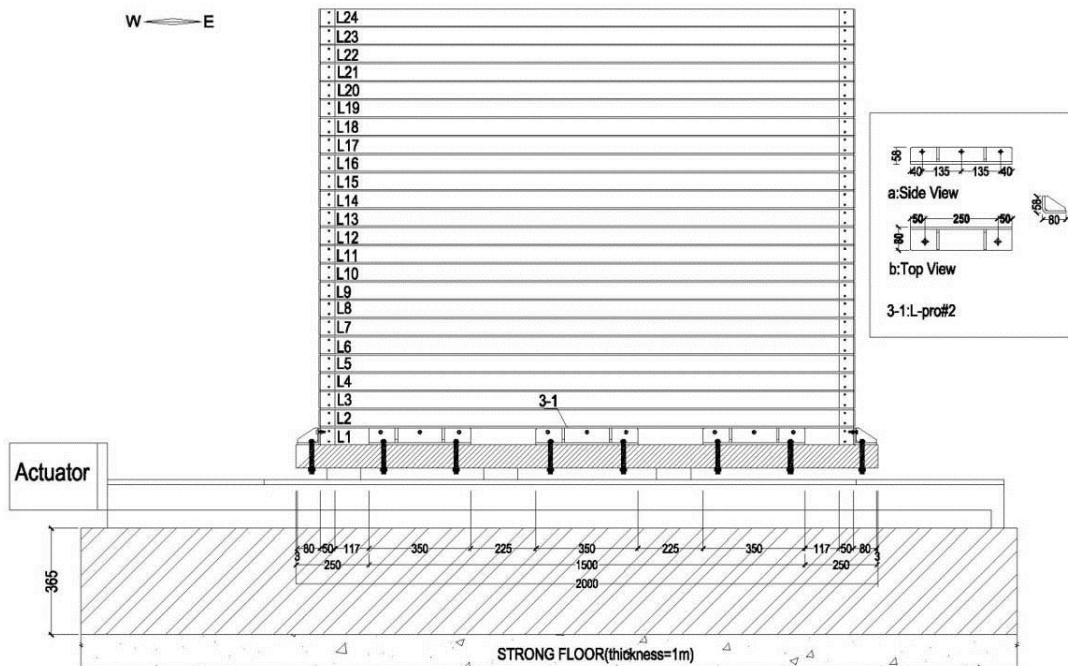


Figure A.9. Side View of Laminar Box (W-E)

Table A.2 Laboratory Equipment and Laminar Box System Components

AVAILABLE STRUCTURAL LABORATORY EQUIPMENT						
Equipment	Capacity	Maximum Displacement	Material	Dimension	Area	Comment
	ton	m	-	m	m ²	
Crane	3	-	-	-	-	Velocity=8.13 (cm/sec)
Strong Floor	-	-	C25-S420	-	51	-
Shake Table	3 (limited to 1 ton)	1	Aluminium	Length=2.04 Width=0.820 Thickness=0.008	1.67	See Fig. A.1

LAMINAR BOX PROPERTIES	
Box Height	1.49 m
Number of Laminates	24
Empty Box Weight	770 kg
Soil Weight	1776 kg
Soil+Box+Membrane Weight	2560 kg
Allowable displacement / Laminate	0.014 m
Maximum cumulative displacement at the top laminate	0.33 m
Gap between the laminates	0.005 m

LAMINAR BOX EQUIPMENT								
No.	Equipment	Name	Dimension	Number	Weight	Total Weight	Material	Comment
			m	-	kg	kg	-	
1	Bottom laminate (L1)	L1	Length = 1.834 Width=0.620	1	12.86	12.86	Aluminium Alloy 6063 I-profile (108.5x57.5x5)	Laminate Parameters : Density = 2.7 g/cm ³ n = 0.33
2	Laminates between top and bottom laminates	L2, L3, L24	Length = 1.834 Width=0.620	22	12.86	282.92	Aluminium Alloy 6063 I-profile (108.5x57.5x5)	
3	Top Laminate (L24)	L24	Length = 1.834 Width=0.620	1	12.86	12.86	Aluminium Alloy 6063 I-profile (108.5x57.5x5)	
4	Footprint area of soil	-	0.65	-	-	-	-	
5	Box Stopper / Laminate (at long edge)	BS #1	Length = 0.18 Length=0.180 Width=0.045 Thickness=0.001	2	0.36	0.72	Aluminium Alloy 6063 Box profile (50x50x4)	For dimensions of the Profile see Fig. A.2
6	Rubber Stopper / Laminate (at long edge)	RS #1	Length = 0.66 Width=0.045 Thickness=0.001	4	0.27	1.08	Rubber	For dimensions of the Profile see Fig. A.2
7	Box Stopper / Laminate (at short edge)	BS #2	Length = 0.66 Length=0.66 Width=0.045 Thickness=0.001	2	1.18	2.36	Aluminium Alloy 6063 Box profile (50x50x4)	For dimensions of the Profile see Fig. A.2
8	Rubber Stopper / Laminate (at short edge)	RS #2	Length = 0.66 Width=0.045 Thickness=0.001	4	0.08	0.32	Rubber	For dimensions of the Profile see Fig. A.2
9	Plates under Rollers / Laminate	-	Length=0.150 Width=0.085 Thickness=0.006	8	0.58	4.64	Steel S235 (S137-2)	Density = 7.85 g/cm ³ n = 0.25-0.30 E= 200 Gpa
10	Profiles near Rollers / Laminate	-	Length=0.150 Width=0.042 Thickness=0.008 Length = 0.06	16	0.28	4.48	Steel S235 (S137-2)	For dimensions of the Profile see Fig. A.4
11	Rollers / Laminate	-	Ø47	8	1.84	14.72	Stainless steel AISI 304	For dimensions of the Profile see Fig. A.4
12	Profiles to connect the bottom laminate to short edge	L-Pro #1	Length = 0.5	2	3.83	7.66	Steel S235 (S137-2) L-profile (80x58x8)	For dimensions of the Profile see Fig. A.9
13	Profiles to connect the bottom laminate to long edge	L-Pro #2	Length = 0.35	6	2.69	16.14	Steel S235 (S137-2) L-profile (80x58x8)	For dimensions of the Profile see Fig. A.9
14	Triangle support on profiles to connect the bottom laminate to short edge	T-pro	Length=0.07 Width=0.05 Thickness=0.008	20	0.14	2.8	Steel S235 (S137-2) Triangle support	For dimensions of the Profile see Fig. A.8
15	Angle bracket on reinforced welding / Laminate	A-pro	Length=0.130-0.092 Width=0.130-0.092 Thickness=0.004	4	0.07	0.28	Aluminium Alloy 6063 L-profile (50x50x5)	For dimensions of the Profile see Fig. A.8
16	Plate on reinforced welding / ring	-	Length = 0.130 Width=0.130 Thickness=0.092	4	0.46	1.84	Steel S235 (S137-2)	Put the profile under per ring for reinforced welding - Fig. A.6
17	Box profile for lifting the laminates	-	Length = 1.9	4	-	-	Steel S235 (S137-2) Box-profile (60x40x3)	For dimensions of the Profile see Fig. A.7
18	C-frame #1 for lifting the laminates	-	Length=0.62	3	2.61	7.83	Steel S235 (S137-2) Box-profile (60x40x3)	For dimensions of the Profile see Fig. A.7
19	C-frame #2 for lifting the laminates	-	Length=1.16	2	4.89	9.78	Steel S235 (S137-2) Box-profile (60x40x3)	For dimensions of the Profile see Fig. A.7
20	Cable lugs to connect the crane to C-Frame	-	M16	4	-	-	Steel (Standard)	For dimensions of the Profile see Fig. A.7
21	Frame	Cable Lug	M16	4	-	-	Steel (Standard)	For dimensions of the Profile see Fig. A.7
22	Chain lock to connect cable lock to the laminate	Chain Lug	-	4	-	-	Steel (Standard)	See Fig. A.7
23	Bars (trondela) to connect the L-pro to shake table	-	M14	20	-	-	-	See Fig. A.8
24	Nuts to connect the L-pro to shake table	-	M14	20	-	-	-	See Fig. A.8
25	Screws to connect the L-pro to shake table	-	M14x110	20	-	-	-	See Fig. A.8
26	Bolts to connect the L-pro at long edge and short edge to bottom laminate	-	M8x16	18	-	-	-	See Fig. A.8
27	Bolts to connect the L-pro at short edge to bottom laminate	-	M8x25	8	-	-	-	See Fig. A.8
28	Nuts to connect the L-pro at short edge to bottom laminate	-	M8	8	-	-	-	See Fig. A.8
29	Rubber Membrane	-	0.460x2.100x1.670x thickness = 0.0015	1	14.39	14.39	641 Complan Membrane	See Fig. 8